

THE CFTR FOLDING PATHWAY: IMPLICATIONS FOR
THE IDENTIFICATION AND DEVELOPMENT OF
CF THERAPEUTICS

APPROVED BY SUPERVISORY COMMITTEE

Philip J. Thomas, Ph.D.

Joseph Albanesi, Ph.D.

Nick V. Grishin, Ph.D.

Youxing Jiang, Ph.D.

Dedication

To my family, Luis, Catalina, Noelia and Thao, for all your love and support.

THE CFTR FOLDING PATHWAY: IMPLICATIONS FOR
THE IDENTIFICATION AND DEVELOPMENT OF CF
THERAPEUTICS

by

JUAN LUIS MENDOZA

DISSERTATION

Presented to the Faculty of the Graduate School of Biomedical Sciences

The University of Texas Southwestern Medical Center at Dallas

In Partial Fulfillment of the Requirements

For the Degree of

DOCTOR OF PHILOSOPHY

The University of Texas Southwestern Medical Center at Dallas

Dallas, Texas

October, 2011

Copyright

by

Juan Luis Mendoza, 2011

All Rights Reserved

Acknowledgements

Award of a Ph.D. is a major life accomplishment requiring a great deal of work and personal sacrifice over a period of many years. While the work and responsibilities ultimately belong to the graduate student, the help and support from others is undoubtedly key to the success of every student. At the top of the list is no other than my mentor, Philip J. Thomas. I remember at the end of my rotation, Phil invited me into his office and was direct and offered me a place in the lab. At the time, I did not really have to think about the decision, listened to my gut and quickly answered yes. While Phil's lab is a fully experimental lab, I had some interests in some computational work. Phil was open to this which turned out to an opportunity that far exceeded my wildest dreams. I have to thank Phil for his passion for science, dedication to combat CF, patience with me (really), commitment to training, and incredible vision.

The second person I would like to thank is Linda Millen. Linda has had such a large contribution to the body of work from the lab and to the CF research community. She is such a tremendous resource for her knowledge, experience, and abundance of resources and body of work. She has always made herself available to help all of us in the lab, given advice on our experiments, and provided reagents for not only me but

everyone in the lab. She is a wonderful source of warmth and I will truly miss her.

Phil's lab has a strong tradition of having outstanding students in the Biophysics Program such as Michael Dorwart, Patrick Thibodeau, Jonathan Moody, Anna Patrick and Karen Lewis. Besides the students, the post-doctorate fellows in the lab such as Balajee Somalinga, Li Zhu (my rotation mentor), and John Richardson III were equally amazing. Everyone was helpful, insightful, and tough with each other so as to prepare each other for the outside world. The strength of the people and research of the lab is a direct reflection of Phil and is perpetuated by the current members of the lab and post-docs; Sandra Tjon- Kon-Sang, students: Caroline Ritchie, Cameron Day, Yair Peres, Ali Vetter; post-docs: Andrea Hoffman, Andre Schmidt, and Carlos Huerta. Also, we are fortunate to have great faculty Andrey Karamyshev and Zemfira Karamysheva adding to expertise and experience providing wonderful insight and advice for me at the bench and future in science.

I would also like the members of my dissertation committee Joseph Albanesi, Nick Grishin, and Youxing Jiang. They and their labs have been an amazing source of insight and suggestions. Nick Grishin and my fellow Computational and Systems Biology student Bong-Hyun Kim were extremely helpful in discussions while I was building the multiple

sequence alignment of the eukaryotic ABC transporters. David Sauer and I had many discussions about sequence, alignments and understanding the role of amino acids in defining structure and function. Faculty and collaborator on a couple of projects I have been on, Chad Brautigam solved crystal structures and has always been extremely helpful, insightful, and provided feedback quickly.

Prior to joining the Thomas Lab, I did a rotation in Rama Ranganathan's lab where I learned to perform sequence coupling analysis. Bill Russ, Alan Poole, and Richard McLaughlin were very helpful in training me during my rotation and were also very helpful providing tips on high efficiency ligations for use in building a genetic library.

I would also like to thank our collaborators Qin Li and Andrew Feranchak. Qin is an amazing electrophysiologist and I felt very fortunate to have the opportunity to work with her on the patch-clamp experiments. She was able to collect all the data necessary for our submitted manuscript in only a couple weeks. The data is beautiful and reflects her expertise and professionalism.

THE CFTR FOLDING PATHWAY: IMPLICATIONS FOR
THE IDENTIFICATION AND DEVELOPMENT OF CF
THERAPEUTICS

Juan Luis Mendoza, Ph.D.

The University of Texas Southwestern Medical Center at
Dallas, October 2011

Philip J. Thomas, Ph.D.

The Cystic Eibrosis Iransmembrane Conductance Regulator (CFTR) protein is a member of the ABC transporter superfamily, important for Cl⁻ conductance at the apical cell membrane. Loss-of-function of CFTR leads to Cystic Fibrosis (CF), a fatal genetic disease affecting 70,000 people worldwide. There are hundreds of CF causing mutations with the

most common being $\Delta F508$, present in at least one allele in 90% of CF patients.

CFTR, comprising of 1480 amino acids, folds into five domains important for forming the channel through the membrane, and the regulation of channel function. F508 is located in Nucleotide Binding Domain 1 (NBD1) and is predicted to be at the interface with Intracellular Loop 4 (ICL4) of Transmembrane Domain 2 (TMD2). Studies of the isolated NBD1 demonstrate that the $\Delta F508$ mutation impacts the folding pathway and stability of the domain. Misfolding of NBD1 contributes to the trafficking defect of the intact protein and subsequent loss-of-function. Conversely, second-site suppressor mutations, which more than compensate for defects of the mutant NBD1 domain, only partially rescue CFTR trafficking, suggesting that the deletion also affects other steps along the folding pathway.

The aim of this work was to identify positions in CFTR critical for defining the folding pathway. We used a computational approach and two *in vitro* folding assays to monitor folding of the isolated NBD1 domain and trafficking of full-length CFTR. These data establish a correlation between the folding of the isolated NBD1 domain and maturation of full-length CFTR. Further, NBD1 second-site suppressor mutations in the $\Delta F508$, F508K (NBD1/ICL4 interface disrupting mutation), and R1070W ($\Delta F508$ NBD1/ICL4 interface stabilizing mutation) backgrounds suggest that

$\Delta F508$ CFTR is defective in two steps of CFTR biogenesis: 1) stability and efficiency of folding of the NBD1 domain, and 2) NBD1/ICL4 docking. We demonstrate that efficient rescue of $\Delta F508$ CFTR requires correction the two distinct defects. This work has implications for the discovery and development of CF therapeutics by providing a framework for understanding the observed ceiling in the efficacy of either suppressor mutations or corrector compounds, which likely correct a single defect.

Table of Contents

Dedication	ii
Acknowledgments	v
Abstract	viii
Table of Contents	xi
Publications From Graduate Work at UTSW	xiii
List of Figures	xiv
List of Tables	xvii
List of Appendices	xviii
Chapter 1: Introduction to the ABC Transporter Cystic Fibrosis Transmembrane Conductance Regulator (CFTR)	
<i>Introduction</i> _____	1
Chapter 2: Analyses of Evolved Sequences and Structure Reveal the Requirements for Efficient Corrected Folding of $\Delta F508$ CFTR	
<i>Introduction</i> _____	25
<i>Results</i> _____	34
<i>Discussion</i> _____	63
<i>Experimental Procedures</i> _____	67
Chapter 3: Perspectives and Future Directions	
<i>Introduction</i> _____	78
<i>Results</i> _____	81
<i>Discussion</i> _____	91
<i>Future Directions</i> _____	99
<i>Experimental Procedures</i> _____	100

Appendices	101
Bibliography	109
Vitae	125

Publications From Graduate Work at UTSW

Mendoza, J.L., Schmidt, A., Li, Q., Caspa, E., Barrett, T., Bridges, R.J., Feranchak, A.P., Brautigam, C.A., and Thomas, P.J. "Requirements for Efficient Correction of $\Delta F508$ CFTR Revealed by Analyses of Evolved Sequences." *Cell* (In Press).

Mendoza, J.L., Schmidt, A., Thomas, P.J. "Chapter 21. Introduction: Biophysical Methods to Approach CFTR Structure *Cystic Fibrosis Methods and Protocols*," ed M. Amaral, **Humana Press**, Totowa, New Jersey. *Methods Mol Biol.*, **741:321-7** (2011). [[PubMed](#)]

Schmidt, A., **Mendoza, J.L.**, Thomas, P.J. "Chapter 24. Introduction: Biophysical Methods to Approach CFTR Structure *Cystic Fibrosis Methods and Protocols*," ed M. Amaral, **Humana Press**, Totowa, New Jersey. *Methods Mol Biol.*, **741:365-76** (2011). [[PubMed](#)]

Zhu, L., Millen, L., **Mendoza, J.L.**, Thomas, P.J. "A unique redox-sensing sensor-II motif in *TorsinA* plays a critical role in nucleotide and partner binding." *J Biol Chem.*, **285** (2010) **37271-37280**. [[PubMed](#)]

Thibodeau, P.H., Richardson, J.M. 3rd, Wang, W., Millen, L., Watson, J, **Mendoza, J.L.**, Du, K., Fischman, S., Senderowitz, H., Lukacs, G.L., Kirk, K., Thomas, P.J. "The Cystic Fibrosis-causing Mutation $\Delta F508$ Affects Multiple Steps in Cystic Fibrosis Transmembrane Conductance Regulator Biogenesis." *J Biol Chem.*, **285** (2010) **35825-35**. [[PubMed](#)]

Mendoza, J.L., Thomas, P.J. "Building an understanding of cystic fibrosis on the foundation of ABC transporter structures." *J Bioenerg Biomembr.* **39** (2007) **499-505**. [[PubMed](#)]

List of Figures

Figure 1-1	TMD/NBD interactions in intact ABC transporter structures.	11
Figure 1-2	Model of TMD and NBD interactions in CFTR .	14
Figure 2-1	Predicted Relationship of CFTR Domains to the F508 Position.	27
Figure 2-2	Δ F508 CFTR is a Misfolding Mutation and is Unable to Traffic to the Plasma Membrane.	28
Figure 2-3	Characterization of Δ F508 NBD1 Reveals the Mutation Affects Folding of NBD1.	29
Figure 2-4	Second-Site Suppressor Mutations Identified by the Genetic Screen are Distal to the F508 Position.	31
Figure 2-5	Second-Site Suppressor Mutations Correction of Δ F508 Mediated Misfolding.	32
Figure 2-6	Positional Conservation Scores in Human Numbering in the MSA of 493 ABC Transporters.	36
Figure 2-7	CFTR Inter-Residue Coupling Matrix Calculated from an ABC Transporter Sequence Alignment.	38
Figure 2-8	NBD1 Inter-Residue Coupling Matrix Calculated from an ABC Transporter Sequence Alignment.	39
Figure 2-9	Statistics and Structural Context of the 16 Representative Coupled Positions in NBD1 Structure.	41
Figure 2-10	Representation of the β -galactosidase Complementation Assay.	44
Figure 2-11	Effects of 508-Coupled Mutations and Second-Site Suppressors on NBD1 Folding.	45
Figure 2-12	S573E Increases the Stability of NBD1, D529F Does Not	46
Figure 2-13	Structural Context of D529F and S573E Suppressor Mutations.	47

Figure 2-14	Effects of 508-Coupled and Second-Site Suppressor Mutations on CFTR Maturation and Correlation with NBD1 Folding Yield.	50
Figure 2-15	Effects of 508-Coupled and Second-Site Suppressor Mutations on CFTR Maturation and Correlation with NBD1 Folding Yield.	51
Figure 2-16	Δ F508 and 508 Missense Mutations Influence the Correlation of CFTR Maturation with NBD1 Folding Yield by Disrupting the ICL4/NBD1 Interface.	54
Figure 2-17	Structure of Unmodified Murine Δ F508 NBD1 Shows Changes in the Backbone Local to the Site of the Deletion.	55
Figure 2-18	Δ F508 and 508 Missense Mutations Influence the Correlation of CFTR Maturation with NBD1 Folding Yield by Disrupting the ICL4/NBD1 Interface.	56
Figure 2-19	R1070W Improves Δ F508, Interferes with WT Maturation.	59
Figure 2-20	Correction of the Δ F508 NBD1/ICL4 Interface Defect is Synergistic with Correction of the Δ F508 NBD1 Folding Yield Defect.	61
Figure 2-21	Correction of the Δ F508 NBD1/ICL4 Interface Defect is Synergistic with Correction of the Δ F508 NBD1 Function.	62
Figure 3-1	Effect of 19 NBD1 CF-causing mutations on maturation.	83
Figure 3-2	Effects of 19 CF-causing mutations on NBD1 folding.	85
Figure 3-3	Evidence leading to a new mutation sub-classification.	86
Figure 3-4	Temperature rescue of mutations with reduced NBD1 folding.	89
Figure 3-5	Rescue of misfolding mutants by second-site suppressors.	90

Figure 3-6 Structural Context of a Select number of Mutants.

98

List of Tables

Table 1-1	Representative ABC Transporter Structures in the Research Collaboratory for Structural Bioinformatics (RCSB) Database	9
Table 2-1	Identification of NBD1 Positions Coupled to F508 Using Four Independent Statistical Methods.	41
Table 3-1	Classification of CF-causing Mutations by Molecular Defect	82
Table 3-2	Extending the Classification of CF-causing Mutations	97

List of Appendices

Figure S1	Δ F508 Forms a Cavity at the NBD1/ICL4 Interface in CFTR.	101
Figure S2	Independent Coupling Matrices for Each of the Four Methods.	102
Figure S3	Positions in NBD1 Coupled to F508, Related to Table 2-1.	103
Figure S4	Structural Context of S573E Suppressor Mutations.	104
Figure S5	Comparison of Various Methods for Quantification of Maturation of CFTR.	105
Table S1	Crystallographic and Refinement Data for Murine DF508 Structure	106
Table S2	Impact of Suppressor Mutations on DF508 NBD1 Folding, Maturation.	108

List of Abbreviations

CF	Cystic Fibrosis
CFTR	Cystic Fibrosis Transmembrane Conductance Regulator
ABC transporter	ATP Binding Cassette transporter
3M	G550E-R553M-R555K mutations in <i>cis</i>
SSS	Second-Site Suppressor(s)
TMD	Transmembrane Domain
RD	Regulatory Domain
NBD	Nucleotide Binding Domain
ECL	Extracellular Loop
ICL	Intracellular Loop
RI	Regulatory Insertion
RE	Regulatory Extension
ER	Endoplasmic Reticulum
SCA	Statistical Coupling Analysis
ELSC	Explicit-Likelihood Subset of Covariation
McBASC	McLachlan Based Substitution correlation

Chapter 1: Introduction to the ABC Transporter Cystic Fibrosis Transmembrane Conductance Regulator (CFTR)

Introduction

Cystic fibrosis (CF) is a fatal disease affecting the lungs and digestive system by impairment of the Cystic Fibrosis Transmembrane Conductance Regulator (CFTR). While hundreds of mutations in CFTR have been associated with CF, the majority of cases are linked to the deletion of phenylalanine 508 (F508). F508 is located in the first nucleotide binding domain (NBD1) of CFTR. This mutation is sufficient to impair the trafficking of CFTR to the plasma membrane and, thus, its function. As an ABC transporter, recent structural data from the family provide a framework on which to consider the effect of the F508 mutation on CFTR. There are hundreds of structures of ABC transporters and domains thereof. Only 20 structures are of the intact transporters. In addition, modern bioinformatic tools provide a wealth of sequence and structural information on the family. We will review the structural information from the RCSB structure repository and sequence databases of the ABC transporters. The available structural information was used to construct a model for CFTR based on the ABC transporter homologue, Sav1866, and provide a context for understanding the molecular pathology of Cystic Fibrosis.

Domain Organization of ABC Transporters

CFTR is a member of the ABC Transporter family of mechanochemical machines that couple ATPase activity to the movement of solutes across a membrane. They function as multi-domain proteins in a diverse number of configurations. The minimum functional unit of the family consists of two nucleotide binding domains (NBDs) and two transmembrane domains (TMDs) (Higgins 1992). ATP binding and hydrolysis at the NBDs transmit chemical work to domain rearrangements in the TMDs that allow for solute movement (Dassa and Hofnung 1985; Schmitt and Tampe 2002; Smith *et al.* 2002; Jones and George 2004).

The largest proteins in the family are the full-length transporters such as CFTR with all four domains on a single polypeptide chain (Higgins 1992). CFTR is 1480 amino acids long with a mass of approximately 170 kDa. At the N-terminus of the CFTR chain is the first TMD containing 6 transmembrane spans as typical for the family, followed by the first of the two NBDs. Unique to CFTR proteins is the insertion of a regulatory domain, the R-domain, following the first NBD. The R-domain is highly disordered and interacts with NBD1 in a phosphorylation-dependent manner (Baker *et al.* 2007). Following the R-domain is a second TMD and then the second NBD (NBD2) at the C-terminus. This order of domain organization is the most prevalent for ABC transporters, however, there are predicted full-length transporters with other domain organizations. In these cases, the N-terminus is initiated by a NBD domain and is continued

alternating NBDs and TMDs. Half-transporters consist of a single TMD and NBD domain translated on a single polypeptide. Both eukaryotic as well as some microbial exporters, are arranged in this manner (Dawson et al. 2007). In this organization, half-transporters fulfill the ABC transporter minimum functional units by forming either homo or heterodimers. For the homodimeric bacterial transporter, Sav1866, the TMD is at the N-terminus followed by the NBD at the C-terminus. Similar to most full-transporters, half-transporters typically have the TMD at the N-terminus as is the case with Sav1866. However, proteins with the reverse TMD/NBD order also exist. The greatest number of ABC transporters, found in archae and bacteria, contain each domain on a separate chain and are expressed modularly. A single microbial operon typically contains the genes for each of the domains required to form the functional complex. Additionally, there are a small number of ABC transporters, which have two fused NBDs on a single polypeptide.

Nucleotide Binding Domains

There are 163,029 sequences from 3,369 species included in the Pfam-A component for the NBDs of ABC transporters, PF00005 (Sonnhammer et al. 1997). Pfam reports that there are 233 structures of ATP-binding domains solved to date. The members which include two NBDs in a single polypeptide chain have both NBDs included in the multiple sequence alignment (MSA). Both CFTR NBD1 and NBD2 are included in

the NBD MSA. Highlighting the high degree of conservation in the NBD region, the percent identity of a previously reported representative alignment was 26% (Mendoza and Thomas, 2007). The NBDs of ABC transporters belong to the α/β class of proteins. Structural classification databases such as SCOP and CATH classify the NBDs as homologous and members of the P-loop containing nucleotide triphosphate hydrolases Superfamily (Murzin et al. 1995; Orengo et al. 1997). SCOP includes 25 different families including AAA- ATPases, motor proteins, G proteins, and several kinase families. The P-loop is also commonly known as the Walker A (GXXGXGKS/T) motif (Saraste et al. 1990). This is the glycine rich region with a conserved lysine and serine, which coordinate ligand binding of the ATP phosphates in other ATPases (Leslie et al. 2001). This sequence motif, along with the Walker B motif ($\phi\phi\phi\phi$ D, where ϕ is a hydrophobic residue), was one of the first identified and is highly conserved in different hydrolases regardless of the family (Walker et al. 1982; Jones and George 2004).

As of this writing, 254 structures of ABC transporters or their domains are available. Most are of the NBDs and of the periplasmic solute binding proteins utilized by bacterial import ABC transporters. We do not further consider these domains here as they are not found in eukaryotic ABC systems including CFTR. The structures available have been solved in apo, ligand bound, and mutant forms. The first structure of a core ABC transporter domain was published by Hung et al of the HisP NBD protein

of the histidine permease (PDB 1B0U) (Hung et al. 1998). The initial structure was of monomeric HisP with ATP bound. The fold was unlike any other known structures at the time, but contained a core α/β domain similar to RecA (Story et al. 1992; Jones and George 1999). The P-loop is found in this subdomain, which also contains the Walker B motif. The Signature motif (LSGGQ) that identifies the ABC transporter family was located in a smaller α -helical subdomain. The α -helical subdomain also contains the F508 residue in CFTR NBD1.

From biochemical studies, HisP was known to function as a dimer and the Signature motif was known to play a vital role in ATP binding and hydrolysis (Nikaido et al. 1997; Fetsch and Davidson 2002; Loo et al. 2002). Yet, in the crystal structure of the monomer, the Signature motif was not in contact distance with the single ATP molecule. This left unresolved the question as to how the Signature sequence contributed to the enzymatic function of NBD proteins. A model that resolved the conundrum was proposed placing the ATP in the interface of an NBD dimer (Jones and George 1999). The first suggestion that this model might be correct came from a structure of Rad50. A member of the Structural and Maintenance of Chromosome (SMC) family of proteins; Rad50 is involved in DNA double-stranded break repair. Although, Rad50 is not an ABC Transporter, it was believed to be related to ABC transporters due to the similarity of fold (Hopfner et al. 2000). Rad50 makes a dimer pairing the Signature sequence from one chain to the Walker A and B motifs of

the opposing chain with ATP sandwiched in between. In 2002, a structure of an ABC transporter NBD dimer (the *Methanococcus jannaschii* protein, MJ0796) was solved (Smith et al. 2002). The dimer was trapped by mutating the catalytic base (E171Q) (Moody et al. 2002). This structure revealed that the Signature motif was involved in coordinating with the γ -phosphate of ATP in the dimeric form in a head to tail sandwich, consistent with biochemical data (Moody et al. 2002; Fetsch and Davidson 2002). In this sandwich dimer, the Signature motif residues of the second NBD complete the active site with the Walker A and B residues of the first NBD (Smith et al. 2002). This arrangement also explains the positive cooperativity of the ATPase.

ICL/NBD Interactions

Alignments of transmembrane regions are more problematic due to the low level of conservation. In contrast to the large number of sequences available for the NBD alignments in Pfam, only 23,148 transmembrane sequences from 2,534 species are in the MSA of ABC transporter TMDs, PF00664 (Sonnhammer et al. 1997). The average percent identity of a representative set of sequences from an alignment as previously reported was only 14% (Mendoza and Thomas, 2007). Thus, even with the most robust methodologies, alignments of transmembrane regions are susceptible to inaccuracies and motifs are more difficult to identify. One such sequence in the intercellular loops connecting the TM segments of

ABC transporter uptake proteins is the EAA-X(3)-G-X(9)-LP motif (Doige and Ames 1993; Saurin and Dassa 1994; Biemans-Oldehinkel et al. 2006). This motif is not ubiquitous throughout the family (Dassa and Hofnung 1985; Schmitt and Tampe 2002; Biemans-Oldehinkel et al. 2006). Thus, quality assessments of the transmembrane domains are not possible due to low conservation across the family in these regions, consistent with their role in mediating movement of a wide variety of structurally diverse solutes.

Of the available ABC transporter structures, only 20 structures, which include the proteins BtuCD, HI1470/1, ModBC, MsbA, MalEFGK₂ and Sav1866, contain the NBDs in complex with the transmembrane domains. One of the early structures of a, MsbA (PDB 1Z2R and 1PF4), have been retracted due to software problems in generating the structure models (Chang and Roth 2001; Reyes and Chang 2005; Chang et al. 2006; Matthews 2007) and has since been replaced by five structures (PDBs 3B5W-Z and 3B60). BtuCD is an ABC vitamin B12 importer and was the first ABC transporter to be crystallized with both NBD and TMD components (PDB 1L7V) (Locher et al. 2002). Unlike other ABC transporters, each half of the TMD region of BtuCD has 10 transmembrane spans with 4 ICLs. Moreover, BtuCD has different ICL/NBD interactions from the other known intact transporters. A single TMD interacts with a single NBD by way of three of the four ICLs (Figure 1-1A). In addition, the N-terminus packs against the outside of the α -helical

subdomain. The first ICL only has two residues within contact distance of the NBD and contacts the α -helical subdomain. ICL2 is not in a close enough proximity to directly interact with either of the two NBDs. The nearest atom of the NBD to ICL2 is approximately 7.7 angstroms. ICL3 has the greatest amount of interaction surface area and interacts with the NBD between both the α -helical and α/β subdomains. In this region of the interface, the ICLs and NBDs share both polar and hydrophobic interactions. The fourth ICL (ICL4) sits above the α -helical subdomain centered between the N and C-termini of the TMD and ICLs 1 and 3.

More prototypical of the transporter family are ModBC and Sav1866. ModBC (PDB 2ONK) is a modular archaeal importer, which has 6 transmembrane spans and two ICLs in each of the TMDs (Hollenstein et al. 2007). Unlike the BtuCD structure in which a single TMD interacts with a single NBD, in ModBC, each of the N-termini cross over to the opposing NBD (Figure 1-1B). The N-terminus of each TMD is positioned within 4.4 angstroms of the outer face of the opposing NBD. ICL1 makes contacts with the N and C-termini of the opposing TMD and does not come in contact with either of the NBDs. ICL2 is positioned in the groove between the α/β and α -helical subdomains. The C-terminus of the ModBC TMDs rest above the NBD α -helical subdomains but are not within contact distance of the NBDs.

Table 1-1 Representative ABC Transporter Structures in the Research Collaboratory for Structural Bioinformatics (RCSB) Database

	Release Date	PDB	Structure Title	Resolution	Species
CFTR Structures	Apr-99	1CKW	CYSTIC FIBROSIS TRANSMEMBRANE CONDUCTANCE REGULATOR: SOLUTION STRUCTURES OF PEPTIDES BASED ON THE PHE508 REGION, THE MOST COMMON SITE OF DISEASE-CAUSING DELTA-F508 MUTATION	NMR	<i>Synthetic</i>
	Apr-99	1CKX	Cystic fibrosis transmembrane conductance regulator: Solution structures of peptides based on the Phe508 region, the most common site of disease-causing Delta-F508 mutation	NMR	<i>Synthetic</i>
	Apr-99	1CKY	CYSTIC FIBROSIS TRANSMEMBRANE CONDUCTANCE REGULATOR: SOLUTION STRUCTURES OF PEPTIDES BASED ON THE PHE508 REGION, THE MOST COMMON SITE OF DISEASE-CAUSING DELTA-F508 MUTATION	NMR	<i>Synthetic</i>
	Apr-99	1CKZ	CYSTIC FIBROSIS TRANSMEMBRANE CONDUCTANCE REGULATOR: SOLUTION STRUCTURES OF PEPTIDES BASED ON THE PHE508 REGION, THE MOST COMMON SITE OF DISEASE-CAUSING DELTA-F508 MUTATION	NMR	<i>Synthetic</i>
	Jul-03	1Q3H	mouse CFTR NBD1 with AMP.PNP	2.50	<i>Mus musculus</i>
	Sep-03	1R0W	Cystic fibrosis transmembrane conductance regulator (CFTR) nucleotide-binding domain one (NBD1) apo	2.20	<i>Mus musculus</i>
	Sep-03	1R0X	Cystic fibrosis transmembrane conductance regulator (CFTR) nucleotide-binding domain one (NBD1) with ATP	2.20	<i>Mus musculus</i>
	Sep-03	1R0Y	Cystic fibrosis transmembrane conductance regulator (CFTR) nucleotide-binding domain one (NBD1) with ADP	2.55	<i>Mus musculus</i>
	Sep-03	1R0Z	Phosphorylated Cystic fibrosis transmembrane conductance regulator (CFTR) nucleotide-binding domain one (NBD1) with ATP	2.35	<i>Mus musculus</i>
	Sep-03	1R10	Cystic fibrosis transmembrane conductance regulator (CFTR) nucleotide-binding domain one (NBD1) with ATP, I4122 space group	3.00	<i>Mus musculus</i>
	Sep-04	1XF9	Structure of NBD1 from murine CFTR- F508S mutant	2.70	<i>Mus musculus</i>
	Sep-04	1XFA	Structure of NBD1 from murine CFTR- F508R mutant	3.10	<i>Mus musculus</i>
	Jun-11	3SI7	The crystal structure of the NBD1 domain of the mouse CFTR protein, deltaF508 mutant		<i>Mus musculus</i>
	Oct-04	1XMI	Crystal structure of human F508A NBD1 domain with ATP	2.25	<i>Homo sapiens</i>
	Oct-04	1XMJ	Crystal structure of human deltaF508 human NBD1 domain with ATP	2.30	<i>Homo sapiens</i>
	Oct-05	2BBO	Human NBD1 with Phe508	2.55	<i>Homo sapiens</i>
	Oct-05	2BBS	Human deltaF508 NBD1 with three solubilizing mutations	2.05	<i>Homo sapiens</i>
	Oct-05	2BBT	Human deltaF508 NBD1 with two solubilizing mutations.	2.30	<i>Homo sapiens</i>
	May-07	2PZE	Minimal human CFTR first nucleotide binding domain as a head-to-tail dimer	1.70	<i>Homo sapiens</i>
	May-07	2PZF	Minimal human CFTR first nucleotide binding domain as a head-to-tail dimer with delta F508	2.00	<i>Homo sapiens</i>
May-07	2PZG	Minimal human CFTR first nucleotide binding domain as a monomer	1.80	<i>Homo sapiens</i>	
Feb-09	3GD7	Crystal structure of human NBD2 complexed with N6-Phenylethyl-ATP (P-ATP)	2.70	<i>Homo sapiens</i>	

<i>(Continued)</i>					
TMD/NBD	Mar-02	1L7V	Bacterial ABC Transporter Involved in B12 Uptake	3.20	<i>Escherichia coli</i>
Complex Structures	Aug-06	2HYD	Multidrug ABC transporter SAV1866 An inward-facing conformation of a putative metal-chelate type	3.00	<i>Staphylococcus aureus</i>
	Oct-06	2NQ2	ABC transporter.	2.40	<i>Haemophilus influenzae</i>
	Sep-07	2R6G	The Crystal Structure of the E. coli Maltose Transporter	2.80	<i>Escherichia coli</i>
	May-08	3D31	ModBC from Methanosarcina acetivorans Crystal structure of the resting state maltose transporter from E. coli	3.00	<i>Methanosarcina acetivorans</i>
	Dec-08	3FH6	Crystal Structure of an outward-facing MBP-Maltose transporter complex bound to ADP-VO4	4.50	<i>Escherichia coli</i>
	Dec-10	3PUV	Crystal Structure of an outward-facing MBP-Maltose transporter complex bound to ADP-ALF4	2.40	<i>Escherichia coli</i>
	Dec-10	3PUW	Crystal Structure of an outward-facing MBP-Maltose transporter complex bound to ADP-BeF3	2.30	<i>Escherichia coli</i>
	Dec-10	3PUX	Crystal Structure of an outward-facing MBP-Maltose transporter complex bound to AMP-PNP after crystal soaking of the pretranslocation state	2.30	<i>Escherichia coli</i>
	Dec-10	3PUY	Crystal Structure of a pre-translocation state MBP-Maltose transporter complex bound to AMP-PNP	3.10	<i>Escherichia coli</i>
	Dec-10	3PUZ	Crystal structure of the maltose-binding protein/maltose transporter complex in an outward-facing conformation bound to MgAMPPNP	2.90	<i>Escherichia coli</i>
	Apr-11	3RLF	ABC-transporter BtuCD in complex with its periplasmic binding protein BtuF	2.20	<i>Escherichia coli</i>
	Jul-07	2QI9	Structure of the multidrug ABC transporter Sav1866 from <i>Staphylococcus aureus</i> in complex with AMP-PNP.	2.60	<i>Escherichia coli</i>
	Jan-07	2ONJ	ABC transporter ModBC in complex with its binding protein ModA	3.40	<i>Staphylococcus aureus</i>
	Jan-07	2ONK	Crystal Structure of Escherichia coli MsbA	3.10	<i>Archaeoglobus fulgidus</i>
	Oct-07	3B5W	Crystal Structure of MsbA from <i>Vibrio cholerae</i>	5.30	<i>Escherichia coli</i>
	Oct-07	3B5X	Crystal Structure of MsbA from <i>Salmonella typhimurium</i> with AMPPNP	5.50	<i>Vibrio cholerae</i>
	Oct-07	3B5Y	Crystal Structure of MsbA from <i>Salmonella typhimurium</i> with ADP Vanadate	4.50	<i>Salmonella typhimurium</i>
	Oct-07	3B5Z	Crystal Structure of MsbA from <i>Salmonella typhimurium</i> with AMPPNP, higher resolution form	4.20	<i>Salmonella typhimurium</i>
	Oct-07	3B60		3.70	<i>Salmonella typhimurium</i>

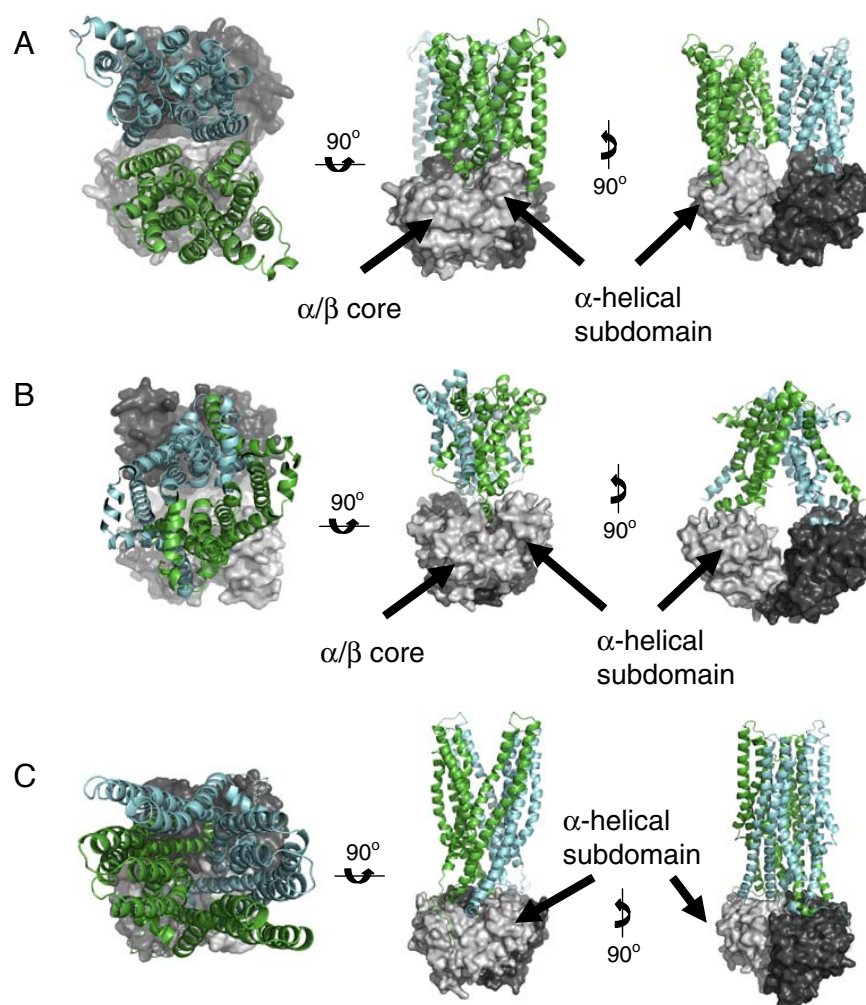


Figure 1-1 TMD/NBD interactions in intact ABC transporter structures (PDB 1L7V, 2ONK and 2HYD). **(A)** The structure of BtuCD. NBDs are represented in surface models in light gray and dark gray. Ribbon representations of the TMDs with their ICLs cyan and green. Each of the BtuC TMDs contain ten transmembrane spans and four ICLs. Three of the four ICLs are within contact distance of the proximal NBD. In this structure, ICLs from one TMD interact with a single NBD. Left Top view from the perspective of the membrane. Center Rotation by 90° in the plane of the page from the prior view. Right Side view of the prior view by rotating 90° out of the plane of the page. **(B)** The structure of ModBC. NBDs are represented in surface models in light gray and dark gray. Ribbon representations of the TMDs are in cyan and green. Each of the ModB TMDs contain six transmembrane spans with 2 ICLs. In this structure, two ICLs from one TMD interact with a single NBD and the N-terminus of each of the TMDs “swap” and are within contact distance of the distal NBD. Left Top view from the perspective of the membrane. Center Rotation by 90° in the plane of the page from the prior view. Right Side view of the prior view by rotating 90° out of the plane of the page. **(C)** The structure of Sav1866. NBDs are represented in surface models in light gray and dark gray. Ribbon representations of the TMDs are in cyan and green. Each of the Sav1866 TMDs contain six transmembrane spans with 2 ICLs. In this structure, both ICLs from one TMD interact with each of the two NBDs. Left Top view from the perspective of the membrane. Center Rotation by 90° in the plane of the page from the prior view. Right Side view of the prior view by rotating 90° out of the plane of the page.

A third arrangement is seen in Sav1866 (2HYD PDB), a bacterial multi-drug transporter containing a single TMD and NBD on a single polypeptide (Dawson and Locher 2006). Of the four, structures with the complex of TMD and NBDs, Sav1866 is the only half-transporter. The Sav1866 TMD has six transmembrane spans located at the N-terminus of the protein. The NBD is at the C-terminus. In the Sav1866 homodimer structure, ICLs form interactions with both NBDs (Figure 1-1C). Thus, each of the NBDs are contacted by both the TMDs. ICL1 sits directly above the P-loop interacting with its own NBD at the α/β subdomain. The interface has approximately 132 angstroms² of surface area with a near equal number of polar and non-polar atoms, 56% and 44%, respectively. The ATP adenine ring is within 4.2 angstroms of ICL1. Additionally, ICL1 interacts with the α -helical subdomain of the opposing NBD near the Signature motif. This interface has approximately 187 angstroms² of surface area with nearly equal number of polar to non-polar atoms, 46% and 54%, respectively. ICL2 solely interacts with the NBD of the opposing dimer chain. The nidus of the ICL2/NBD interaction occurs at the groove between the α/β and α -helical subdomains of the dimer NBD chain. There are approximately 725 angstroms² of surface area at the ICL2/NBD interface. Furthermore, this interface is strongly characterized by a hydrophobic interface with a 32% and 68% polar to non-polar atoms, respectively. Sav1866 is the closest homologue of CFTR for which a structure is available.

A Model for CFTR

The large majority of CF patients have the disease linked to the deletion of phenylalanine 508 in the N-terminal NBD1 of CFTR. The F508 CFTR misfolds at physiological conditions and does not traffic efficiently beyond the endoplasmic reticulum as monitored by complex glycosylation (Cheng et al. 1990). The mutant also affects the isolated NBD1 (Thibodeau et al. 2005). In the cell, F508 CFTR is targeted for degradation (Lukacs et al. 1994). Notably, electrophysiological studies indicate that when F508 CFTR is temperature-rescued the channel has activity (Denning et al., 1992). Thus, the primary cause of this form of CF disease is due to the disruption of the folding pathway of CFTR (Thomas et al., 1992). Understanding the structural perturbations which occur due to the deletion of F508 is of great interest and practical importance, as correcting CFTR's inability to reach the plasma membrane should be of therapeutic benefit. Because there is no structure of full-length CFTR, models provide important insight into elucidating the interactions within CFTR and the effect of disease-causing mutations.

At present there are structures for the first NBD (NBD1) of CFTR (Table 1-1). Also available are F508 NBD1s containing mutants that enable folding. Six years after the first NBD1 structure was solved, NBD2 was solved in 2009 by Atwell et al. A structure of the NBD1/2 heterodimer has yet to be determined. However, like other ABC transporters, the two NBDs of CFTR are expected to interact and bind two molecules of ATP

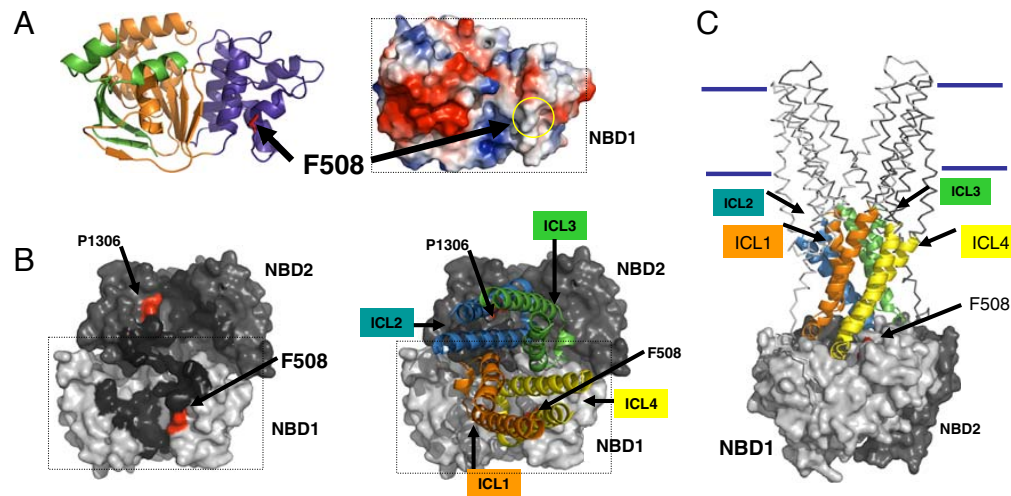


Figure 1-2 Model of TMD and NBD interactions in CFTR (Based on: 1R0W and 2HYD). (A) Structure of CFTR NBD1 looking from the perspective of the membrane plane. Left Ribbon representation of the CFTR NBD1. The N-terminal region is colored in green. The Walker A and B motifs are located in the α/β -core subdomain orange. The Signature “LSGGQ” and F508 residue red are located in the α -helical subdomain dark blue. Right, electrostatic surface representation with negative-red and positive-blue. The hydrophobic-white 508 position is exposed and is indicated by the yellow circle. (B) The Sav1866 structure was used to produce a working model for CFTR. The relative interactions of the NBDs, the ICLs, and specific CFTR residues are indicated. The two NBDs dimerize with the two ATPs (not shown) sandwiched between the interface, analogous to the MJ0796 sandwich dimer structure. Left The NBD sandwich dimer is shown stripped of the TMDs and connecting ICLs. The surfaces covered by the ICLs are shown in black and the surface exposed positions of F508 and P1306 (predicted) are shown in red. Right Same view with the ICLs in place. ICL4 sits in a groove on the surface of NBD1 between the α -helical subdomain and the α/β -core and near the F508 position (partially hidden). (C) A side view of the CFTR model.

(Vergani et al. 2005). If NBD1/NBD2 forms such a sandwich dimer then only one of these two sites will be enzymatically active, because the catalytic glutamate is absent in the Walker B motif in CFTR NBD1 (Lewis et al. 2004).

Mutations at three positions (G550, R553, and R5550) in NBD1 have been found to correct the folding defect of F508 solubility (Dork et al. 1991; Teem et al. 1993, 1996; DeCarvalho et al. 2002). All three second-site suppressor mutations are located in the α -helical subdomain. A crystal structure has been solved of F508 NBD1 containing these three suppressor mutations (Lewis et al. 2005). Comparison of the structures for wild-type NBD1 and the F508 NBD1 with the three solubilizing mutations do not reveal any significant rearrangements. Alignments of the mutant structure against wild-type NBD1 are within 0.6 angstroms RMS deviation. In addition to the effect of the disease causing mutation on isolated NBD1 folding, the structures place the F508 mutation on the surface of the domain in a position predicted to interact with the ICLs in other ABC transporters. In this regard, Lewis et al propose that one effect of F508 CFTR is the disruption of interdomain interactions with the membrane spans (Lewis et al. 2004).

A current open question is what is the nature of this interface. That is, how do the ICLs interact with the NBDs in CFTR? If CFTR is arranged like the exporter, Sav1866, CFTR ICL2 (predicted 242 to 307) and ICL3

(predicted 930 to 990) would interact with NBD2 (Seibert et al. 1996; Wigley et al. 1998). CFTR ICLs 1 (predicted 141–194) and 4 (predicted 1037 to 1095) would interact with NBD1 (Cotten et al. 1996; Wigley et al. 1998) (Figure 1-2). In this model, CFTR ICL4 makes contacts with the F508 position of NBD1, whereas ICL2 makes contacts with the equivalent P1306 position in NBD2. The Sav1866-based model predicts CFTR ICL4 will have the largest contribution to the ICL/NBD interaction surface area of NBD1. Consistent with this prediction, biochemical studies showed CF-causing mutations in ICL4 altered the gating of the channel in response to stimuli (Cotten et al. 1996).

Due to the lack of efficient expression systems to yield large amounts of CFTR, and the presence of large disordered regions in the R-domain; CFTR has proven to be a difficult target for structural analysis. In spite of this difficulty, significant progress has been made in understanding the molecular pathology. The availability of CFTR NBD1 structures in addition to structures of intact homologous transporter proteins, allows construction of structural models suggesting specific interactions between the ICLs and NBDs. Zolnerciks et al. have recently reported biochemical experiments providing for Sav1866-like TMD/ NBD interactions with another human ABC transporter, the multi-drug transporter P-glycoprotein (Zolnerciks et al. 2007). Thus, models built on structural and biochemical studies can generate testable hypotheses that lead to a deeper understanding of the mechanism of CF-causing mutations.

Biophysical Methods to Approach CFTR Structure

Inefficient folding of CFTR into a functional three-dimensional structure is the basic pathophysiologic mechanism leading to most cases of cystic fibrosis. Knowledge of the structure of CFTR and placement of these mutations into a structural context would provide key information for developing targeted therapeutic approaches for cystic fibrosis. As a large polytopic membrane protein containing disordered regions, intact CFTR has been refractory to efforts to solve a high-resolution structure using X-ray crystallography. The chapters in the text *Cystic Fibrosis Methods and Protocols* summarize current efforts to circumvent these obstacles by utilizing NMR, electron microscopy, and computational methodologies and by development of experimental models of the relevant domains of CFTR.

Mutations in the cystic fibrosis transmembrane conductance regulator (CFTR) lead to the development of cystic fibrosis (CF), one of the most common, fatal autosomal-recessive diseases (Cutting, 1993; Riordan et al., 1989). CFTR is a large membrane protein composed of at least five individual domains: two nucleotide-binding domains (NBDs), two transmembrane domains (TMDs), and a regulatory domain (RD). The NBDs and TMDs are common to the ABC transporter supergene family, of which CFTR is a member of the C subfamily (ABCC7). These domains (Mendoza and Thomas, 2007; Riordan, 2008) allow CFTR to mediate chloride conductance (Choi et al., 2007; Devor et al., 2000; Quinton and Reddy, 1992) and regulate the activity of several other critical transport

systems in the apical membrane of epithelial cells (Ko et al., 2004; Kunzelmann et al., 1997; Mall et al., 1999; Schreiber et al., 1999). Detailed structural information at a variety of resolutions is critical for understanding how the protein functions. The presence of disease-causing mutations in the CFTR gene leads to an absence of function. Such loss-of-function effects can arise from one or more of several distinct mechanisms including, direct effects on channel function (Linsdell et al., 1998; McCarty, 2000; Sheppard et al., 1993), effects on regulation (Fulmer et al., 1995), or effects that cause aberrant folding (Qu et al., 1997; Thomas et al., 1992) and trafficking (Gregory et al., 1991) or a combination of these. Whereas the primary sequence of a protein contains the information required for achieving a functional, native conformation, it is not surprising that defective CFTR folding is the most common of the mechanisms leading to dysfunction (Qu et al., 1997; Thomas et al., 1992). Again, structural information can provide critical insight into the molecular pathogenesis of these mutations and the means to counter the aberrant steps.

Information about the structure of the CFTR molecule can be generated at several different levels of detail. First, biochemical and immunochemical methods can reveal the presence of post-translational modifications that reflect the enzymes CFTR has come in contact with, and, thus, its history in a cell. The cell has its own intricate methods for distinguishing and sorting aberrant protein molecules from those that

continue on to a functional native structure, which are reflected in these changes (Hutt et al.; Wang et al., 2006; Younger et al., 2005). This information indicates, at an extremely reliable, albeit gross level; whether or not CFTR has folded into a native structure. These approaches are covered in great detail in a number of chapters within Part III of *Cystic Fibrosis Methods and Protocols*. At the next level of detail, studies of full-length CFTR can provide information about the state of individual domains by combining limited proteolysis and electrophoretic separation with identification of domains using antibodies with known CFTR epitopes. In this manner, the effects of specific mutations on domains can be assessed by comparisons to the wild-type protein (Awayn et al., 2005; Cui et al., 2007; Kleizen et al., 2005). Low-resolution approaches have greatly informed our understanding of the structure and function of CFTR and the molecular pathology of many of the disease-causing mutations. However, a desire to understand function and dysfunction at a structural level motivates the difficult goal of determining higher-resolution structures of CFTR and its domains that are summarized in Chapters 22-25 in the text *Cystic Fibrosis Methods and Protocols*.

The structure of full-length CFTR at a resolution that allows for determining the relative apposition of the domains can be elucidated experimentally using incisive biophysical approaches such as electron microscopy and electron crystallography as described in Chapter 18 of *Cystic Fibrosis Methods and Protocols* by Ford et al (Awayn et al., 2005;

Rosenberg et al., 2004; Zhang et al., 2009). These approaches require significant amounts of purified full-length CFTR and are sample preparation, data collection and computationally intensive. The structures produced to date provide information about the identity of domains in the structure and changes in their relationship that correlate with alterations in nucleotide content and phosphorylation state, two parameters known to regulate the activity of CFTR. These methods hold great promise for the future in that resolution in the single digit Ångstrom level can be achieved and the presence of disordered regions in CFTR do not interfere as much as they might in the case of X-ray crystallography.

While full-length CFTR has proven refractory to X-ray crystallography to date, structures of other members of the ABC transporter family have been solved to high-resolution utilizing this approach (Aller et al., 2009; Dawson and Locher, 2006; Locher et al., 2002). While these homologues lack some important features of CFTR, for example the R-domain and regulatory insertion (RI) and regulatory extension (RE) within NBD1, they share the four fundamental domains and, can thus, act as a starting point for producing structural models of CFTR. This approach, described in Chapter 19 of *Cystic Fibrosis Methods and Protocols* by Serohijos et al., can provide molecular models useful for formulating specific hypotheses for experimental testing (Huang et al., 2009; Mendoza and Thomas, 2007; Moran; Mornon et al., 2009; Serohijos et al., 2008). More sophisticated computational approaches that calculate

the folding trajectories of CFTR-NBD1 have been developed and utilized to identify differences between wild type and F508del and residues important in these differences (Serohijos et al., 2008). This work points the way to novel therapeutic interventions by small molecules to circumvent the differences in the mutant and wild type folding.

An ultimate goal remains, however, the solution of high-resolution structures of the intact CFTR and mutants thereof in a variety of states that define the functional and pathogenic mechanisms. In particular, structures in the low Ångstrom resolution range will be required to reveal the conformation of the side chains as would be required for defining the binding mode of CFTR ligands. Also, information about the structural dynamics is also likely to be key and will come from NMR, as discussed in Chapter 21 of *Cystic Fibrosis Methods and Protocols* by Kanelis *et al*, and related experiments. A dissect and build approach has been utilized in the absence of technology to produce and analyze the full-length CFTR at this resolution at the present time. The assumption underlying this operation is that the domains of CFTR can be isolated as independent units that retain structure and at least partial function. This dissection has proven valid for the case of the NBDs and the R-domain. The second half of the operation is to build by recombining the high-resolution information garnered from the component domains, perhaps as directed by electron microscopy results.

To date, high-resolution structures have been produced for the NBD1 domains from murine and human CFTR (Atwell et al.; Lewis et al., 2004; Lewis et al.; Thibodeau et al., 2005) and human NBD2 (in fusion with a portion of the related bacterial NBD, MalK) (PDB 3GD7). These structures have provided important insight into the fold of the CFTR NBDs, the details of how they interact with nucleotide ligands, and the position of the critical F508 residue and other positions mutated in CF (Lewis et al., 2004). The B-factors for these structures point to increased dynamics of particular regions when specific mutations or phosphorylations are introduced (Lewis et al.). Methods for producing and characterizing these domains are presented in Chapter 19, 20 and 21. Chapter 20 of *Cystic Fibrosis Methods and Protocols* focuses on the history of development of systems for producing CFTR-NBD1 as an illustrative example.

Dynamical changes in the conformation of CFTR are important at a variety of levels. Changes in conformation and in the relative orientation of the domains define the mechano-chemical reaction cycle of gating. Order-disorder transitions and conformational rearrangements underlie control of these domain rearrangements and, thus, the mechanisms by which nucleotide binding and hydrolysis and CFTR phosphorylation regulate the activity of the channel (Baker et al., 2007; Kanelis et al.). Folding is by definition the dynamic changes in conformation that occur as the native state is assembled. Where static structural information is difficult, dynamic structural information requires temporal information about the structure

over many different time scales. Chapter 21 of *Cystic Fibrosis Methods and Protocols*, by Kanelis *et al*, summarizes the use of NMR spectroscopy to address many of the critical questions about the regulation of CFTR and the effects of mutations on the dynamics of the domains.

Structural information relevant to the function and dysfunction of CFTR forms the basis of a rational approach to therapeutic discovery and development. However, CFTR is an integral membrane protein that is produced in cells in low abundance creating significant obstacles to structural studies. Moreover, it contains significant regions of disorder even when it is in its native state--disorder that is central to its function, but that impedes many structural experiments--obviating a need for information about the dynamics of these structures. Finally, in several cases, including the prevalent F508del mutation, the mutant protein does not fold efficiently into the final structure. Since many of these disease-causing folding mutants retain at least partial function when they are induced to fold *in vitro* or in cell culture systems (Brown *et al.*, 1996; Denning *et al.*, 1992), a critical challenge is to produce structural information relevant to these partially folded or misfolded states. Computational methods have a key advantage for directing work in this difficult area. Several chapters in *Cystic Fibrosis Methods and Protocols* provide a primer on current experimental and computational methods for structural work on full-length CFTR, its domains and the dynamical states central to folding and function. Understanding the structural details of

function and the folding process may provide not only fundamental knowledge, but also have practical application in the development of future treatments for the disease.

**This chapter is adapted and updated from Mendoza and Thomas 2007 and Mendoza, Schmidt, and Thomas 2011.*

Chapter 2: Analyses of Evolved Sequences and Structure Reveal the Requirements for Efficient Corrected Folding of $\Delta F508$ CFTR

Introduction

Cystic fibrosis (CF) is a lethal, monogenic disease caused by dysfunction of the Cystic Fibrosis Transmembrane Conductance Regulator (CFTR). CFTR is a member of the ATP-Binding Cassette (ABC) transporter sub-family class C that functions as a chloride channel. This polytopic integral membrane protein is composed of five domains: two transmembrane domains (TMDs) which form the channel through the membrane, two nucleotide binding domains (NBDs) which gate the channel through ATP binding and hydrolysis reactions, and a regulatory region (R) which mediates kinase dependent regulation of channel activity (Figures 2-1A and 2-1B) (Berger et al., 2005; McCarty, 2000; Mendoza and Thomas, 2007; Riordan et al., 1989; Vergani et al., 2005). The majority of CF cases are associated with the deletion of a single amino acid, phenylalanine 508, located in the first NBD (NBD1) of CFTR (Figures 2-1A, 1B, and 1C) (Riordan et al., 1989). Upon deletion of this amino acid, CFTR fails to fold properly and does not efficiently traffic to the plasma membrane (Cheng et al., 1990) resulting in a loss-of function (Rich et al., 1990) (Figure 2-2). However, the mutant CFTR is active when induced to fold and traffic to the membrane (Denning et al., 1992; Teem et al., 1993) indicating that compounds that correct the folding defect may have therapeutic benefit.

Studies of the NBD1 of CFTR, and portions thereof, containing the F508 position indicate that the deletion reduces the folding efficiency (Qu and Thomas, 1996; Thibodeau et al., 2005b) and stability (Hoelen et al., 2010; Protasevich et al., 2010; Thibodeau et al., 2010b; Thomas et al., 1992; Wang et al., 2010) of the model polypeptides (Figure 2-3A-B). Consistent with the observed defects in yield, computational folding dynamics studies predict an altered folding pathway of NBD1 upon deletion of F508 (Serohijos et al., 2008). Crystal structures of the isolated CFTR-NBD1 domains reveal that F508 is partially exposed on the surface (Lewis et al., 2004) and that deletion of the residue causes only local rearrangements in the loop following the 508 residue in the context of stabilizing mutations that facilitated crystallization (Atwell et al., 2010; Lewis et al., 2005a) (Figure 2-3C).

Several lines of evidence suggest that Δ F508 CFTR can be targeted to improve folding and restore function. Sequencing identified a patient with a less severe form of CF with the genotype Δ F508-R553Q on one allele and a nonsense mutation on the other allele (Dork et al., 1991). A genetic screen in yeast utilizing a CFTR - Ste6 chimera that supports mating, identified the same R553Q mutation as a suppressor of the loss-of-mating Δ F508 phenotype (Teem et al., 1993). Additional second-site revertant mutations I539T, G550E, R553M, and R555K, within the portion of CFTR NBD1 near F508 that was included in the chimera, were also

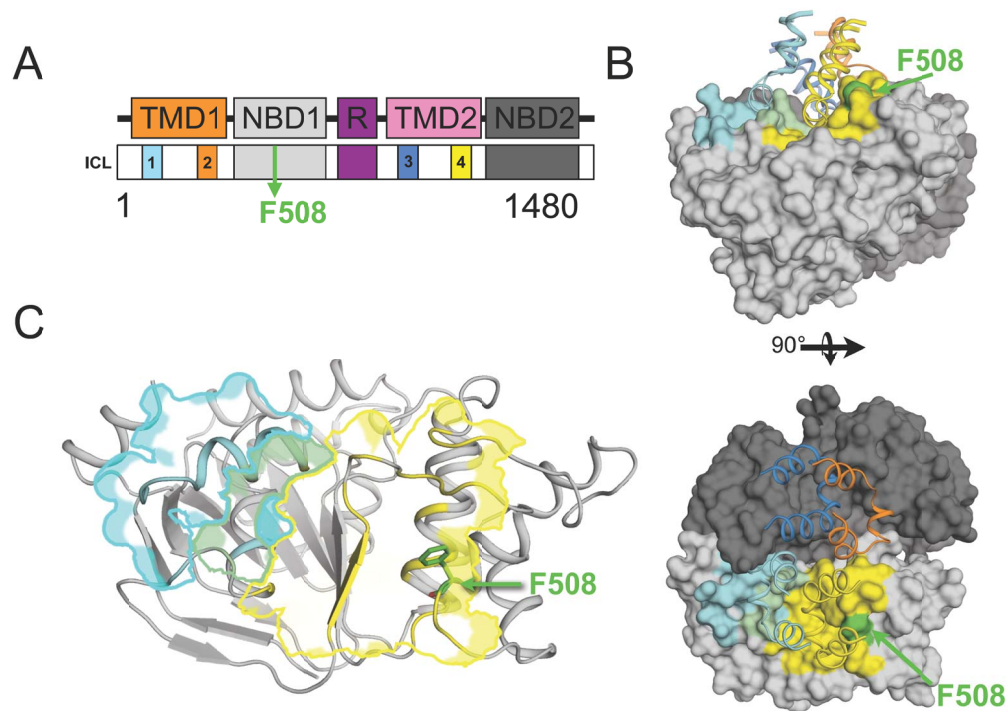


Figure 2-1. Predicted Relationship of CFTR Domains to the F508 Position. (A) CFTR is 1480 amino acids in length and contains two transmembrane domains (TMDs, orange and pink) and four intracellular loops (labeled ICL1-4, cyan, orange, blue, and yellow), two nucleotide binding domains (NBDs, grey and charcoal) and a predicted highly disordered region Regulatory region (R, purple). F508, green is located within the NBD1 domain. (B) The Sav1866 based homology model of CFTR *sans* R-region (PDBs 2HYD, 1R0W, and 3GD7). (*top*) View of the NBDs and ICLs of CFTR parallel to the membrane. The two NBDs associate in a head-to-tail fashion. ICL1 (cyan ribbon) and ICL4 (yellow ribbon) interact with NBD1 and ICL2 (orange ribbon) and ICL3 (blue ribbon) interact with NBD2. F508 (green surface) is at the predicted interface with ICL4. NBD1 surface residues predicted to be within 6 Å of ICL1, ICL4 or both are highlighted in cyan, yellow or light green respectively. (*bottom*) View of the CFTR model looking down from the membrane as previously described in the top panel and rotated by 90° along the x-axis. (C) Ribbon representation of NBD1 (PDB 1R0W) showing relationship of F508 (green sticks) to the predicted interface with ICL4 yellow outline.

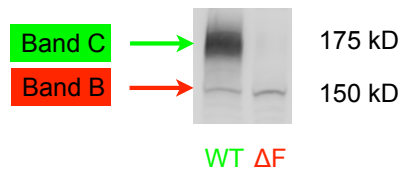


Figure 2-2. $\Delta F508$ CFTR is a Misfolding Mutation and is Unable to Traffic to the Plasma Membrane. CFTR folds co-translationally in the ER and is inserted into the ER membrane where it is core glycosylated approximately 150 kDalton band as visualized on a western blot of SDS PAGE (Band B). If the protein is properly folded, it traffics to the Golgi where it is further post-translationally modified and is complexly glycosylated and finally is trafficked to the plasma membrane where it is required for function. The complexly glycosylated form is visualized on WB as an approximate weight of 175 kDaltons denoted as Band C.

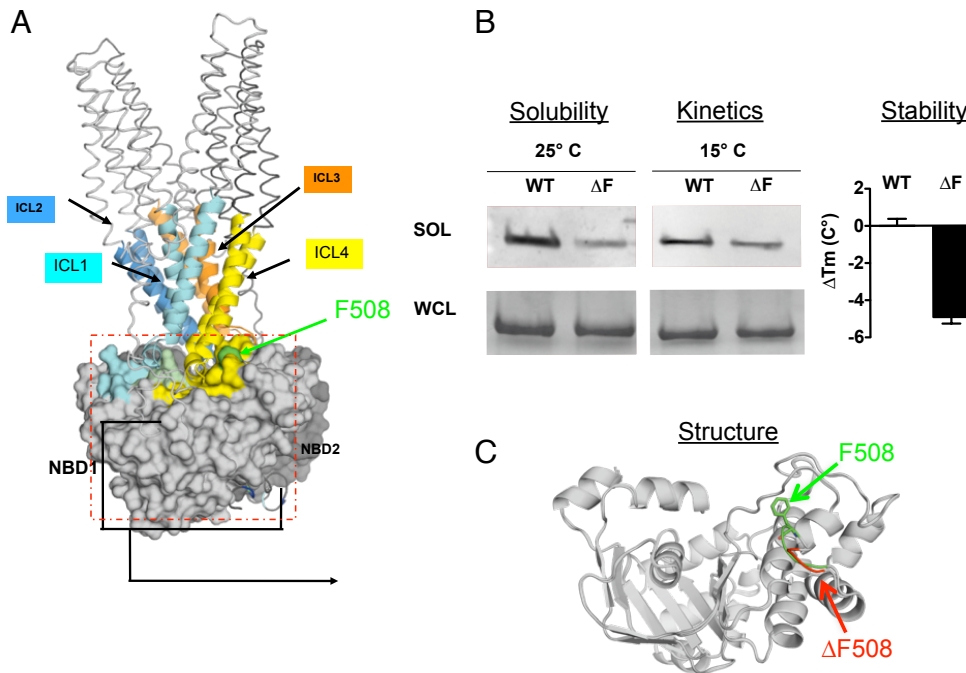


Figure 2-3. Characterization of $\Delta F508$ NBD1 Reveals that the Mutation Affects Folding of NBD1. (leftmost panel) The predicted structure of human CFTR as described in Figure 2-1B,C. The F508 position is at the predicted interface of NBD1 and ICL4. (Solubility of NBD1) Western blot of SDS PAGE of bacterially expressed wild-type and $\Delta F508$ NBD1 reveals the mutation decreases the solubility of NBD1. The difference in solubility is not due to protein production as suggested by western blot of the whole cell lysate (Thibodeau et al., 2010). (Kinetics) Expression of NBD1 at a lower temperature suggests that folding kinetics of the domain is also altered by the deletion mutation as the difference in solubility between wild-type is diminished (Thibodeau et al., 2010). Again, as the WB of the WCL suggests, this is not due to protein production. (Stability) Thermal denaturation studies of purified NBD1 demonstrate that $\Delta F508$ decreases the T_m of NBD1 by nearly 6°C (Hoelen et al., 2010).

identified using this approach (DeCarvalho et al., 2002; Teem et al., 1993; Teem et al., 1996a) (Figure 2-4). The R553M, I539T and the combination of G550E-R553M-R555K (3M) mutations have been shown to correct the folding and stability defects of the Δ F508 NBD1 domain in isolation (DeCarvalho et al., 2002; Hoelen et al., 2010; Pissarra et al., 2008; Qu et al., 1997; Thibodeau et al., 2010a), but only partially restore maturation of the full-length mutant protein (Hoelen et al., 2010; Pissarra et al., 2008; Thibodeau et al., 2010a) (Figure 2-5). These data indicate that correction of the NBD1 folding defect alone only incompletely restores maturation of Δ F508 CFTR.

Based on the hypothesis that compounds that effectively improve the folding of Δ F508 CFTR would be of therapeutic benefit, several cell-based high-throughput screens have been performed (Pedemonte et al., 2005; Robert et al., 2010; Robert et al., 2008; Van Goor et al., 2006). While some of the compounds identified bind to and stabilize NBD1 (Sampson et al., 2011); the mechanism of action of most remains unknown. None of the reported Δ F508 correctors have potency much less than 1 μ M and, like the single intragenic second site-suppressor mutants, efficacy above about 15% of wild-type levels. There is reasonable concern that this degree of correction will not have significant therapeutic benefit based on the promising results with the more potent and efficacious potentiator of the rarer CF-causing G551D

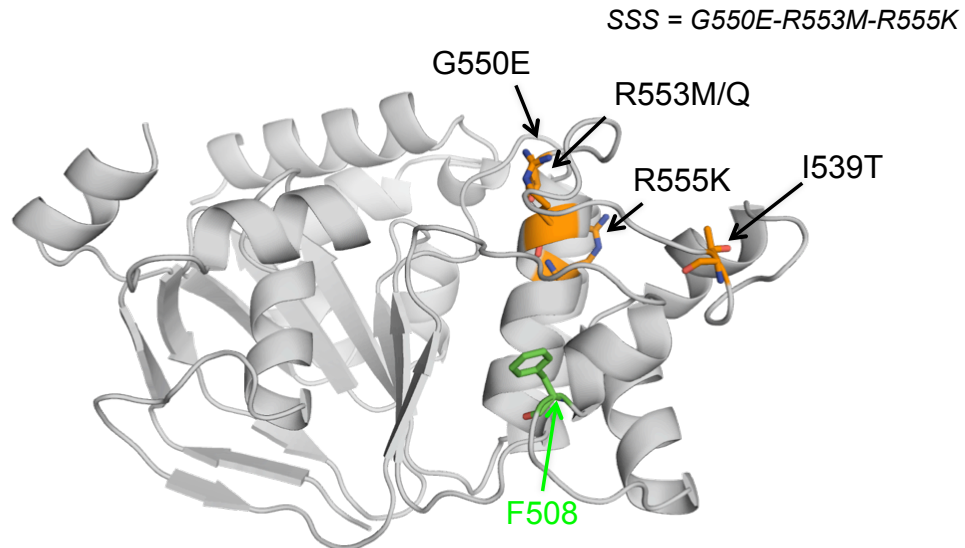


Figure 2-4. Second-Site Suppressor Mutations Identified by the Genetic Screen are Distal to the F508 Position. The structure of human NBD1 (PDB 2BBO) with the three suppressor mutations reveal that the mutations are not in contact with the F508 position. Structural analysis predicts changes in hydrogen bonds between I539T, R555K, and R5553(M/Q) and backbone carbonyls of neighboring residues. The G550E position is predicted to be near the γ -phosphate of ATP at this pocket. G550E is known to alter the gating characteristics of CFTR (Roxo-Rosa et al., 2006).

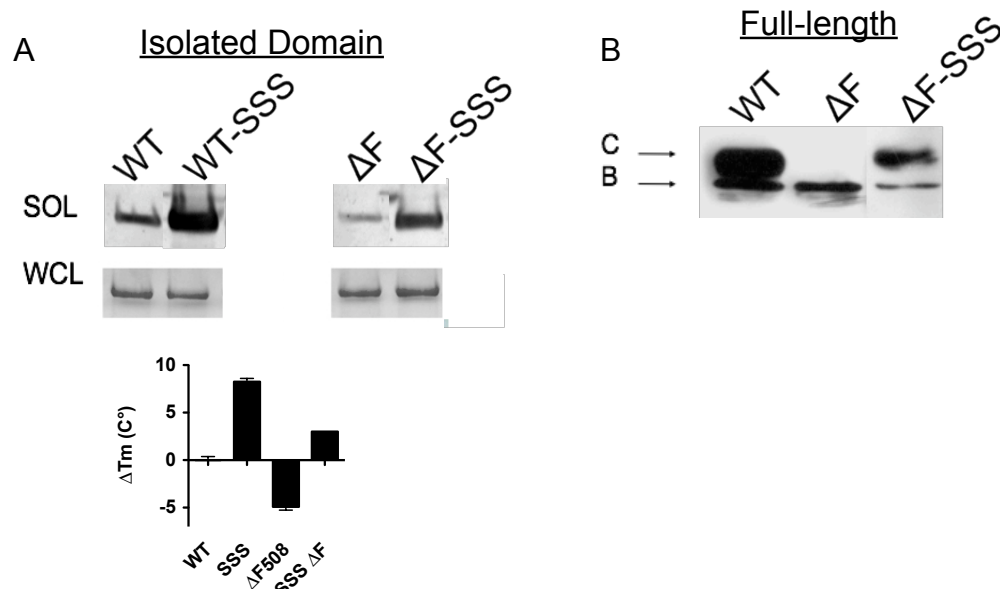


Figure 2-5. Second-Site Suppressor Mutations Correction of $\Delta F508$ Mediated Misfolding. (A) (top panel) Western blot of SDS PAGE of SSS on WT and $\Delta F508$ NBD1 of soluble fraction and whole-cell lysate of protein expressed in a bacterial expression system. Triple suppressor mutations (G550E-R553M-R555K) improve the solubility of NBD1 in both the wild-type and $\Delta F508$ NBD1 backgrounds (Thibodeau et al., 2010). The increase in soluble protein levels of NBD1 with the SSS mutations are not due to protein production (Thibodeau et al., 2010) (bottom panel). The triple suppressor mutation increases the thermal stability of NBD1 by approximately 8°C in both wild-type and $\Delta F508$ backgrounds such that $\Delta F508$ NBD1 is more stable than wild-type as reflected in the soluble fraction of the proteins (Hoelen et al., 2010). (B) Western blot of SDS page of wild-type, $\Delta F508$, SSS- $\Delta F508$ CFTR (Thibodeau et al., 2010). The triple suppressor mutations partially restore trafficking to the plasma membrane despite more than compensating for the folding defects of $\Delta F508$ NBD1 as shown in panel A) (Thibodeau et al., 2010).

gating mutant (Accurso et al., 2010; Van Goor et al., 2009). This potentiator compound, VX-770, clearly demonstrates that pharmacological improvement of mutant CFTR function in adult patients provides a measurable clinical benefit (Accurso et al., 2010), further stimulating the search for effective correctors of $\Delta F508$ folding and function. Understanding the molecular basis of the apparent correction ceiling and the mechanism of action of corrector compounds would provide critical insight for development of more effective corrector compounds.

The identification of positions coupled to F508, provided by the Ste6-CFTR chimera revertant mating screen, has provided critical insights into CFTR folding and the effect of $\Delta F508$, but was necessarily limited to residues immediately proximal to the F508 position in NBD1 by the methodology (Teem et al., 1993; Teem et al., 1996b). Extending such a second-site analysis to the whole of CFTR might be reasonably expected to provide critical new information about the folding and maturation of CFTR and the effect of the $\Delta F508$ mutation thereon—information critical for revealing the mechanism of action of extant correctors, for developing methods capable of identifying better compounds, and for a fundamental understanding of the process of integral membrane protein folding. In the absence of a conveniently assessed phenotype for CFTR function as required to evaluate millions of individual genetic perturbations, the information nature has provided in the sequences of the ABC supergene family offer an alternative. Multiple algorithms have been developed that

can identify residues coupled to specific positions, for example F508, in the evolved sequences of protein homologues (Fodor and Aldrich, 2004; Goh et al., 2000; Kass and Horovitz, 2002; Lockless and Ranganathan, 1999; Pazos and Valencia, 2008; Socolich et al., 2005). The set of residues statistically coupled to the F508 position would be expected to be enriched for positions that interact directly or allosterically in the final structures or transiently during the process of folding. Such interactions should be evident in the stability and folding yield of NBD1 and the maturation of CFTR, which reflects the association of folded NBD1 with ICL4. In the present work we identified positions coupled to F508 in CFTR and determined their effect on both NBD1 folding and CFTR maturation. The results reveal the quantitative effect of the Δ F508 mutation on two distinct steps of folding and, further, suggest mechanistically defined methodologies for identifying compounds targeting either or both steps defective in the mutant protein.

Results

Identification of positions coupled to 508 in the ABC transporter supergene family.

CFTR is a member of the C subgroup of the large ABC transporter supergene family (Dean and Annilo, 2005). Over 2,000 full-length sequences of eukaryotic ABC Transporters (containing two NBDs and two TMDs on a single polypeptide) were obtained from two iterations of a PSI-

Blast default search using the human CFTR protein sequence as the seed (gi 90421313). Four multiple sequence alignments (MSA) were generated using ClustalW (Larkin et al., 2007). After quality assessment of the MSA using the three highly conserved Walker A and B, and Consensus motifs (Dean and Allikmets, 1995; Dean and Annilo, 2005; Jones and George, 2004; Walker et al., 1982), the total number of sequences to be queried was reduced by half. After removing additional sequences that had greater than 90% identity to any other sequence within the alignment, the final alignment contains 493 full-length sequences (MSA available for download at <http://cftrfolding.org>, Figure 2-6). The two NBD domains have the highest number of conserved positions, with the three ATP Binding cassette motifs having the highest conservation scores in the MSA. Four positions in CFTR are invariant in the alignment, K464 and G1244 in the Walker A motifs of NBD1 and NBD2, respectively, Q1292, the Q-loop residue in NBD2, and D1370 of the NBD2 Walker B motif. The TMDs have positions of high conservation clustered at or near the ICLs. The conservation scores in the R-domain approach randomness (conservation score of -1). Phenylalanine is the most common amino acid at the 508 position followed by tyrosine at frequencies of 0.86 and 0.11, respectively. Matrices of the pairwise correlation scores were calculated using the MSA by four independent, statistical methods; Statistical Coupling Analysis (SCA), Explicit Likelihood of Co-variation (ELSC), OMES, and McBASC (Figures 2-7A, 2-8A, and S1) (Matlab file available for download at <http://>

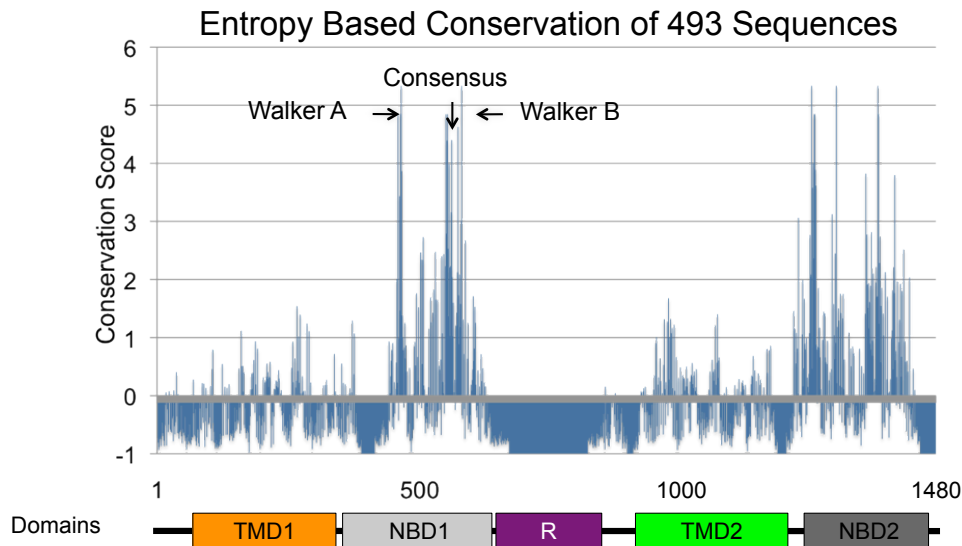


Figure 2-6. Positional Conservation Scores in Human Numbering in the MSA of 493 ABC Transporters. Entropy based conservation scores were calculated for the Multiple Sequence Alignment of 493 full-length ABC transporter and plotted with human CFTR numbering. Approximate boundaries of each of the five domains of CFTR are shown below the plot. The two NBDs have the highest level of conservation. Amongst the most conserved positions are those important for ATP binding and hydrolysis and identified as the Walker A/B and Consensus motif for NBD1 for reference. In contrast, the R-domain approaches randomness (a entropy conservation score of -1). The two TMDs while largely not conserved, have several positions with a high degree of conservation. These positions correspond to or are near to, the ECLs and ICLs.

cftrfolding.org) (Dekker et al., 2004; Fodor and Aldrich, 2004; Lockless and Ranganathan, 1999). The top 20 statistical 508-coupled positions for the four methods formed a set of 45 positions (Table 2-1). A sample set of 16 of these 45 508-coupled positions, including those most common and unique to all methods (Table 2-1 and Figure **S3**), were selected for experimental assessment of impact on CFTR folding. The 16 positions represent ~78% coverage of the top ten 508-coupled positions for all four methods, and include 6 positions common among all 4 methods, 2 positions in common among 3 methods, 6 positions common among 2 methods, and 2 positions unique to a single method (Table 2-1 and Figure 2-9). The 6 coupled positions common among all 4 methods are located in the α -helical subdomain (Table 2-1 and Figure S3). Ten of the 16 positions are surface exposed, F490L and W496, like F508, are predicted to be at the ICL4 interface (Table 2-1 and Figures 2-9 and S3). Additional positions reside within the coupling helix boundaries of ICL1 and ICL4 (Figure 2-7B). The amino acid at each of the 16 positions in CFTR was changed to the most common non-CFTR amino acid (Table 2-1) and the effect on both NBD1 folding and CFTR maturation was assessed.

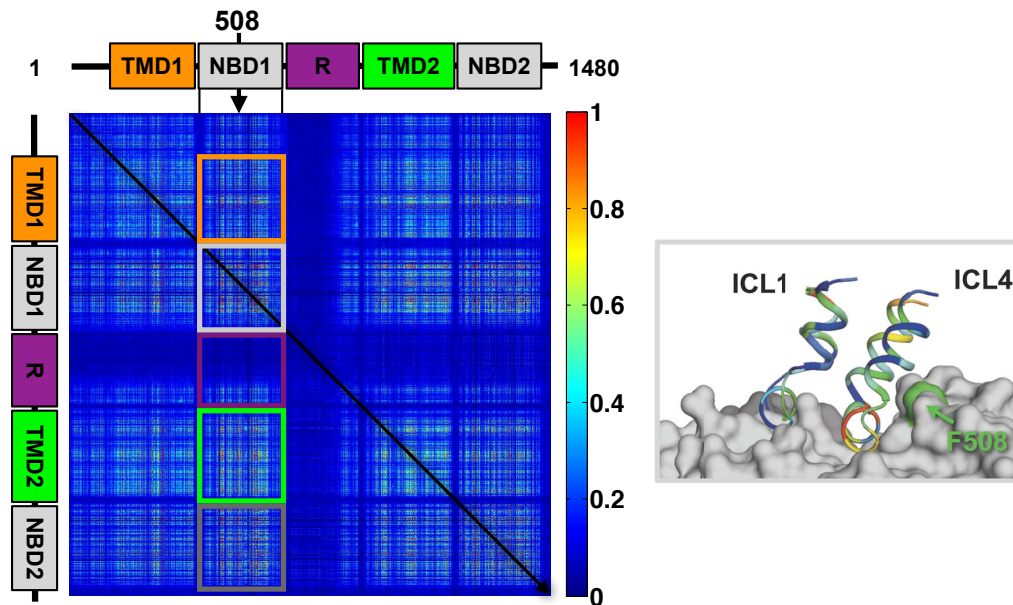


Figure 2-7. CFTR Inter-Residue Coupling Matrix Calculated from an ABC Transporter Sequence Alignment. (*left*) Heat map of the 1480 x 1480 matrix representing a linear combination of four statistical methods (SCA, ELSC, OMES, McBASC). The color scale is located on the right side of the panel with statistical scores approaching zero represented by dark blue and scores of high statistical significance in red. The diagonal denotes identity. Coupling of each of the five domains of CFTR to NBD1 are shown in squares with TMD1 in orange, NBD1 coupling to itself in light gray, the R-region in purple, TMD2 in pink, and NBD2 in dark gray. (*right*) The 508-coupling scores in ICL1 (residues 158-184) and ICL4 (residues 1050-1080) of the CFTR model (Figure 2-1B). The surface corresponding to the F508 position is colored in green and is predicted to be in contact with ICL4.

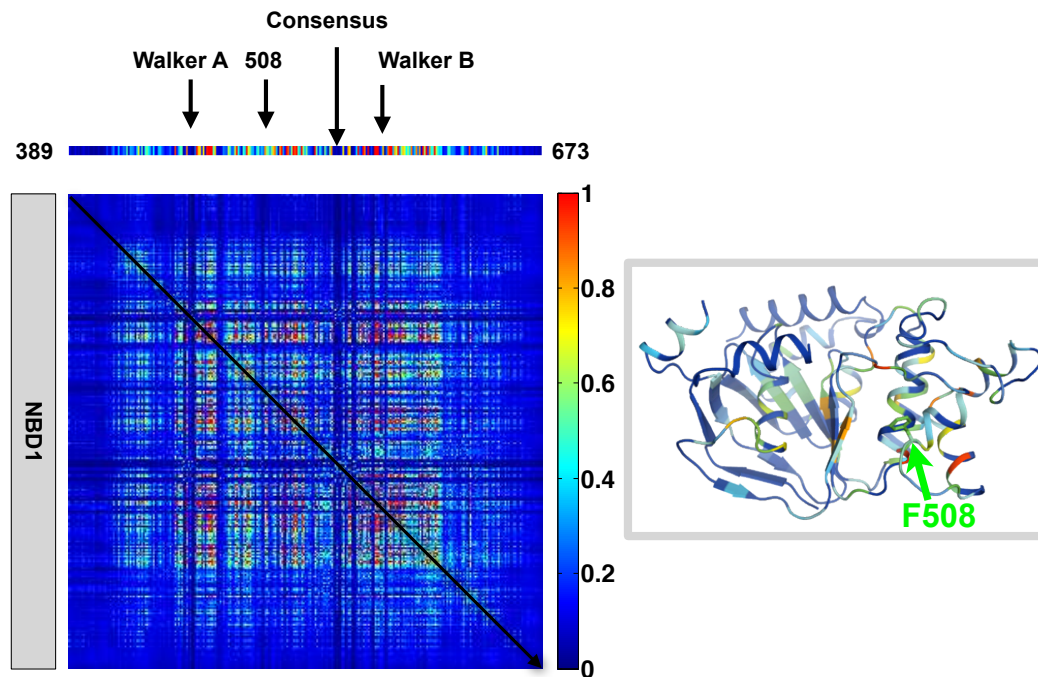


Figure 2-8. NBD1 Inter-Residue Coupling Matrix Calculated from an ABC Transporter Sequence Alignment. (*left*) Heat map of the 285 x 285 matrix representing a linear combination of four statistical methods (SCA, ELSC, OMES, McBASC). The color scale is located on the right side of the panel with statistical scores approaching zero represented by dark blue and scores of high statistical significance in red. The diagonal denotes identity. NBD1 coupling to itself in light gray, the R-region in purple, TMD2 in pink, and NBD2 in dark gray. (*right*) A view of NBD1 (pdb 1R0W) colored with normalized scores from heat map, *left* and *top left*. The F508 position is shown in green.

ELSC	mcBASC	Omes	SCA
			435
		453	
		460	
		S466T	S466T
	468		
		470	
	472		
		473	473
		474	474
L475Y		<u>L475Y</u>	<u>L475Y</u>
	F490L		F490L
<u>W496V</u>	W496V	<u>W496V</u>	W496V
	503		
	505		
	507		
	509		
512			
513			
Y517I	Y517I	Y517I	Y517I
		520	520
	521		
<u>C524A</u>	<u>C524A</u>	C524A	C524A
<u>L526A</u>	L526A	L526A	L526A
D529F	D529F	D529F	D529F
D537F			D537F
	543		
Y563V	Y563V	<u>Y563V</u>	Y563V
A566P		<u>A566P</u>	
		569	569
			S573E
P574A		P574A	<u>P574A</u>
F575T		F575T	
			578
582			
E583G		<u>E583G</u>	
587			
	591		
	595		
	598		
	602		
604		604	604
H609T			
	617		
630			630
640			

Table 2-1. Identification of NBD1 Positions Coupled to F508 Using Four Independent Statistical Methods. The alignment of 493 sequences was used to calculate pairwise coupling scores using each method (ELSC, SCA, McBASC, and OMES). The top ten highest scoring positions are shown in bold for each method. The representative set of sixteen 508-coupled positions and the missense mutations selected for experimental analysis are underlined.

A

Statistics

# of Methods	# of Positions
4	6
3	2
2	6
1	2

Structural

Location	# of Positions
Interface (ICLs)	2
Surface	10
Core	4

B

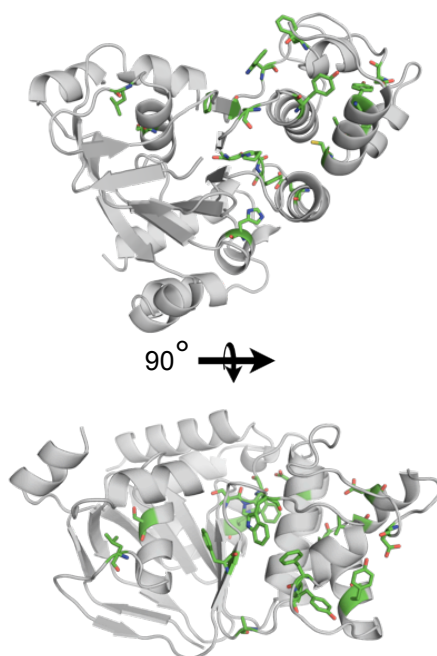


Figure 2-9. Statistics and Structural Context of the 16 Representative Coupled Positions in NBD1 Structure. (A) (top) Table summarizing coverage of the representative 16 coupled positions. The 16 coupled positions sample positions in common among each of the four methods as well as including positions unique to a single method. (bottom) The 16 positions are distributed throughout the NBD1 structure as summarized in the table. (B) Structural context of the 16 coupled positions in NBD1 (PDB 2R0W) and as summarized in Table 2-1 (green sticks).

Effects of 508-Coupled Positions on NBD1 Folding

Each of the 16 508-coupled positions, as well as the previously identified second-site suppressor mutations and combinations thereof, were evaluated for effects on the folding of the isolated human CFTR NBD1 using a structural complementation assay for folding as previously described (Thibodeau et al., 2010a; Wigley et al., 2001) (Figure 2-10). In the current implementation of the assay, the folding signal of $\Delta F508$ NBD1 was 0.43 ± 0.03 relative to wild-type NBD1, 1.00 ± 0.03 . All 16 508-coupled and second-site suppressor mutations had a significant effect on the folding of the isolated domain relative to wild-type (Figure 2-11) suggesting that the statistical analyses identified a set enriched for biological relevance. Fourteen of the 508-coupled mutations interfered with NBD1 folding (Figure 2-11, green bars). The significance of the decrease in folding was less than $6E-6$ for 13 of the mutants and 0.002 for the least significant, E583G. Two 508-coupled mutants, D529F and S573E, dramatically increased the relative folding yield of NBD1 by 3.07 ± 0.13 and 1.85 ± 0.06 fold, respectively, a level comparable to that of the second-site suppressors identified in the STE6 chimera screen (Figure 2-11).

Thermal denaturation of purified D529F and S573E NBD1 revealed that S573E raised the T_m by 2 to 5 °C relative to wild-type depending on ATP concentration (Figures 2-12 and S4), indicating that the improved folding yield reported by the structural complementation assay could be

accounted for by increased stability of the native state (Figure 2-12). In stark contrast, D529F had no measureable effect on T_m indicating the structural complementation folding assay reflects changes in yield and pathway as well as changes in stability or solubility. D529 is located in the α -helical sub-domain of NBD1 near the NBD1/NBD2 interface (Figure 2-13). Analysis of the human NBD1 crystal structures (PDB 2BBO and 1XMI) reveals that this aspartic acid side chain forms a salt bridge with R555. The R555 side chain also makes a hydrogen bond with the backbone carbonyl of Q525 (Figure 2-13). The R555K missense mutation has been one of the well-characterized intragenic second-site suppressors of $\Delta F508$ NBD1 mediated misfolding (Roxo-Rosa et al., 2006; Teem et al., 1996a). The R555K mutation increases the folding yield of NBD1, 3.26 ± 0.07 fold over wild-type (Figure 2-12). The T_m of R555K NBD1 was 6.4°C higher than wild-type in 2 mM ATP. A glutamate or aspartic acid at the CFTR equivalent 573 position is the catalytic base in the highly conserved Walker B motif in the ABC Transporter family (Jones and George, 2004; Mendoza and Thomas, 2007; Walker et al., 1982). The serine present in CFTR at this position accounts for the lack of ATP hydrolysis at this site as central to the mechanochemistry of the gating cycle (Figure 2-13) (Vergani et al., 2003).

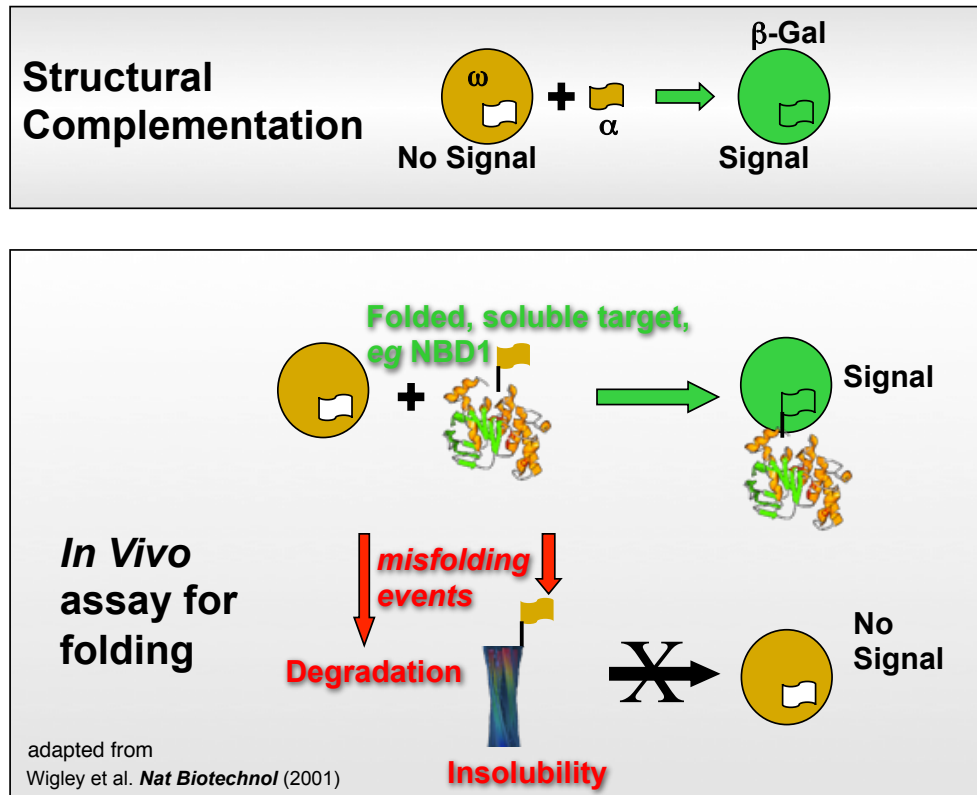


Figure 2-10. Representation of the β -galactosidase Complementation Assay. The β -galactosidase enzyme is fragmented into two pieces, α and ω . The α fragment is tagged on the C-terminus of NBD1. When the NBD1 fusion protein is co-expressed with a plasmid containing the ω fragment in mammalian cells, the two fragments can complement to make an active enzyme. Previous work has shown, when a mutation, such as $\Delta F508$, causes NBD1 to misfold, the fusion protein is either targeted for degradation or forms insoluble aggregates, both of which to lead to a decrease in measured enzymatic activity monitored by fluorescence signal.

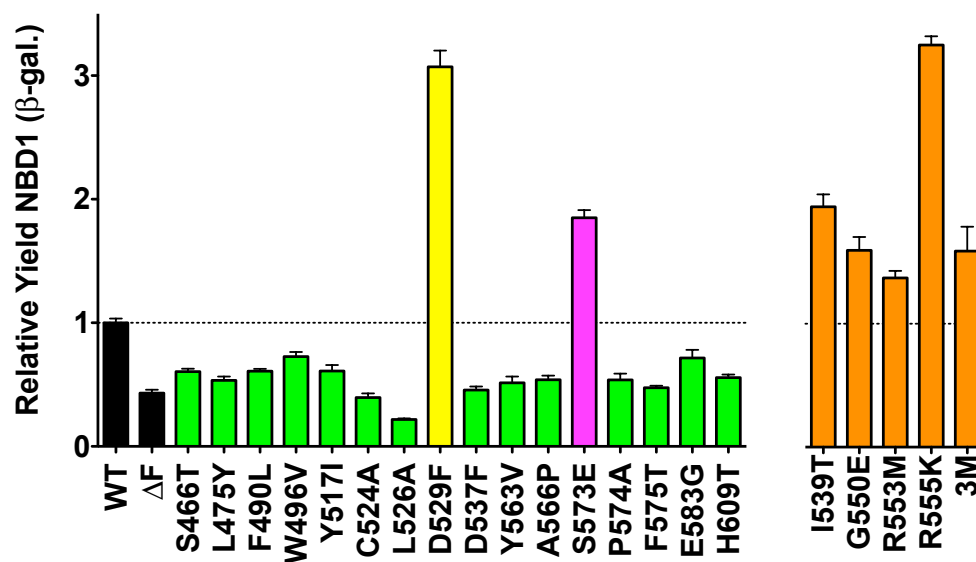


Figure 2-11. Effects of 508-Coupled Mutations and Second-Site Suppressors on NBD1 Folding. (A) The relative yield of NBD1 folding was determined using an in vitro folding assay. All mutations altered the relative yield relative to wild-type NBD1 as shown in the bar chart (\pm -SEM, $n=9$ except for WT, $\Delta F508$, D529F, and S573E where $n=18$). Two of the 508-coupled positions, D529F and S573E, increase the yield of NBD1. The remaining mutations decrease the yield of soluble NBD1.

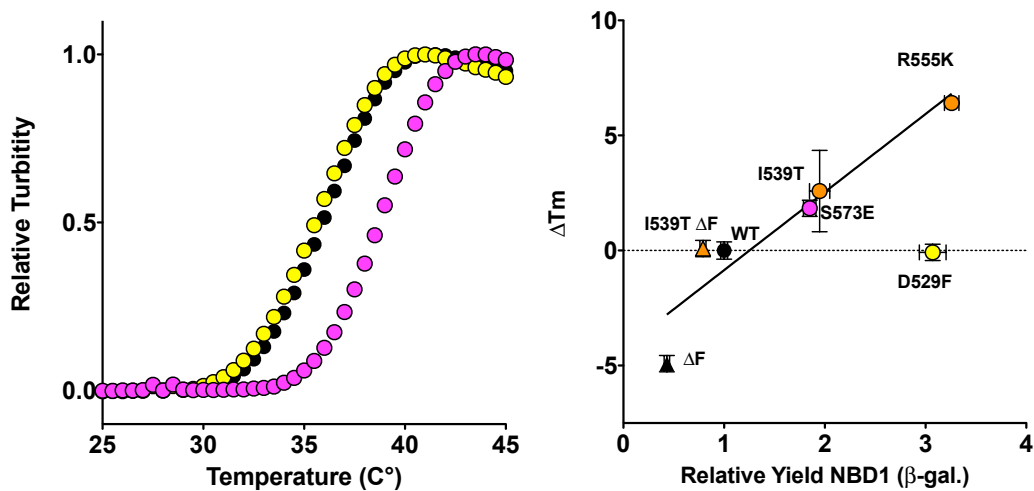


Figure 2-12. S573E Increases the Stability of NBD1, D529F Does Not. (A) (top panel) Thermal denaturation of 5 μ M purified recombinant WT, D529F, and S573E NBD1 in the presence of 2 mM ATP. By contrast to the increased NBD1 folding yield, the D529F mutation (yellow circles) has no observable effect on thermal stability relative to WT (black circles). S573E (magenta circles) increased the melting temperature 2° C relative to WT. (lower panel) Correlation between thermal stability of bacterially expressed and purified NBD1 and NBD1 folding yield as measured by the mammalian in vitro folding assay. For mutants on either WT (circles) or ΔF (triangles) backgrounds, the correlation between stability and folding yield, R, is 0.94 when D529F is excluded (yellow circle). While D529F increases the folding yield of NBD1 on the WT background, it has no effect on the thermal stability as shown in the upper graph.

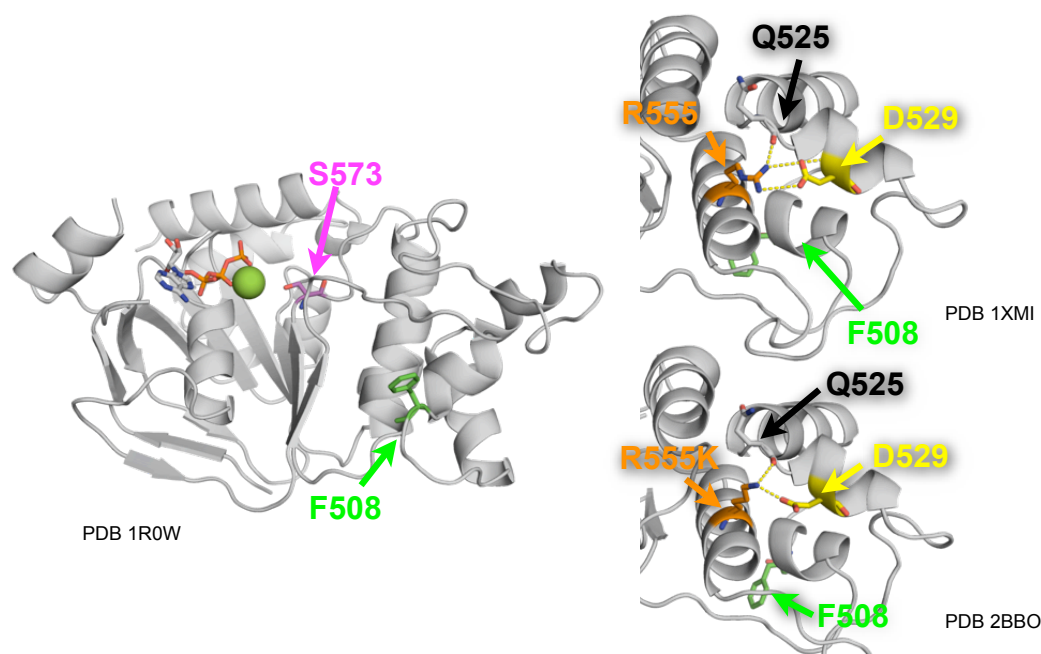


Figure 2-13. Structural Context of D529F and S573E Suppressor Mutations.

The mutations D529F and S573E increase the folding efficiency of NBD1 by different mechanisms (Figure 3). (A) View of the helical subdomain of human NBD1 (PDB 1XMI), F494-A566, from the perspective of the NBD1/NBD2 domain interface. Left panel, D529 is shown in yellow, F508 in green, R555, one of the previously identified second-site suppressor mutations is shown in orange sticks, and Q525 is shown in grey sticks. R555 makes a salt bridge with D529 as well as a hydrogen bond with the carbonyl backbone of Q525. Right, structure of human NBD1 with second-site suppressors (PDB 2BBO). Identical view as left panel but contains the R555K suppressor mutation. (B) Left, the S573 position, shown in magenta, is typically an Asp or Glu residue, serving as the catalytic base, in the vast majority of the Walker B motifs in the ABC transporter superfamily. This is a canonical view of the α/β core of human NBD1 (PDB 1XMI) from the perspective of the membrane. The adenosine head group of ATP is shown in grey and the three phosphates of ATP are shown in orange. Mg^{2+} is represented as a green sphere while F508 is shown in a green stick representation. Right panel, T_m of human WT and S573E as a function of ATP concentration. For every ATP concentration assessed (40 μM – 100 mM), the T_m is higher for S573E.

Effects of 508-Coupled Positions on CFTR Maturation

To examine the relationship of NBD1 folding and stability to full-length CFTR folding, the mutant CFTRs were expressed in HeLa cells and CFTR maturation was determined by two methods. As CFTR folds, it traffics from the ER to the Golgi where it attains complex glycosylation prior to reaching the plasma membrane. The resulting increase in molecular mass can be detected by western blotting of SDS-PAGE (Figure 2-14). The slower migrating complex glycosylated Band C reflects the folded, mature CFTR while the more rapidly migrating Band B reflects core glycosylated CFTR that has not reached the Golgi (Cheng et al., 1990). These data have been utilized in several ways to monitor the effect of mutations and compounds on CFTR folding. The ratio of Band C to Band B is linear with both CFTR at the surface as monitored by biotinylation and with Band C itself (Figure S5C). By contrast the ratio of Band C over total CFTR has a nonlinear relationship, with mature surface CFTR being more sensitive to changes at low folding yields (Figure S5B). In these analyses it was noted that none of the mutants tested had a significant effect on the amount of Band B and thus, the total CFTR was linear with the amount at the surface (Figure S5C). An ELISA assay for total CFTR quantitation was developed and used to monitor CFTR maturation. The signal from this method is linear with the relevant process, the procedure is less cumbersome and the methods produces lower noise data than prior methods (Figure S5C). The influence of all the 508-coupled mutants on CFTR folding was

assessed by ELISA western blot analysis (Figure 2-14). All sixteen of the 508-coupled mutations and second-site suppressor mutations altered the yield of full-length CFTR relative to wild-type. The same 14 mutations that reduced the yield of NBD1 folding, reduced the maturation of full-length CFTR (Figure 2-14, green bars). The P-value for all is less than 0.04. The same two mutations that improved NBD1 folding yield, D529F and S573E, increased the maturation efficiency of CFTR (Figure 2-14, yellow and magenta bars, respectively). The previously identified second-site suppressor mutants also improved CFTR maturation in a manner consistent with their effects on NBD1 folding. The correlation between NBD1 folding and CFTR maturation is formalized in Figure 2-15. The data indicate a linear relationship of good correlation ($R = 0.85$) with a slope of 0.75. Thus, NBD1 folding is necessary for CFTR folding and for every fold change in NBD1 yield a concomitant change of 0.75 in CFTR yield is observed. The position along the x axis thus reflects the amount of folded NBD1 and the slope of the line likely reflects later steps in folding during which folding NBD1 associates with other parts of the CFTR protein.

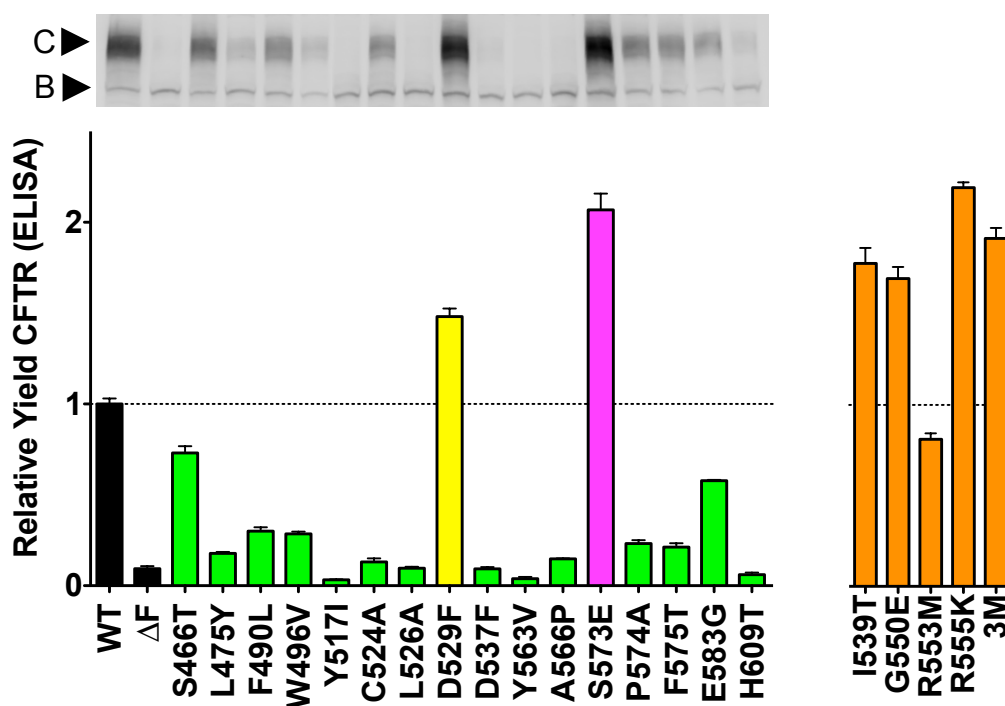


Figure 2-14. Effects of 508-Coupled and Second-Site Suppressor Mutations on CFTR Maturation and Correlation with NBD1 Folding Yield. Effects of 508-coupled mutations (green, yellow, and magenta) and second-site suppressors (orange) on the maturation of full-length CFTR and correlation with NBD1 folding yield. (A) The efficiency of full-length CFTR maturation was determined by ELISA (+/- SEM, n=6 for WT, ΔF508, D529F, and S573E, n=3 for other mutants). A representative western blot for one of the experiments is shown above the bar graph. All mutations altered maturation relative to wild-type CFTR. The two 508-coupled positions that increased NBD1 folding yield, D529F and S573E, also increased the maturation yield of CFTR (yellow and magenta bars, respectively).

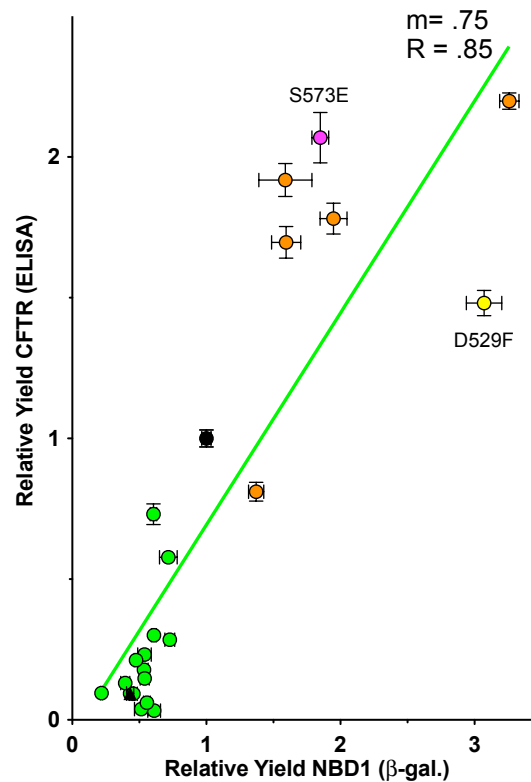


Figure 2-15. Effects of 508-Coupled and Second-Site Suppressor Mutations on CFTR Maturation and Correlation with NBD1 Folding Yield. The influence of the 508-coupled mutations (green circles), four individual second-site suppressor mutations (I539T, G550E, R553M, and R555K) and three suppressors in combination (G550E, R553M, and R555K) (orange circles) on F508 background on relative maturation of full-length CFTR and on relative NBD1 folding yield is directly correlated (green line, $m = 0.75$, $R = 0.85$). The two F508 coupled position mutations, D529F and S573E, are colored in yellow and magenta circles, respectively.

Quantitative Influence of $\Delta F508$ on NBD1 Folding and Later Steps in CFTR Maturation.

To determine whether in addition to its known effects on NBD1 folding and stability, $\Delta F508$ interferes with later steps in CFTR folding, the differential effects of the NBD1 suppressor mutations on the wild-type and $\Delta F508$ NBD1 folding yield and CFTR maturation yield were measured and correlated (Figure 2-16). Interestingly, the two suppressors identified by the coupling analysis, D529F and S573E, had much more modest effects on NBD1 yield in the presence of the $\Delta F508$ mutant, as might be expected. Taken together, the six suppressors and the combination define a line ($m = 0.10$, $R = 0.36$) in the context of $\Delta F508$ indicating the mutation interferes with a later step in CFTR folding in addition to its defect in NBD1 folding yield. Thus, the mutation decreases NBD1 folding yield approximately three fold and later CFTR folding steps by approximately seven fold.

Extant structures of CFTR $\Delta F508$ NBD1 contain a series of the previously identified second-site mutations that improve folding and solubility of the model domain. To simplify structural interpretation of the current results, a high resolution structure of murine $\Delta F508$ NBD1 without any mutations or deletions was solved (Table S1).

Comparison of the backbones of the murine wild-type (PDB 1R0W)

and $\Delta F508$ NBD1 (PDB 3SI7) structures reveal nearly identical structures, RMS 0.249 Å, with backbone shifts immediately following the 508 position (Figure 2-17). The largest shift in C α between the two structures is G509 shifting by 3.5 Å followed by a 1.5 Å shift for V510 before the $\Delta F508$ backbone converges with WT. Analysis of a surface view of the two structures further suggests local changes to the surface near the site of the deletion (Figure S1) similar to the structures containing the second-site mutations (Lewis et al., 2010; Lewis et al., 2005b). The absence of the F508 side chain creates a significant pocket on the surface of NBD1 at the predicted interface between ICL4 and NBD1 (Figure S1B). Additionally, the V510 side chain rotates outwardly 3.6 Å (C β) from the core in the mutant structure, further increasing the size of the pocket.

To better understand the molecular basis of the later step in folding effected by the $\Delta F508$ mutation, we built upon earlier work indicating that most missense mutations at the 508 position do not have dramatic effects on NBD1 but rather interfere with CFTR maturation (Du et al., 2005; Thibodeau et al., 2005a), the current assay battery was applied to a set of these mutations alone or in combination with the NBD1 suppressors (Figure 2-18). When F508 is replaced by lysine very little CFTR maturation is observed regardless of the ability of the NBD1 to fold ($m = 0.03$, $R = 0.38$) (Figure 2-18). The model of CFTR (Mendoza and Thomas, 2007) based on alignment with Sav1866 (Dawson and Locher, 2007) places

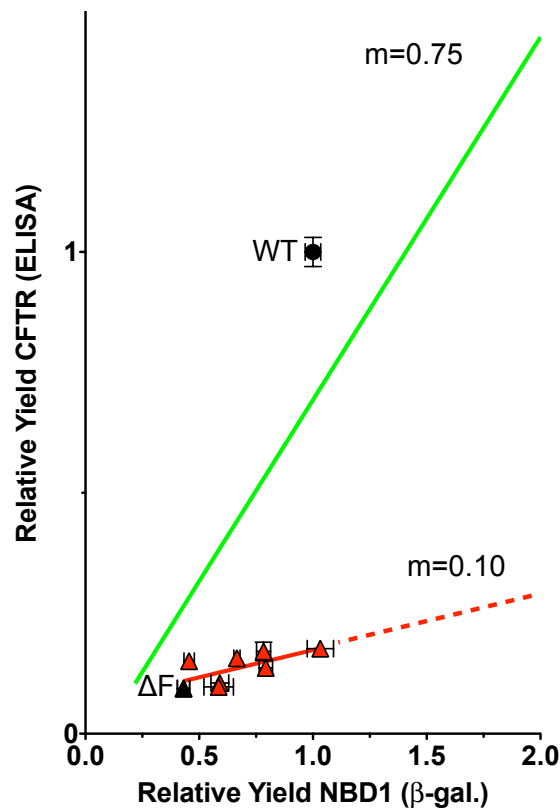


Figure 2-16. $\Delta F508$ and 508 Missense Mutations Influence the Correlation of CFTR Maturation with NBD1 Folding Yield by Disrupting the ICL4/NBD1 Interface. (A) View of the CFTR NBD1 ICL1/4 interface, as described in Figure 1C. (B) Deletion of the F508 residue creates a pocket on the NBD1 surface near the predicted ICL4 interface (compare $\Delta F508$ Figure 5B, PDB 3SI7, to wild-type Figure 1C, PDB 1R0W). Previously identified second-site suppressor (I539T, G550E, R553M, R555K, and 3M) but not the 508-coupled mutants (D529F and S573E), increase the yield of $\Delta F508$ NBD1. The correlation between increased NBD1 yield and relative yield of $\Delta F508$ CFTR is shallower (red line, $m = 0.10$, $R = 0.36$) than on the wild-type background (green line, $m = 0.75$, $R = 0.85$).

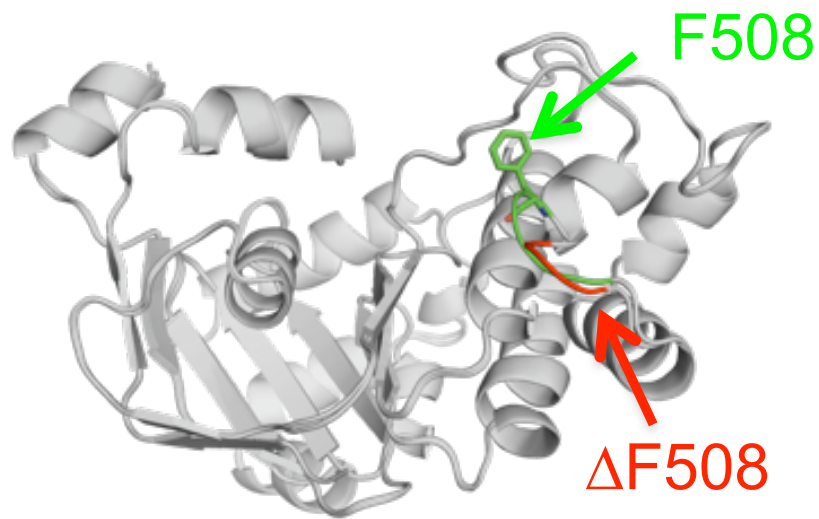


Figure 2-17. Structure of Unmodified Murine Δ F508 NBD1 Shows Changes in the Backbone Local to the Site of the Deletion. Structural alignment of murine wild-type and Δ F508 NBD1 solved for this study (PDB 1R0W and 3S17) show nearly identical structures (RMS 0.249 Å). The solved structure is complete in the domain boundaries (389-673) and is without mutations present in other Δ F508 NBD1 structures needed to stabilize or improve solubility facilitating crystallization.

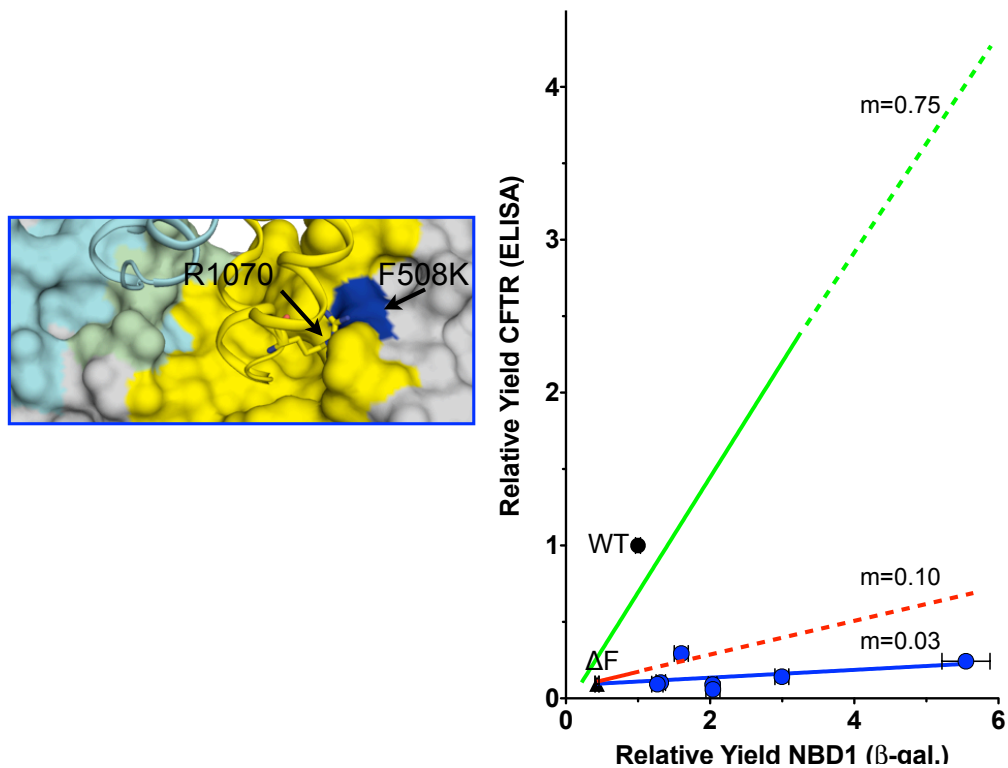


Figure 2-18. Δ F508 and 508 Missense Mutations Influence the Correlation of CFTR Maturation with NBD1 Folding Yield by Disrupting the ICL4/NBD1 Interface. (A) View of the CFTR NBD1 ICL1/4 interface, as described in Figure 2-1C. (B) Deletion of the F508 residue creates a pocket on the NBD1 surface near the predicted ICL4 interface (compare Δ F508 Figure 5B, PDB 3SI7, to wild-type Figure 1C, PDB 1R0W). Previously identified second-site suppressor (I539T, G550E, R553M, R555K, and 3M) but not the 508-coupled mutants (D529F and S573E), increase the yield of Δ F508 NBD1. The correlation between increased NBD1 yield and relative yield of Δ F508 CFTR is shallower (red line, $m = 0.10$, $R = 0.36$) than on the wild-type background (green line, $m = 0.75$, $R = 0.85$).

F508 (or the Δ F508 pocket) near R1070 in ICL4 (I218 in ICL2 of Sav1866) (Figure 2-19, *left*). Residues in ICL4 coupled to the 508 position exhibit a helical pattern consistent with the structural model. To assess the NBD1 ICL4 interface from the ICL4 side of the interface, a large tryptophan side chain replaced the native arginine. The bulk of the R1070W sterically clashes with the F508 position in the structural model (Figure 2-19, *left*) a prediction consistent with fact that this is a CF-causing mutation (Krasnov et al., 2008) and the observation that it inhibits CFTR maturation when F508 is present (open circle, Figure 2-19, *right*). By contrast, the introduction of the larger side chain at 1070 is accommodated by the Δ F508 pocket in the mutant NBD1, and, in fact may allow for better packing (Figure 2-19, *left*) that promotes improvement in folding (open triangle, Figure 2-19, *right*) due to correction of the ICL4 - Δ F508 NBD1 interface defect.

The ability of the R1070W mutation to counteract the ICL4 - NBD1 interface defect caused by the Δ F508 mutation, allowed assessment of the quantitative effects of suppression of both defects concurrently. When NBD1 suppressor mutations were introduced on top of R1070W and Δ F508, the slope was restored ($m = 0.77$, $R = 0.47$) (Figure 2-20). Thus, correction of the two defects results in near total rescue of the mutant folding phenotype. A three-fold improvement in Δ F508 NBD1 folding yield alone, correcting the NBD1 to wild-type levels, is reflected as a more

modest improvement in CFTR maturation (0.10 slope). Similarly the R1070W interface mutant, which produces an approximately seven fold increase in the slope, produces a more modest improvement in CFTR maturation. However, when the two effects are combined, they have a multiplicative effect on folding.

In order to determine whether the dual correction of $\Delta F508$ CFTR restores function in a synergistic manner reflective by maturation yields, two independent functional studies were performed of cells transiently expressing CFTR; conductance measurements of Fischer Rat Thyroid (FRT) cell monolayers and single cell patch clamp measurements of HeLa TetOn cells. FRT cells were transfected and grown on Transwell permeable supports. Conductance responses to agonists (forskolin plus IBMX) and Inhibitor 172 were measured for wild-type, R1070W, $\Delta F508$, single suppressor mutants (I539T and R555K) on both $\Delta F508$ and $\Delta F508$ -R1070W CFTR backgrounds. R1070W decreases function in the wild-type background while increasing function in the $\Delta F508$ background (Figure 2-21A, top, open bar, right side of graph) reflecting protein levels as shown in Figure 2-20, $.47 \pm .03$ and $.48 \pm .07$ relative conductance to wild-type ($1.0 \pm .1$), respectively. Single mutants on the $\Delta F508$ background were limited in their correction of function with maximum conductance achieved by $\Delta F508$ -R1070W CFTR (Figure 2-21A, top, red and open bars). Correcting both $\Delta F508$ CFTR folding defects had a synergistic effect on

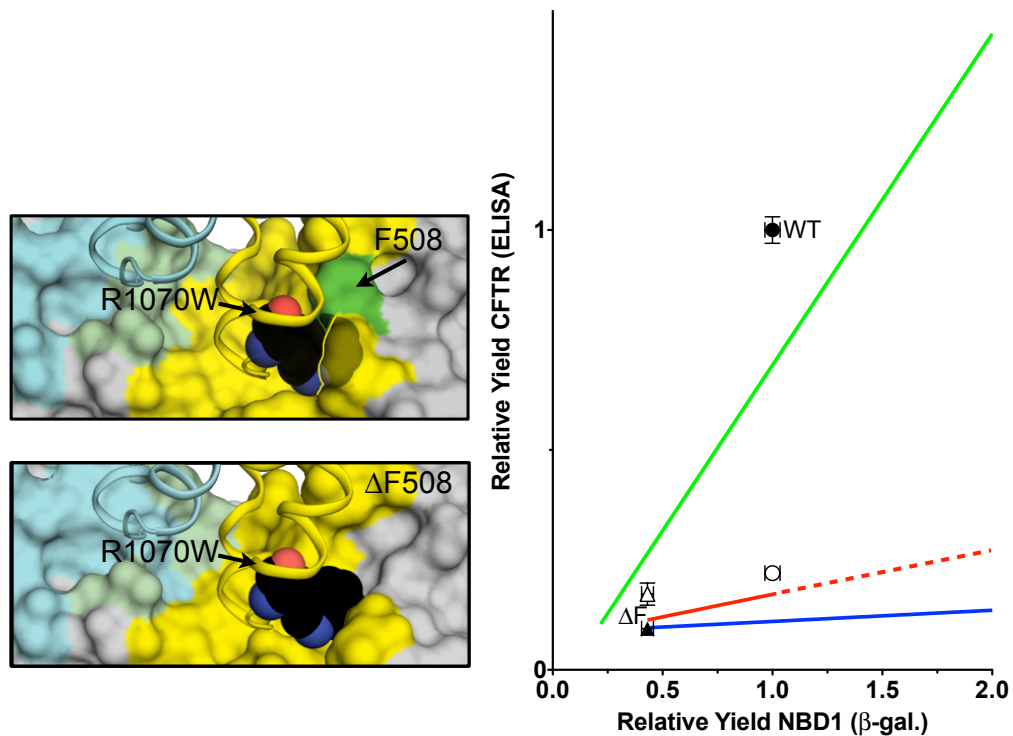


Figure 2-19. R1070W Improves $\Delta F508$, Interferes with WT Maturation. *Right*, CFTR maturation yield as a function of NBD1 folding yield for wild-type, $\Delta F508$, and the ICL4/NBD1 interface mutants are shown as green, red and dark blue lines for comparison. The R1070W (open triangle) mutation in ICL4 modestly improves the relative yield of $\Delta F508$ CFTR maturation and decreases the relative yield for CFTR wild-type (open circle) consistent with the predicted steric clash with the F508 side-chain (*top left*). By contrast, in the model tryptophan is accommodated by the pocket formed by the $\Delta F508$ mutant (PDB 3Si7) (*bottom left*).

function with measured conductance of I539T and R555K on Δ F508-R1070W measuring at $1.71 \pm .23$ and $1.90 \pm .42$ relative conductance (Figure 2-21A, top, cyan bars). The measured function for all constructs was ablated by the presence of Inh. 172 (Figure 2-21A, bottom). Patch clamp studies of transiently expressing HeLaTetOn cells further demonstrate the synergistic effects of correcting both NBD1 folding and the ICL4/NBD1 interface defects of the aberrant Δ F508 CFTR protein. Upon agonist stimulation by Forskolin, I539T and R555K on the Δ F508-R1070W CFTR background restore current density to wild-type levels, 88 ± 8 , 76 ± 5 , and 82 ± 2 pA/pF, respectively. This study establishes a direct correlation between maturation and agonist-stimulated CFTR function (Figure 2-21B, black line, $R= 0.94$, $m= 101$). The change in the slope of the dotted line in the presence of antagonist, Inh.-172, demonstrates measured currents are due, specifically, to CFTR function (Figure 2-21B, $R= 0.68$, $m =1$). Trace of the R555K-R1070W dual corrected Δ F508 CFTR protein has a wild-type-like response to Forskolin and Inh.-172 (Figure 2-21B, inset). A detailed table of NBD1 folding, Maturation, and functional values for single and double mutant studies is summarized in Table S2.

**Data was taken from Thibodeau et al. 2010, Hoelen et al. 2010, and Mendoza et al. 2011. Contributions to this study: C. Brautigam solved the structure of murine Δ F508 NBD1 (PDB 3SI7) which was purified by E. Caspa. A. Schmidt purified and performed thermal denaturation studies of D529F, S573E, and R555K NBD1. T. Barrett cloned D529F NBD1. Q. Li measured whole-cell Cl^- current using the patch-clamp technique.*

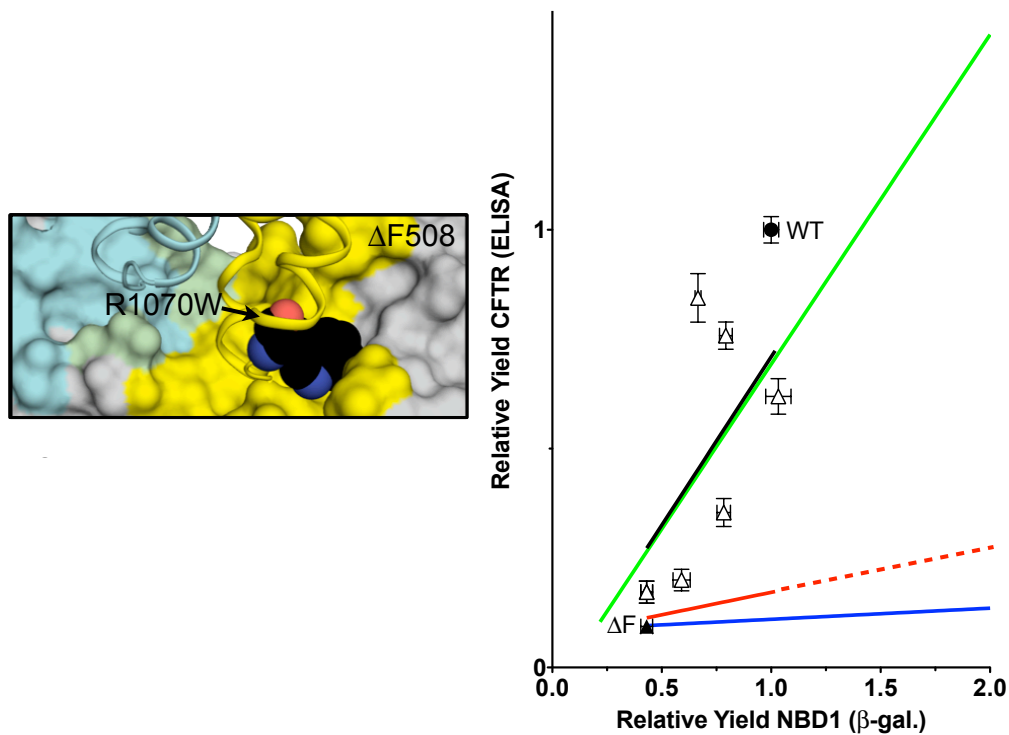


Figure 2-20. Correction of the $\Delta F508$ NBD1/ICL4 Interface Defect is Synergistic with Correction of the $\Delta F508$ NBD1 Folding Yield Defect. By contrast to the wild-type model, the larger tryptophan side chain can be accommodated by the NBD1 pocket formed by the $\Delta F508$ mutant (pdb 3SI7) and the attendant local conformational changes in the model (*left*). When R1070W is combined with mutations that improve $\Delta F508$ NBD1 folding yield, I539T, G550E, R553M, R555K, and 3M (open triangles), the correlation between NBD1 folding and CFTR maturation in the wild type protein is restored ($m = 0.77$, $R = 0.47$, black line) (*Right*).

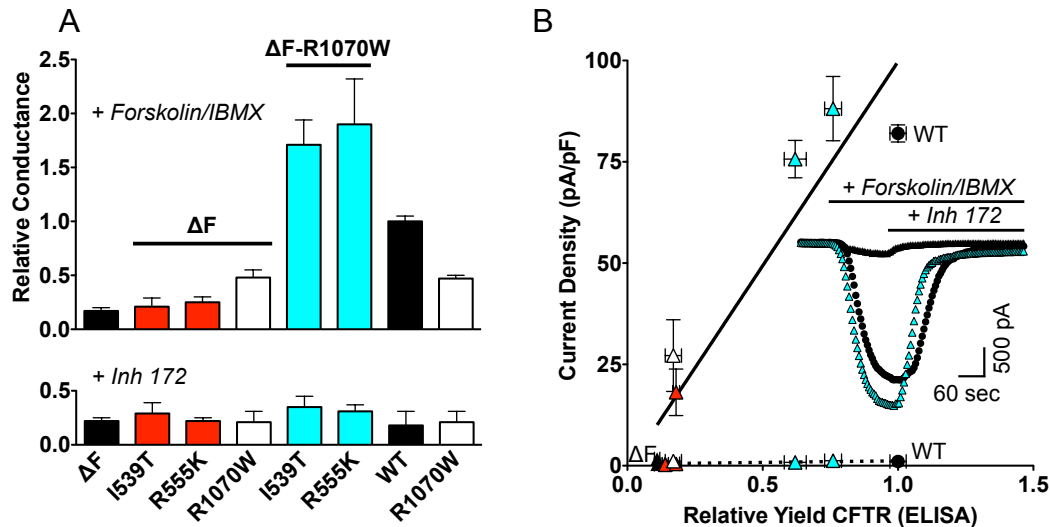


Figure 2-21. Correction of the $\Delta F508$ NBD1/ICL4 Interface Defect is Synergistic with Correction of the $\Delta F508$ NBD1 Function. (A) CFTR-dependent transepithelial conductance. Monolayers of FRT cells transiently expressing CFTR were stimulated with 10 μ M Forskolin + 100 μ M IBMX and transepithelial conductance measured (*top*, \pm SE, $n=3$, average conductance for wild type = 1.24 mS). The CFTR dependence of conductance is indicated by the sensitivity to 20 μ M Inh-172 (*bottom*) (B) Forskolin stimulated, Inh-172 sensitive whole cell currents of HeLa cells transiently expressing CFTR reveal a correlation between Current Density after activation (10 μ M forskolin + 100 μ M IBMX) with relative yield of CFTR (black line, $n = 5-6$) and in the presence of Inhibitor 172 (10 μ M) dotted line ($n=4-6$). A representative trace of the corrected mutant, $\Delta F508$ -R555K-R1070W CFTR (cyan triangles) is more like wild type (filled circles) than $\Delta F508$ (filled triangles) (inset).

Discussion

It is well established that the most common cystic fibrosis causing mutation, $\Delta F508$, disrupts the normal folding pathway of CFTR leading to the loss of function that underlies pathogenesis (Cheng et al., 1990). The fact that the mutant protein is produced and is active when induced to fold (Denning et al., 1992; Teem et al., 1993) suggests a novel pharmacological approach to treating CF. Small molecules that bind to and counteract the folding $\Delta F508$ defect would provide a means of repairing the protein (Thomas et al., 1992) and maintaining normal regulation and expression patterns. Multiple efforts to identify such compounds have been reported (Pedemonte et al., 2005; Robert et al., 2010; Robert et al., 2008; Sampson et al., 2011; Van Goor et al., 2006), but the identified molecules are typically not very potent and almost invariably unable to correct mutant CFTR folding to more than 15% of the wild-type levels. Understanding the basis of the observed efficacy ceiling would provide information critical for determining the feasibility of the corrector approach and guide any future discovery efforts. Although it is known that CFTR folding is a hierarchical process that occurs partially during translation (Du et al., 2005; Hoelen et al., 2010; Thibodeau et al., 2005a) and that the $\Delta F508$ mutation interferes with NBD1 folding (Hoelen et al., 2010; Protasevich et al., 2010; Thibodeau et al., 2005a; Thomas et al., 1992) and the changes are reflected in other CFTR domains (Du et al., 2005), fundamental details of the folding pathway and its disruption are lacking.

To gain insight into the folding process, we identified residues coupled to the 508 position utilizing a computational approach. Several methods have been developed to use evolutionary sequence analysis to identify networks of residues within proteins important for function, to improve native intermolecular contact prediction algorithms, and to identify hot spots of ligand binding or protein-protein interactions (Dekker et al., 2004; Goh et al., 2000; Lockless and Ranganathan, 1999; Madaoui and Guerois, 2008; Pazos and Valencia, 2008; Socolich et al., 2005). We sought to use the evolutionary record of the ABC transporter family to identify positions related to F508 and its important role in folding. Multiple independent evolutionary coupling algorithms were utilized to improve the chance of finding relevant positions. Remarkably, the 16 508- coupled mutants selected and tested all affect the folding of both the isolated domain and the full-length proteins. Fourteen mutations made folding worse and two improved the folding. These results are not likely to occur by random chance. For example, two examples of random mutant library folding screens found 0.03% of clones in the library improved folding, while, 20% of mutants misfolded with an average of two mutations per clone, demonstrating the inherent mutational robustness of proteins (Kunichika et al., 2002; Pjura et al., 1993) and the utility of the computational methods. In comparison to the random screens, we were 400 times more likely to identify mutations which improve folding and 4

times more likely to identify mutations which result in misfolding.

Identified from the evolutionary sequence analysis in this study, D529F and S573E improve folding of NBD1 in isolation and maturation of full-length CFTR in the wild-type background. The human CFTR 573 position corresponds to a highly conserved glutamic acid, the catalytic base, of the Walker B motif in other members of the ABC transporter family and in the second NBD of CFTR (Walker et al., 1982). However, CFTR proteins have evolved to have a serine at this position, a major contributing factor to the loss of ATPase activity at this site. However, reversion to Glu alone does not restore catalytic activity at this site as there are likely other changes important in the evolution of CFTR as a channel from a family of transporters (Stratford et al., 2007; Vergani et al., 2003). In this work, we found the wild-type protein is less stable than the mutant containing the conserved residue; the S573E mutation increases the thermal stability of NBD1 (Figure 2-12).

In the structure of human NBD1, there is a salt bridge observed between D529 and R555. R555K is one of the second-site suppressors identified by a genetics screen (Teem, Carson et al. 1996). The R555 residue has been suggested to play a role as a retention motif (Roxo-Rosa, Xu et al. 2006; Thibodeau, Richardson et al. 2010). In this work we demonstrate the R555K mutation increases the stability of the isolated domain and, thus, providing a mechanism by which it most likely corrects

the $\Delta F508$ NBD1 folding defect. Interestingly, the D529F mutation does not have a measurable impact on the stability of the domain, yet, significantly improves the folding yield of both NBD1 and full-length CFTR in the WT background (Figures 2-11, 2-12, and 2-14). However, it is unable to rescue maturation of $\Delta F508$ CFTR to a detectable level by western blot analysis. One explanation is that the D529F mutation alters the recognition by the quality control machinery of the cell via the retention motif, however, it is most likely, this mutation acts on the folding pathway, as phenylalanine is not expected to be a solubilizing mutation.

Analysis of the coupled mutations identified in the wild-type and $\Delta F508$ backgrounds, utilizing methodologies to facilitate the large number of samples, demonstrated that there are two steps in CFTR folding in which $\Delta F508$ is defective; NBD1 folding and an association step between NBD1 and ICL4, specifically an interaction with R1070. The correction of only one of the defects by either suppressor mutations or compounds are limited in efficacy as is reflected in the partial maturation of $\Delta F508$ CFTR to less than 20% of wild-type, the previously observed “ceiling”. In plots of CFTR folding yield against NBD1 folding yield, the position along the x axis reflects the first step in folding and the slope of the line reflects the later step of formation of the NBD1/ICL4 interface.

As demonstrated by the experiments with the second-site suppressor mutations on the F508K background, regardless of how well NBD1 folds,

CFTR is unable to mature if the NBD1/ICL4 is disrupted; likewise, CFTR cannot mature if NBD1 is unable to form a native structure. These findings predict that screens for compounds that improve CFTR along the y axis might be biased against compounds that act specifically against either individual folding defect as they would produce improved position on the x axis or a steeper slope, but little actual improvement of CFTR folding yield on the y axis. Unless single compounds can correct both steps, the set of highest hits in such screens are likely to be significantly populated with compounds that do not directly act on CFTR. Thus, these findings have significant implications for the discovery and development of CF therapeutics. Compounds, or combinations of compounds, that correct both defective steps would provide both specificity and efficacy of action. The assay systems and second-site mutants developed may also find utility in establishing a mechanism of action of extant correctors and aid in the identification of new compounds.

Experimental Procedures

Bioinformatics

The human CFTR protein sequence (gi|90421313) was used as a seed for PSI-Blast (Altschul et al., 1997) and run against the non-redundant database. Sub-alignments were performed using ClustalW and quality was assessed (Larkin et al., 2007), where sequences lacking any of the conserved ABC Transporter motifs (Walker A, B, and/or Consensus motifs)

(Walker et al., 1982) were removed from the alignment. The final alignment was generated online using the Promals 3D web server (Pei et al., 2008a; Pei et al., 2008b). Proteins with greater than 90% identity to any other protein in the alignment were removed prior to statistical analyses. The final alignment contains 493 sequences and has 1480 columns, numbered to the human CFTR sequence. Positional entropy based conservation scores were calculated using AL2CO (Pei and Grishin, 2001) and frequencies of the most common amino acid position identified and calculated via Perl scripting.

The multiple sequence alignment was used to calculate pairwise correlation matrices using Statistical Coupling Analysis (Lockless and Ranganathan, 1999), Explicit Likelihood Subset of Co-variation (Dekker et al., 2004), OMES (Kass and Horovitz, 2002; Larson et al., 2000)(Fodor and Aldrich, 2004; Kass and Horovitz, 2002), and McBASC (Gobel et al., 1994; Olmea et al., 1999). Pairwise correlation scores for SCA were calculated in Matlab (The MathWorks Inc.) using the SCA algorithm provided by R. Ranganathan. ELSC, OMES, and McBASC scores were calculated using the downloaded package from A. Fodor (afodor.net). Missense mutations at each of the positions were selected utilizing amino acid distribution profiles complementing correlated changes at the 508 position.

NBD1 Folding Yield

The pcDNA 3.1(+) constructs containing human WT and Δ F508 CFTR NBD1 (residues 389-673) were used as previously described (Thibodeau et al., 2010a; Wigley et al., 2001). Site directed mutagenesis was used to introduce missense mutations onto the WT and Δ F508 backgrounds (Stratagene). HeLa TetOn (Clontech Laboratories Inc.) cells were transiently transfected using Lipofectamine 2000 (Invitrogen Corp.) following recommended protocols at a cell density of 320,000 cells/ml. After transfection, cells were grown at 37°C for 18-24 hours. Media was aspirated from each well and 50 λ of a 2.5 mM fluorescein-di- β -D-galactopyranoside (FDG) (Sigma-Aldrich Corp.) substrate in Reporter lysis buffer (Promega Corp.) was added. Fluorescence measurements were made every minute for 24 hours on a BIOTEK Synergy MX (BioTek USA), a Spectramax M5 or a Gemini (Molecular Devices Inc.). Enzymatic rates were determined from the linear portions of the time course data. Reported P-values were determined using the Student's T-test with a two-tail distribution of a two-sample heteroscedastic test.

CFTR Maturation Yield

Site-directed mutagenesis was used to introduce missense mutations (Stratagene) on WT and Δ F508 pCMV-CFTR, a gift from J. Rommens. HeLa TetOn (Clontech) cells were transiently transfected in suspension using Lipofectamine 2000 (Invitrogen) using manufacturer recommended

conditions and incubated at 37°C for 24 hours. Effects of the mutations on maturation of CFTR was visualized by western blot analysis and quantitated by a sandwich ELISA utilizing A596 (provided by J. Riordan, UNC) as the capture antibody and 3G11 (provided by W. Balch, Scripps) as the detection antibody. Characterization of the ELISA maturation assay and detailed methods are included in the Extended Experimental Procedures and Figure S5.

Protein Expression, Purification, and Characterization

Murine Δ F508 NBD1 with no additional mutations, 389-673 human numbering, was expressed and purified as previously described except bacterial pellets were not frozen (Lewis et al., 2004). Quickchange mutagenesis was used to introduce the D529F, S573E, and R555K mutations onto human wild-type NBD1 in the expression system and expressed and purified as previously described (Lewis et al., 2004; Thibodeau et al., 2005a). The temperature melts were performed at 2 mM ATP as previously described (Hoelen et al., 2010).

Measurements of CFTR Function

HeLa TetOn (Clontech) cells were transfected with the plasmids used for the CFTR maturation experiments. 1 μ g of CFTR plasmids and 100 ng of PCMV GFP were co-transfected using 2 λ of Lipofectamine 2000 (Invitrogen) in a 6-well format. 24 hours post-transfection, the whole-cell

configuration of the patch-clamp technique was used to measure the Cl^- current. The pipette solution contained (mM) 145 $\text{NMDG}^+\text{-Cl}^-$, 1 MgCl_2 , 2 EGTA, 5 ATP, and 10 HEPES (pH 7.3 with Tris). The bath solution was (mM) 145 $\text{NMDG}^+\text{-Cl}^-$, 1 MgCl_2 , 1 Ca Cl_2 , 10 HEPES and 10 Glucose (pH 7.4 with Tris). The current was recorded with an Axopatch 200B patch-clamp amplifier and digitized at 2 kHz. The membrane conductance was probed by stepping the membrane potential from a holding potential of 0 mV to membrane potentials -40 and $+40$ mV steps for 200 ms. Pipettes had resistance between 3 and 5 $\text{M}\Omega$ when filled with pipette solution and seal resistance was always more than 8 $\text{G}\Omega$. Current recording and analysis was performed with pClamp 9.2 software and analyzed with Origin 8 software.

FRT cells were transfected with the plasmids as previously described with Lipofectamine LTX with Plus solution. 1 μg of plasmids were complexed with 1.2 λ of Plus solution and 1.5 λ of Lipofectamine LTX transfection reagent in 100 λ of Optimem (Gibco) solution. 500 λ of cells at a concentration of 600,000 cells/mL were combined with the DNA complexes and 200 λ plated in transwell with 750 λ of growth media in the outer well. 72 hours post-transfection, resistance measurements were conducted using an Epithelial. The plate was incubated for 15 minutes prior to measuring baseline resistance on a peltier set at 37°C . Resistance was measured 10 minutes after treatment with final

concentration of 10 μ M Forskolin (Sigma) + 100 μ M IBMX (Sigma) and after 5 minutes addition of 20 μ M Inhibitor 172 (CFFT). Conductance, where $I = 1/R$, was calculated from resistance measurements before and after treatments and adjusting for the surface area of the well.

Δ F508 NBD1 Crystallization and Structure Determination

Crystals of murine CFTR NBD1 Δ F508 were grown using the vapor-diffusion method by mixing 1 μ L of 10 mg/ml of the murine Δ F508 NBD1 protein with 1 μ L of the well solution (containing 3.5-4 M sodium acetate, pH 7.5) as previously described (Lewis et al., 2004; Thibodeau et al., 2005a). The crystals used for data collection were flash-cooled by suspending in a nylon loop directly out of their mother liquor and then plunging into liquid propane. X-ray diffraction data were acquired at beamline 19-ID at the Structural Biology Center of the Advanced Photon Source at Argonne National Laboratories. Statistical details of the final model are found in Table S1.

Homology Model of CFTR

A model of CFTR was constructed as previously described (Mendoza and Thomas, 2007). Either, murine NBD1 or Δ F508 (PDB 1R0W or 3SI7) and human NBD2 (PDB 3GD7) were docked onto the Sav1866 structure (PDB 2HYD) (Dawson and Locher, 2007; Lewis et al., 2004). A set of sequences containing of the ICL4 segments of CFTR proteins and Sav1866 ICL2 was used to generate an alignment using the JalView ClustalW function (Clamp et al., 2004; Waterhouse et al., 2009). On either the WT or Δ F508 CFTR models, F508K, R1070, R1070W residues were modeled using the Pymol (Schrodinger, 2010) mutagenesis function. Contact distances between CFTR ICL1 and ICL4 residues and murine WT or Δ F508 NBD1 residues were calculated via a Perl script using the atomic coordinates from these CFTR homology models.

Δ F508 NBD1 Structure Determination

The crystals had the symmetry of space group P4212, and they diffracted X-rays to a dmin value of 2.25 Å. The diffraction data were indexed, integrated, and scaled using HKL2000 (Otwinowski and Minor, 1997). Statistics regarding the data set are found in Table S1. Negative intensities were corrected using the TRUNCATE procedure (French and Wilson, 1978). The crystal appeared to be isomorphous with that used to determine the structure of wild-type murine NBD1 (Lewis et al., 2004a) (PDB accession code 1R0W). The 1R0W model, stripped of waters and

heterogens, was therefore used as the starting model for the current structure. To eliminate statistical bias and allow for a random assignment of reflections to the “free” set for the calculation of R_{free} , the starting coordinates were “shaken” such that they adopted new positions, resulting in a coordinate rms deviation between the starting and shaken coordinates of 0.5 Å. The shaken coordinates were then subjected to the rigid-body, simulated annealing, individual ADP, and TLS refinement protocols available in PHENIX (Adams et al., 2010). Coot (Emsley and Cowtan, 2004) was used to manipulate the model between rounds of refinement. The statistics from the final model are found in Table S1.

Homology Model of $\Delta F508$ CFTR

The crystal structures of murine WT (PDB 1R0W) and $\Delta F508$ (PDB 3S17) NBD1 were docked onto the Sav1866 (2HYD) structure as described in the main text using Pymol (Schrodinger, 2010). Contact distances were calculated from the atomic coordinates of the homology models using Perl scripts.

Analyses of Evolved Sequences

The coupling matrices for each of the four independent methods SCA (Lockless and Ranganathan, 1999), ELSC (Dekker et al., 2004), McBASC (Fodor and Aldrich, 2004; McLachlan, 1971), and OMES (Fodor and

Aldrich, 2004; Olmea and Valencia, 1997) were calculated as described in the main text.

ATP Dependence on Stability of NBD1

Human WT and S573E NBD1 proteins were expressed and purified as described in the main text. Additionally, each T_m for the two proteins was determined as a function of ATP concentration from 40 μ M to 100 mM.

Quantification Methods for Mature CFTR

Plasmids that express each of the sixteen 508-coupled mutants were used to transfect HeLa TetOn cells (Clontech). The sandwich ELISA was performed as follows: 100 λ of capture anti-body, A596 (provided by J. Riordan, UNC) was bound to Nunc Immobilizer plates (Nalgene Nunc Intl.) at a dilution of 1:1000 in binding buffer (100 mM Phosphate buffer, pH 8.0). After 24 hours, the cells were lysed using CRIPA buffer, a modified RIPA, (20 mM Tris pH 7.5, 150 mM NaCl, 0.5% CHAPS w/v, 0.5% DOCA, 0.1% SDS, and Complete Mini Protease Inhibitor tablet (Roche Applied Science) for one hour at 4°C. The antibody bound plates were washed three times with TBST and loaded with 100 λ of lysate clarified by centrifugation at 16,000 rcf and normalized to total protein. After an overnight incubation, the plates were washed three times with TBST and incubated for two hours with 100 λ of detection primary (3G11, W. Balch, Scripps) at a 1:1000 dilution in blocking buffer (3% BSA in PBS and

sodium azide), washed three times with PBST, and then incubated for two hours with 100 λ of diluted (1:2000 in blocking buffer) HRP conjugated α -rat secondary (The Jackson Laboratory). The plates were then washed three times with PBST and 100 λ of HRP colorogenic *o*-Phenylenediamine (OPD) substrate was added (Sigma-Aldrich Corp.). After 30 minutes, the reaction was stopped by adding 100 λ of 2.5 M Sulfuric Acid and absorbance read at 490 nm on either a Spectramax M5 or a Gemini plate reader (Molecular Devices Inc.). Western blot analysis of samples was performed as previously described (Thibodeau et al., 2005; Thibodeau et al., 2010) using the A596 antibody (provided by J. Riordan, UNC) at 1:5000 dilution.

Cell surface biotinylation experiments were performed using [EZ-Link Sulfo-NHS-SS-Biotin](#) and [NeutrAvidin Agarose Resin](#) as recommended by the manufacturer (Thermo Scientific). The samples were then analyzed by western blot analysis as previously described. Densitometry measurements from western blots of Band B and Band C from three independent experiments of whole cell lysate samples or samples derived from cell surface biotinylation experiments were performed using ImageJ (NIH). Ratio of Band C/Band B and Band C/Total were calculated, normalized to the respective WT CFTR ratio for each transfection set, and plotted against relative Band C using Prism (Prism

Software Corp.). Band C/Band B was fit to a straight line and Band C/Total was fit to the equation $y=x/(x+C)$, where C is a constant.

ELISA measurements, Total CFTR (Band B + Band C), cell surface biotinylation (CSB) were plotted against the relative intensity of Band C from WT CFTR and all fit to a linear equation. Comparison of the five quantification methods (ELISA, Band C, Total CFTR, Band B, and Band C/Total) was performed using a Student's T-test (two tail, heteroscedastic) between three independent experiments. The p-values for each of the methods and mutants were calculated against $\Delta F508$. The p-values for the Student's T-test between $\Delta F508$ and W496V and each of the five methods was plotted

Chapter 3: Perspectives and Future Directions

Introduction

While the $\Delta F508$ is by far the most prevalent mutation in the population of people living with Cystic Fibrosis, there are hundreds of Cystic Fibrosis mutations which are associated with the disease (<http://www.genet.sickkids.on.ca/CftrDomainPage.html>). Some of the more common mutations have been previously classified by the molecular defect (Welsh and Smith, 1993). Class I mutations are either a nonsense, frameshift or splicing mutant that results in the failure of the protein being produced (Table 3-1). Class II mutants, includes the $\Delta F508$ mutation, are defined as processing mutations (Table 3-1) (Cheng et al., 1990). In the third class of mutations, regulation mutants, the protein is produced and is processed meaning it reaches the plasma membrane but fails to function, such as G551D (Chang et al., 1993). Finally, the class IV CF causing mutants are termed ion conductance mutants such as R117H, R334W and R347P (Table 3-1) (Sheppard et al., 1993). This class of mutation alters the pore of the channel rather than causing a defect in gating, as with the class III mutants.

For the class II set of mutations, the mutant CFTR proteins are produced but fail to mature, thus, causative for the loss-of function. When comparing $\Delta F508$ and F508K by maturation alone, these two mutations have the same outcome, defective maturation. However, as reported in

the previous chapter, F508K NBD1 folds better than wild-type NBD1 but the full-length proteins with the second-site suppressor mutations mature even less well than in the $\Delta F508$ CFTR background reflected in the slopes of the blue and red lines, respectively (Figures 2-16 and 2-18). In this example, the F508K mutation does not effect NBD1 folding, x-axis, but the mutation has a large impact on maturation by disrupting the NBD1/ICL4 interface. For the case of $\Delta F508$ CFTR, the work in the previous chapter provides evidence that the deletion mutation affects both domain folding in addition to impacting the NBD1/ICL4 domain stability. Finally, it is conceivable within the class II set of mutations, some mutations may alter interactions between various quality control machinery thereby impacting trafficking. For example, a mutation could be within the NBD1 boundaries, distal from predicted inter-domain interfaces but still result in defective processing. Again, this information is lost when only monitoring the gross impact of mutations on maturation. Thus, monitoring only the impact of mutations along the y-axis may not be fully informative in understanding the class II mutations as there are likely to exist subclasses of molecular defects. The molecular defects of specific CF-causing mutations are important in understanding the molecular pathology so directed pharmacological compounds can be developed in an individualized manner.

In this chapter, we will be utilizing the step-wise specific assays developed for the studies of $\Delta F508$ defects on the CFTR folding pathway to more accurately classify NBD1 mutants. Additionally from these studies, we have three mutations suppressor mutations (R555K, D529F, and S573E) which may be informative in understanding other mutations in NBD1. R555K and S573E are both stabilizing mutations, however, each of the mutations are located in different subdomains of NBD1, α -helical and α/β core, respectively. One question to ask: must a second-site suppressor mutation be located on the same sub-domain as the misfolding mutation in order to correct a folding defect or can suppressors act as global stabilizers irrespective of the domain in which the suppressor and misfolding mutations reside. In our studies, while R555K was able to rescue $\Delta F508$ mediated misfolding, the computationally identified S573E suppressor did not have a significantly measurable effect suggesting linkage to the presence of Phe at the 508 position. Similarly, D529F is a folding pathway mutant in the α -helical sub-domain and also does not have a significantly measurable rescue either on $\Delta F508$ NBD1 or CFTR folding. By utilizing double mutant studies in the background of some of the 19 CF-causing mutations, we may be able to define the specific defect(s) of each of the mutations, the mechanism of rescue of different suppressor mutations, and gain useful information in developing individualized and effective therapeutics for specific mutations or classes of mutations.

Results

Impact of 19 NBD1 CF Associated Mutations on CFTR folding.

19 CF-causing mutations were introduced into CFTR using a full-length mammalian expression vector, and maturation was measured by both ELISA and western blot of SDS PAGE. Of the 19 mutant CFTR proteins within the NBD1 domain boundaries (389-673), 5 mutants mature better than wild-type (M470V, S549N, G551D, R668C and G576A) and 14 mutants mature less than wild-type (S492F, A455E, A559T, V520F, Δ I507, Δ F508, R560T, L558S, S549R, L467P, D614G, Y569D, and D579G) (Figure 3-1). In the group of mutants which fold better than wild-type, M470V and G551D are included and have been previously classified as a class III mutations (Chang et al., 1993, Wei et al., 2000).

In order to understand the molecular defects of the mutants with a decrease in the maturation of CFTR, further analysis is required by looking at folding of NBD1. All 19 CF associated mutations were introduced in the β -galactosidase assay vector for mammalian expression and folding was monitored as previously described. The five mutants which mature better than wild-type (M470V, S549N, G551D, R668C, and G576A) the mutant NBD1s also fold better than wild-type. Of the 14 mutant CFTRs which matured less well than wild-type, five mutant NBD1s folded equal to or better than wild-type NBD1 (L558S, L467P, D614G, Y569D, and D579G)

Table 3-1 Classification of CF-causing Mutations by Molecular Defect

Classification	Defect	Mutations
I	Protein Production	Frameshift and Nonsense mutations
II	Protein Processing	Δ F508
III	Regulation	G551D
IV	Conduction	R117H, R334W, and R347P

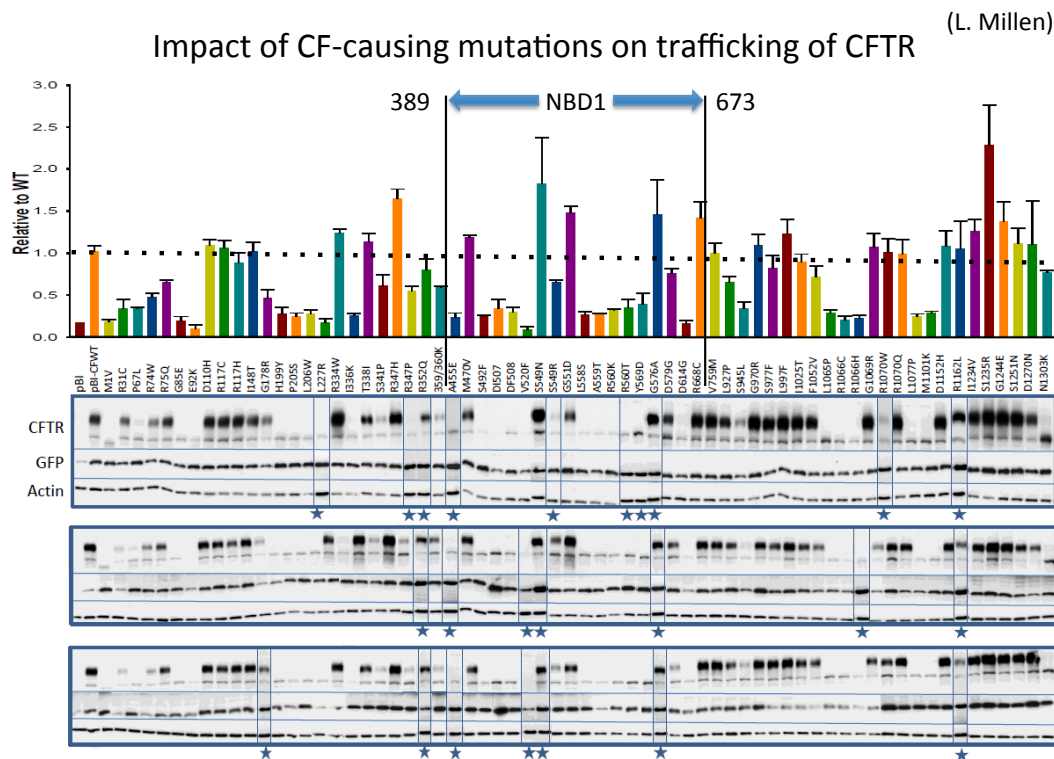


Figure 3-1. Effect of 19 NBD1 CF-Causing Mutations on Maturation. 19 mutations associated with causing CF were analyzed by ELISA and western blot of SDS PAGE. While most mutations decrease the efficiency of CFTR folding and maturation, as would be expected, five mutations, M470V, S492F, G551D, G576A, and R668C, increase the relative quantity of mature CFTR. These results are consistent between both biochemical assays and suggest a loss-of-function by another mechanism other than misfolding. *Mutations from CFTR2 (G. Cutting, Johns Hopkins University and Consortium and data is from L. Millen)

(Figure 3-2). The remaining 9 mutant NBD1s folded less efficiently than wild-type ($\Delta I507$, $\Delta F508$, R560T/K, S492F, A455E, V520F, S549R, and A559T) (Figure 3-2). A559T NBD1 folding is not significantly different from wild-type NBD1.

In order to visualize the impact of each of the 19 CF-causing mutations on NBD1 folding and maturation, maturation was plotted against relative folding of NBD1. This plot reveals the mutations lie within the boundaries of three quadrants, **Quadrant a** bounded by $0 < x < 1$ and $0 < y < 1$, **Quadrant b** bounded by $x \geq 1$ and $y < 1$, and **Quadrant c** bounded by $x > 1$ and $y > 1$ (Figure 3-3). **Quadrant a** consists of mutations in which there is a decrease in NBD1 folding efficiency, thus, impacting the ability of the mutant proteins to mature. The $\Delta F508$ and eight other mutations lie in this quadrant. Mutant proteins in **Quadrant b** have NBD1 folding equal to or better than wild-type NBD1 but are deficient in maturation. These mutations include D614G, Y569D, D579G, and L467P. L558S and V520F, while they lie within **Quadrant a**, may also be similar to the mutations in **Quadrant b** as the NBD1 folding is similar to wild-type fall of the line formed, $m = .75$, defined by 16 coupled mutations in NBD1 background (Chapter 2). Mutations in **Quadrant c** have both improved NBD1 folding and maturation relative to wild-type. Mutations in this quadrant include M470V, S549N, G551D, G576A, and R668C.

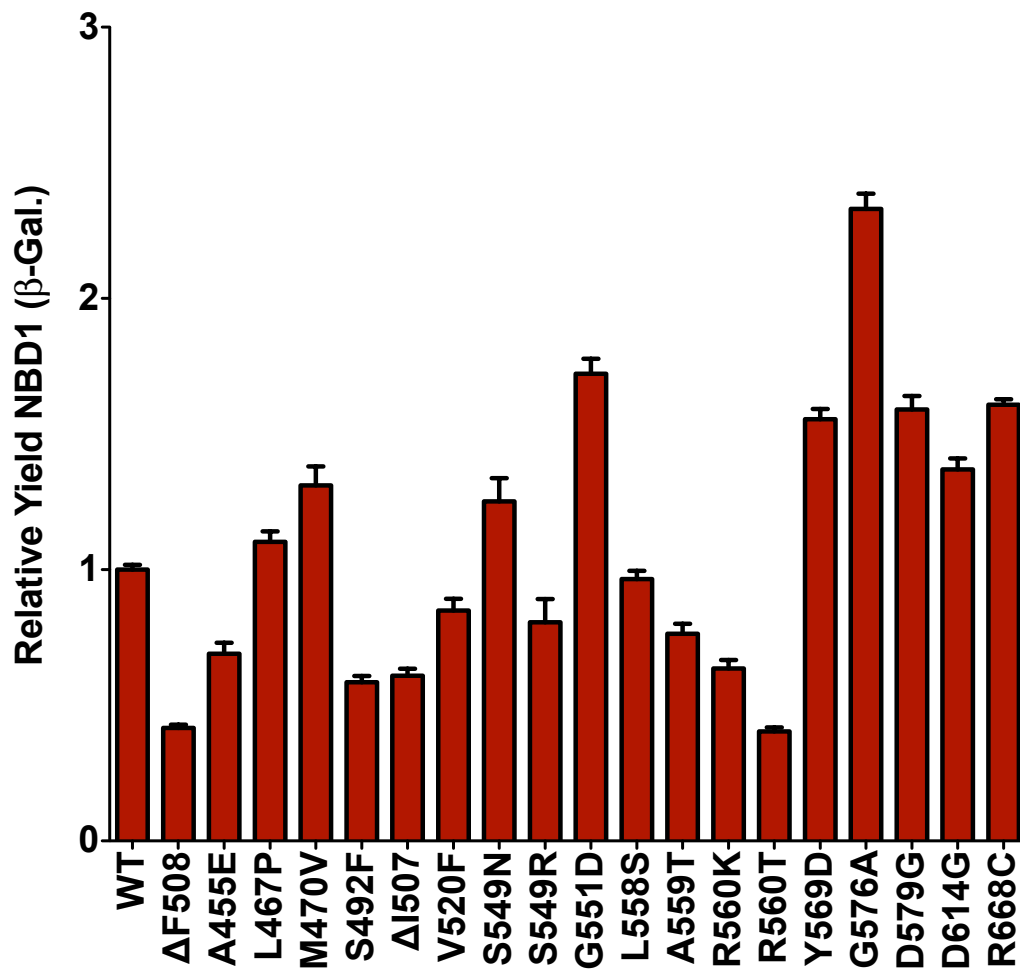


Figure 3-2. Effects of 19 CF-Causing Mutations on NBD1 Folding. Maturation studies of the 19 mutations in CFTR results showed 14 of the 19 mutations led to mistrafficking. NBD1 folding studies using the β -galactosidase folding assay reveals only ten of the mutants impact NBD1 folding, two had no measureable difference while eight mutations improved folding. *M. Fuller and J. Mendoza

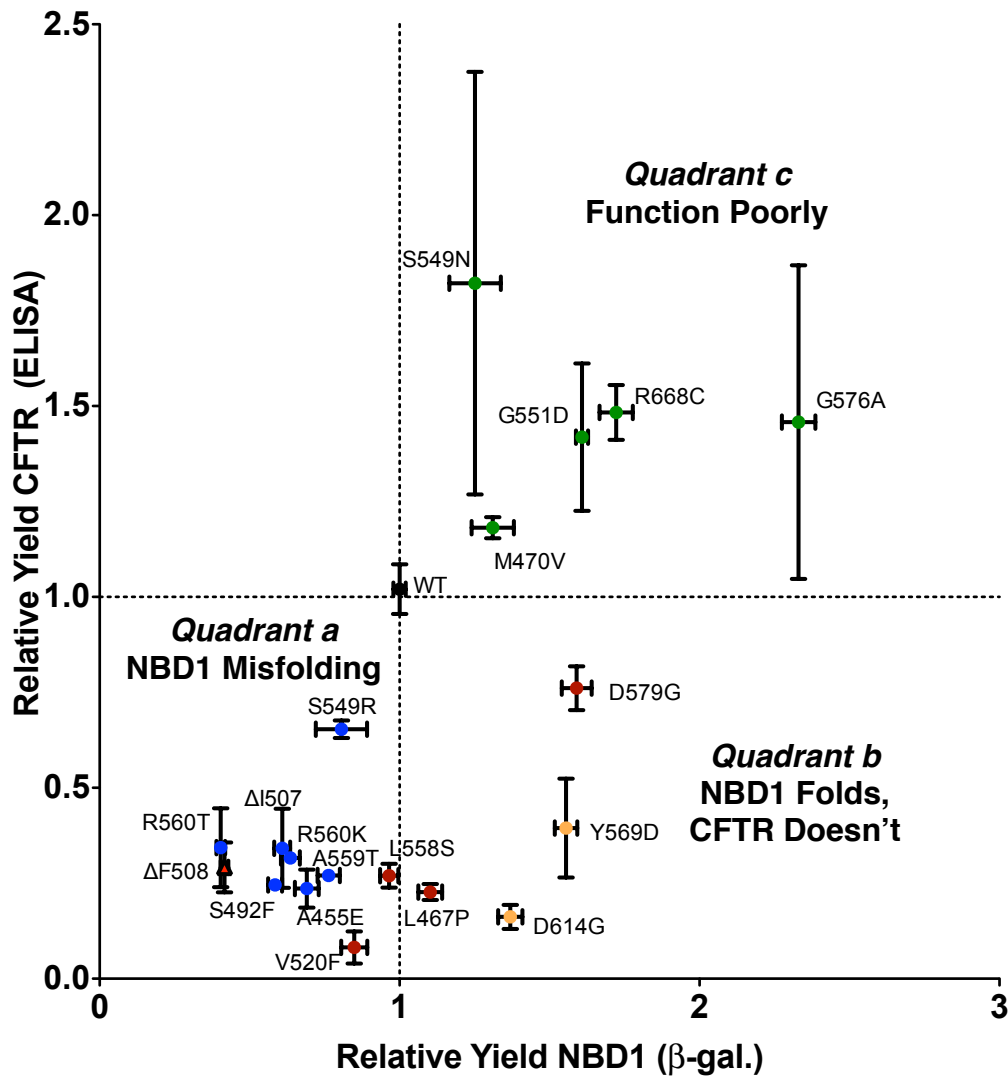


Figure 3-3. Evidence Leading to a New Mutation Sub-Classification. The plot of Total CFTR vs NBD1 Folding reveals three main classes of mutations as previously described in addition to new sub-classes of mutations. As previously classified, Class IV, mutations such as G551D do not decrease folding efficiency with most improving maturation. Several of the mutations in this quadrant of the graph are known to have altered function thus leading to the loss-of-function. For the class III set of mutants, including ΔF508, inefficient folding correlates with reduced trafficking. A new classification system is required to classify mutations which do not affect NBD1 folding but have reduced maturation. Additional, ΔF508 is one mutation also which is a subclass of misfolding mutation as this mutation is known to alter domain-domain interactions. *L. Millen, M. Fuller, and J. Mendoza

Rescue of the nine mutants in **Quadrant a** was assessed by two experiments in context of the isolated NBD1 domain. First, the mutants were expressed at a low temperature, 30°C, to identify mutations which could be improved. Second, an initial screen of the three second-site suppressor mutations in the background of some of these nine mutants as this is a work in progress. In the low temperature rescue experiment, the experiment was repeated once in triplicate where n=9. The results indicate four mutations have NBD1 yields significantly different when expressed at 30°C vs 37°C. Three fold better (Δ F508, S492F, and R560T) and one folds worse (L558S). If temperature rescue is capable of partially correcting folding pathway or stability defects, as has been shown with Δ F508 (Denning et al., 1992), these data suggest a differentiation in the molecular defects of CF-causing mutations in the class II set of mutations as some mutations are not amenable to correction by temperature.

In the second battery of experiments, the three suppressor mutations D529F, S573E and R555K were tested for their ability to rescue each of the 9 NBD1 mutants with less efficient folding than wild-type. Eight of these 9 mutations were available at the time of the experiment which excluded S492F. R555K had a significant improvement in the NBD1 folding yield of five of the eight tested (A455E, Δ I507, Δ F508, R560K, and R560T). This suppressor mutation did not improve folding of the V520F, L558S, and A559T NBD1 mutants. Four of the 9 mutations (S492F,

Δ F508 modestly, V520F, and R560T) were tested for rescue by S573E with all four mutants being improved. Finally, D529F was tested in the Δ F508 and V520F backgrounds. D529F had no impact on Δ F508 while markedly improving the NBD1 folding yield of V520F. These data further demonstrate that D529F and S573E are coupled to Phe at the 508 position, consistent with experiments and analyses of evolved sequence presented in Chapter 2. These data further provide evidence that D529F and S573E are coupled to F508 and lose their effect on folding in the absence of the position as with Δ F508 mutation.

**Contributions to this study: G. Cutting and the CFTR2 consortium provided the curated list of CF-causing mutations. L. Millen performed the cloning and full length maturation studies of the 19 CF mutations and Western Blot of FRT cells transiently expressing CFTR. M. Fuller and J. Mendoza performed mutagenesis and NBD1 folding experiments utilizing the β -galactosidase assay.*

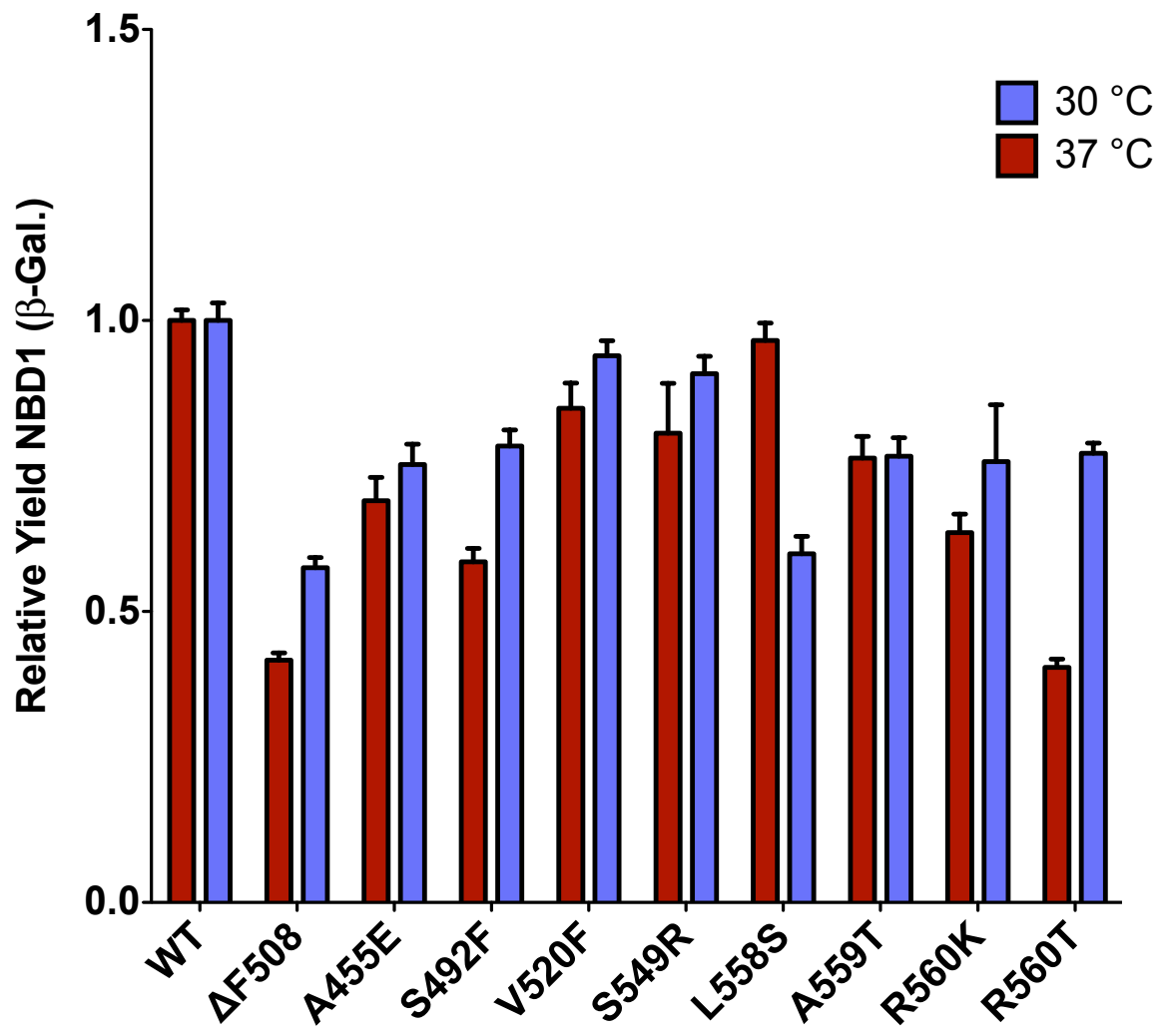


Figure 3-4 Temperature Rescue of *Quadrant a* Mutations with Reduced NBD1 Folding. Nine mutations which altered NBD1 efficiency were expressed at lower temperatures to identify mutations that can be rescued. Low temperature rescue had a positive impact on three mutations, negatively had an impact on a mutation, with no effect on the remaining five.

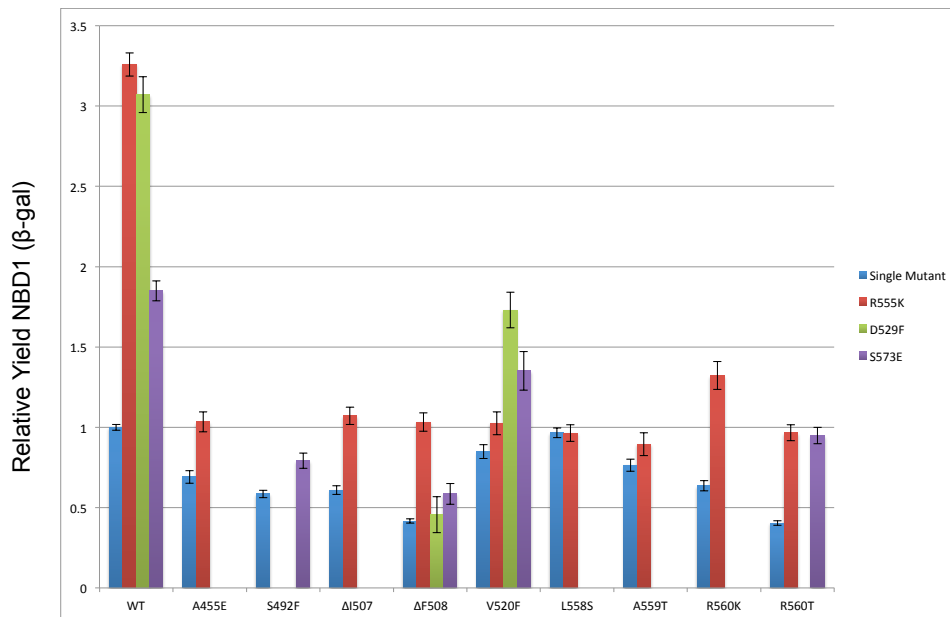


Figure 3-5. Rescue of misfolding mutants by second-site suppressors.

Nine mutations which were previously shown to cause NBD1 to misfold were attempted to be rescued by suppressor mutations (stabilization mutants R555K and S573E, and the D529F pathway mutant). D529F increased the yield of V520F by ~1.5 fold but has no effect on ΔF508. S573E had a significant improvement of NBD1 folding yield of two mutants, R560T and V520F. R555K improved the yield of most mutants but did not effect on the yield of three misfolding mutants, V520F, L558S and A559T.

Discussion

Cystic Fibrosis is a loss-of-function disease. There are three types of mutations which lead to dysfunction: 1) loss of protein production (class I mutants), 2) defective protein processing (class II mutants), or 3) mutations which do not affect protein production or processing but alter function (class III and IV mutants). Methods to distinguish between class II-IV mutants involves a combination of quantification of protein levels ie western blot analysis of mammalian expression systems and functional assays either requiring generating a stable cell line, or transient expression of CFTR for functional studies in patch clamp or single channel measurements. For the class II mutants, contributions or domain folding, domain-domain associations, or CFTR-protein interactions have not been differentiated and would require step-specific assays. The correlative studies presented in the previous chapter presents a systematic study linking folding of a single domain, NBD1, to maturation of the full length protein, CFTR. This step-wise assay system is informative especially when utilizing intragenic manipulations to alter/correct specific defects. Using this methodology, the two defects of $\Delta F508$ CFTR folding were defined and the defects corrected by demonstrating the restoration of corrected maturation and function. Thus, it is likely, mutations previously categorized as class II mutants may have multiple defects contributing to the protein misfolding, like $\Delta F508$.

Perspectives

Beginning with traditional methods to look at protein levels, we identified five mutants increased levels of mature protein relative to wild-type CFTR. 14 mutants altered the ability for CFTR to mature. Location of the mutations in the primary structure, literature reviews, quantification of mature levels of protein along with functional analysis would classify the five mutant CFTRs (M470V, S549N, G551D, G576A, D579G, and R668C) as class III mutants (Chang et al., 1993, Wei et al., 2000). Under the previous classification system as described by Welsh and Smith, the remaining 14 mutations would be labeled as class II or processing mutants. However, NBD1 folding studies suggest this classification system does not fully classify the mutations by molecular defects. The plot of maturation versus NBD1 folding yields of each of the mutant proteins reveals different subclasses of mutations leading to a decrease in mature CFTR. From this plot we defined three quadrants (**Quadrants a-c**) in which the mutant proteins are located. Proteins falling in **Quadrant c** have improved NBD1 folding and maturation relative to wild-type CFTR but have altered function. Mutant proteins in **Quadrants a** and **b** by previous observations would be simply classified as class II mutants. However, the data presented in this chapter suggest this method of classification is not necessarily straight forward. Analysis of the maturation vs NBD1 folding plot reveals the apparent difference between mutations which may affect NBD1 folding, maturation, or both. Loss-of-

function of the mutants in **Quadrant c**, class III, are most likely due to Regulatory defects alone.

From the maturation and NBD1 folding studies in this chapter, there is an opportunity to make sub-classifications for the class II set of mutants. Based on the preliminary data, structural analyses, and coordinates of each of the mutants on the maturation vs NBD1 folding plot, we have classified the 19 mutations in Table 3-2, thereby, extending the sub-classification. Furthermore, this classification methodology allows for complexing of classes and sub-classes as is the case for $\Delta F508$ CFTR. A mutant which alters the folding of the domain, local to the site of the mutation, would be classified as a class IIa mutant which includes $\Delta F508$ CFTR. Mutations which alter association of two or more domains is defined as a class IIb mutation, $\Delta F508$ CFTR is part of this subclass. Under the new classification of $\Delta F508$ CFTR would be class IIab. Combining information from the step-wise folding assays, we can begin to define more of the complex mutants; for example, if the rescued $\Delta F508$ CFTR protein exhibited a defect in Regulation (gating), we would propose such a mutation should be classified as class III,IIab.

Structural analyses of the mutations in context of the homology model of CFTR and folding data assist in the formulation of hypotheses on some of the other mutations. First, we can inspect the location of the 9 mutants in **Quadrant a**, for example, L558S and V520F. Both of these mutations only slightly alter NBD1 folding but have a very large impact on

maturation. Analysis of the CFTR model, places these mutations in the core of the α -helical subdomain but also one layer away from the NBD1/ICL4 interface (Figure 3-6A). One possibility is that the NBD1 may be able to repack to accommodate the mutations in context of the isolated domain, however, this may also alter the topology at the NBD1/ICL4 interface. In turn, these mutations have a large effect on maturation. Based on these observations, we have classified these mutations as class IIb.

D579G from Figure 3-3, we see this mutation actually improves folding of NBD1 as seen in the improvement along the x-axis, however, this mutation is located at the predicted interface of NBD1 and NBD2 near the site of ATP binding and has a lower than expected detectable quantity of Band C (Figure 3-6B). Examination of the preliminary functional data suggest there is a decrease in forskolin dependent activation and no response to Inh172. This mutation may be classified as IIb,III.

Y569D and D614G greatly impact the ability of the full-length protein to mature despite NBD1 folding significantly more efficiently than wild-type NBD1. Analysis of the CFTR homology model locates these positions on the surface of NBD1 distal from any predicted NBD1-domain interfaces. However, these two positions are near the diacidic motif important for the COPII dependent exit of CFTR from the ER (Figure 3-6C) (Stagg et al., 2008). It is possible these mutations either alter the topology or

electrostatics at the surface which is important for trafficking and thus leading to a decrease in maturation. The preliminary functional data, loss of-function, reflects the inability of the mutant proteins to traffic to the plasma membrane. Thus, we have classified these mutants as type IIc.

Based on the currently available information using the step-wise folding assays, functional transepithelial conductance data, literature review, and structural context of the mutations, we have extended the classification of the 19 CF-causing mutations as summarized in Table 3-2. Revisiting the classification of the mutations may find utility in understanding the molecular mechanism of the ultimate loss-of-function leading to Cystic Fibrosis. Furthermore, the work presented in Chapter 3 and 4 demonstrate the complexity and diversity of the defects. Quantification of Band C is not sufficient in describing the defects of the large number of mutations resulting in decreased levels of CFTR at the membrane. This work establishes the groundwork to identify and develop individualized CF therapeutics where one size fits all model is not appropriate. As an example, VX-770 which has profound improvements in patients with the class III mutant, G551D, has little clinical benefit for patients with $\Delta F508$, a class IIa,b mutant. Patient genotyping efforts, extension of the mutation classification, and the stepwise specific assays

developed in this body of work, we hope future screens for CF therapeutics and patients will benefit from these new perspectives.

Table 3-2 Extending the Classification of CF-causing Mutations

Class	Defect	Mutations	Quadrant
I	Protein Production	Nonsense mutations	NA
II	Protein Processing	General Misfolding	
IIa	Domain Folding	Δ I507, Δ F508, S492F, A455E, R560K, A559T, S549R, R560T	a
IIb	Domain-Domain Association	Δ F508, D579G, L558S, L467P, V520F	a,b
IIc	Protein-Protein	D614G, Y569D	a,b
III	Regulation	M470V, S549N, G551D, G576A, D579G, R668C	c
IV	Conduction	R117H, R334W, and R347P	NA

*NA = Not Applicable

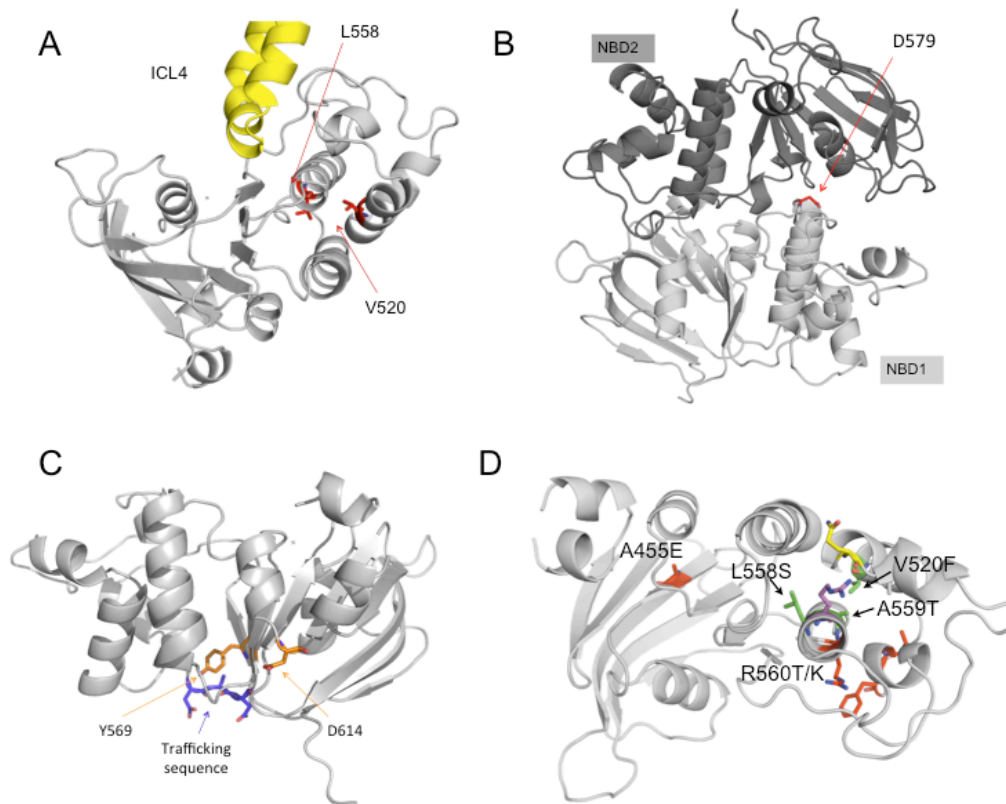


Figure 3-6. Structural Context of a Select number of Mutants. (A) Figure 9 L558S and V520F predicted to disrupt the NBD1-ICL4 interface. The L558 and V520 positions are very close to the interface between NBD1 and the fourth intracellular loop (ICL4), which forms part of the physical ion channel of CFTR. Disrupting the interface could change the conformation of the full-length protein, limiting maturation. (PDBs 2PZE, 2HYD). (B) D579G predicted to disrupt the NBD1-NBD2 interface. The D579 position is right at the interface between the two nucleotide binding domains and is likely necessary for proper interactions between them. If these two domains do not interact normally, it could disrupt the conformation of the whole protein, limiting the amount of CFTR that traffics to the plasma membrane. (PDB 2PZE) (C) Y569D and D614G predicted to disrupt crucial trafficking signal. These mutations are positioned very close to the sequence necessary for binding with trafficking machinery (COPII). This machinery is involved in vesicle formation in the ER, and disruption of this interaction could limit maturation (PDB 2PZE). (D) Structural context of the three mutants which folding yields are unaffected by R555K. View of NBD1 (PDB 1R0W) looking down from the NBD1/NBD2 interface. The mutations which had improved folding yields (A455E, R560T/K, Δ F508) in the presence of the R555K are shown in red sticks. Three mutations (L558S, A559T, and V520F, green sticks) are unaffected by the presence of the R555K suppressor mutation (purple sticks). These three mutations are proximal to the interface of the two helices on which there is a hydrogen bond between R555 and Q525 (purple and yellow sticks, respectively).

Future Directions

The data presented in this chapter is from ongoing work and requires additional experiments to establish a more well defined classification of the 19 CF-causing mutations in NBD1 as examined. Specifically, folding studies of the all three suppressor mutations (R555K, D529F, and S573E) in the background of the 9 NBD1 misfolding mutations should be completed both in the NBD1 folding assay and in context of full-length CFTR. By acquiring this data, we can better understand the vectorial change of the corrected mutants. For example, R555K moves $\Delta F508$ far along the x-axis but with little improvement along the y-axis. If other mutants fail to improve along the y-axis as they do along x-axis, this would be an indication of more than one defect. An example of this, are the three mutations L558S, V520F, and A559T in the NBD1 folding assay are not affected by the stabilizing effects of the R555K mutation (Figures 3-5 and 3-7D). In addition, functional studies should also be performed to identify any possible problems with gating.

D614G and Y569D are near the diacidic motif important for the COPII dependent trafficking of CFTR. We are currently working to produce mutants D614A, D614E, and D614S to further establish a more detailed understanding of this hypothesis. Cross-linking experiments may be useful in identifying altered interactions with the trafficking machinery in response to the identity of the amino acid at 614 and 569.

Experimental Procedures

Measuring the Impact of CF-causing Mutations on NBD1 Folding, Maturation, and Function.

Briefly, the ELISA, western blot analysis, NBD1 folding, and conductance experiments were conducted as detailed in Chapter 2 with the following changes:

The full-length CFTR expression vector used in these studies was pBI-CMV2 (Clontech). Maximal CFTR conductance was measured 30 minutes after activation with 10 μ M forskolin which includes a 15 minute treatment with 10 μ M of the potentiator 2-(2-(1H-indol-3-yl)-N-methylacetamido)-N-(4-isopropylphenyl)-2-phenylacetamide (PG01) (CFFT). Inhibition of CFTR dependent conductance was measured 15 minutes after the addition of 10 μ M Inh.172.

For low temperature expression of 9 NBD1 mutants, the cells were incubated at 37°C for 24 hours post-transfection followed by a 24-hour incubation at 30°C before analysis.

Appendices

The following figures and tables provide additional information to the main text in Chapter 2.

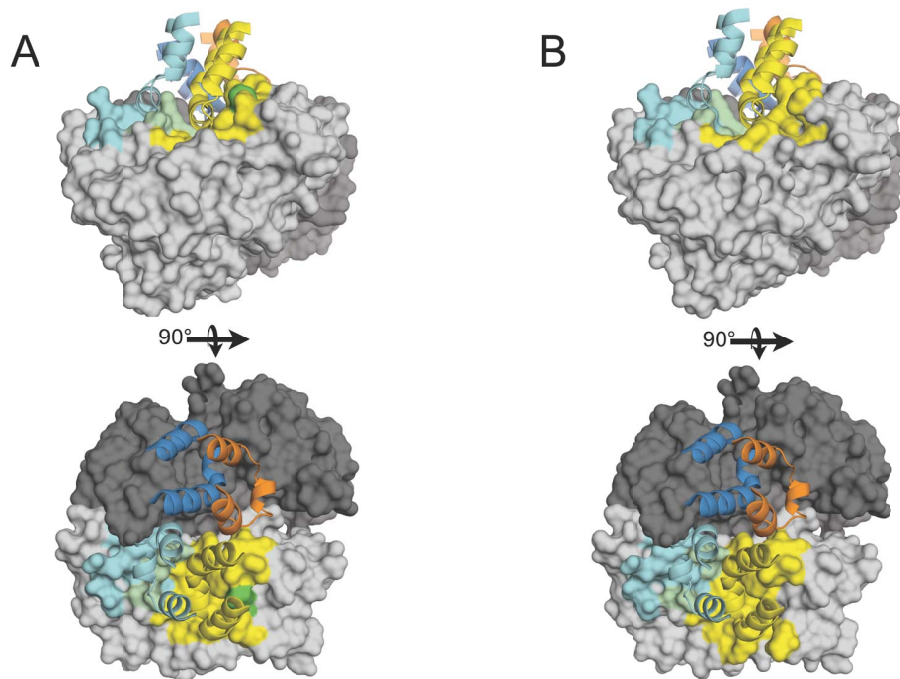


Figure S1. $\Delta F508$ Forms a Cavity at the NBD1/ICL4 Interface in CFTR. (A) View of ICL4 NBD1 interface in the model of WT CFTR as described in Figure 2-1B. (B) Murine $\Delta F508$ NBD1 (pdb 3SI7) docked on the CFTR model as described in Figure 1B. Comparison of the surface between the WT and $\Delta F508$ reveals changes local to F508 forming a pocket and perturbation of the ICL4 interaction surface (Figures 2-1B and S1A).

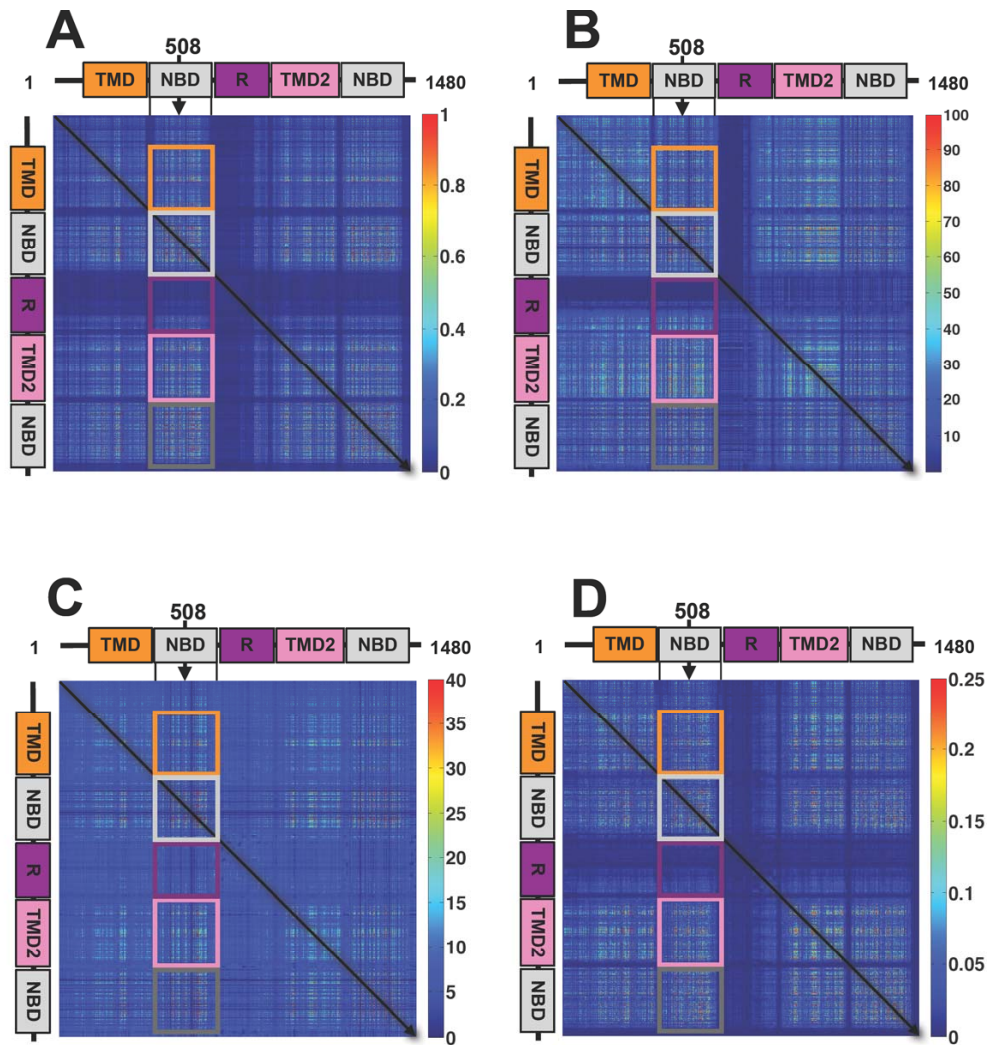


Figure S2. Independent Coupling Matrices for Each of the Four Methods. Four heat maps of coupling values for each statistical method are shown without normalization as described in Figure 2-7A. **(A)** Upper left matrix is from Statistical Coupling Analysis (SCA), **(B)** upper right is from Explicit Likelihood Subset of Covariation (ELSC), **(C)** lower left is OMES, and **(D)** lower right is from McBASC.

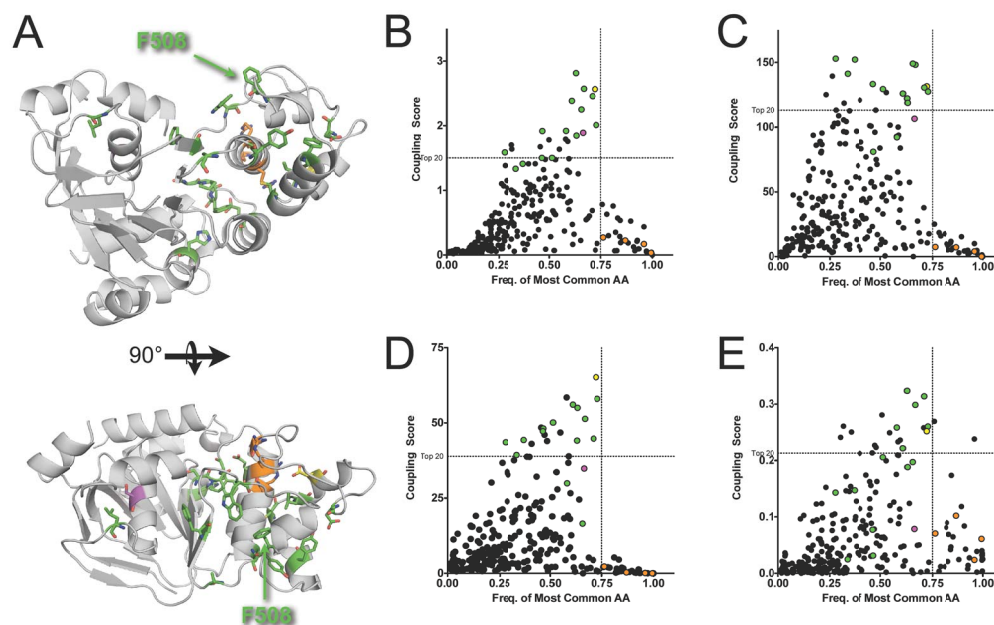


Figure S3. Positions in NBD1 Coupled to F508, Related to Table 2-1. (A) The structure of murine NBD1 (pdb 1R0W, grey ribbon) is shown with the side chains of fourteen 508-coupled positions from Table 1 indicated in green and two positions, D529 and S573, indicated in yellow and magenta, respectively. The four NBD1 previously identified second-site suppressor positions (I539, G550, R553, and R555) are indicated in orange. (Top) Canonical view of NBD1 looking from the perspective of the membrane. (Bottom) A 90° rotation about the x-axis. (B) Plot of coupling scores to the 508 position from SCA versus the frequency of the most common amino acid for every position in NBD1 (389-673). The sixteen representative 508-coupled positions (green, yellow, and magenta circles) account for 60% of the top 20 scoring positions in SCA. Positions in NBD1, which are dominated by a single amino acid, frequency > 0.75, have low coupling scores, right most side of plot. The abrupt drop in coupling scores for these positions is not evident when a similar plot is produced using traditional conservation scores. The four second-site suppressor positions were not identified through the coupling analysis, since these positions have a single amino acid frequency > 0.75 and are thus above the drop off. (C) Plot of coupling scores to the 508 position from ELSC versus the frequency of the most common amino acid in NBD1. (D) Plot of coupling scores to the 508 position from OMES versus the frequency of the most common amino acid in NBD1. (E) Plot of coupling scores to the 508 position from OMES versus the frequency of the most common amino acid in NBD1.

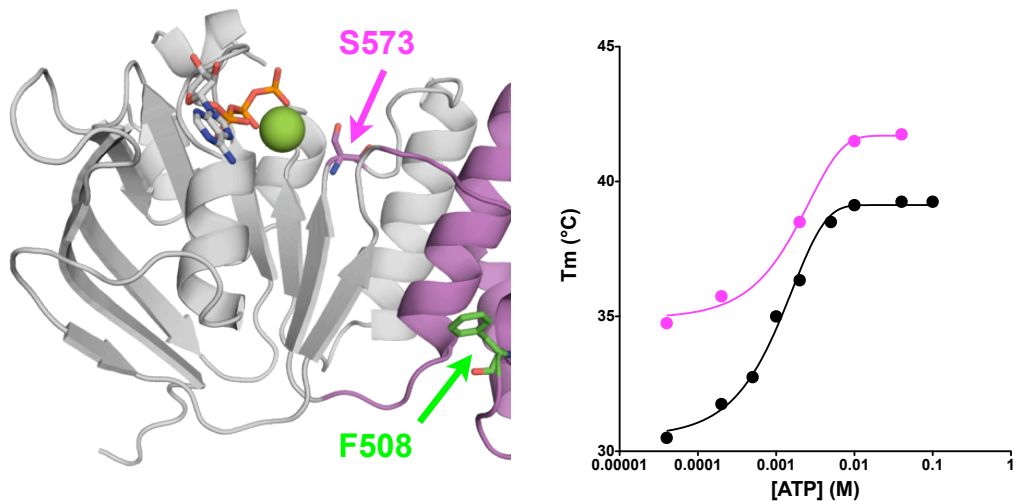


Figure S4. Structural Context of S573E Suppressor Mutations. The mutation S573E increases the folding efficiency of NBD1 (Figure 2-11). Left, the S573 position, shown in magenta, is typically an Asp or Glu residue, serving as the catalytic base, in the vast majority of the Walker B motifs in the ABC transporter superfamily. This is a canonical view of the α/β core of human NBD1 (PDB 1XMI) from the perspective of the membrane. The adenosine head group of ATP is shown in grey and the three phosphates of ATP are shown in orange. Mg^{2+} is represented as a green sphere while F508 is shown in a green stick representation. Right panel, T_m of human WT and S573E as a function of ATP concentration. For every ATP concentration assessed (40 μ M – 100 mM), the T_m is higher for S573E.

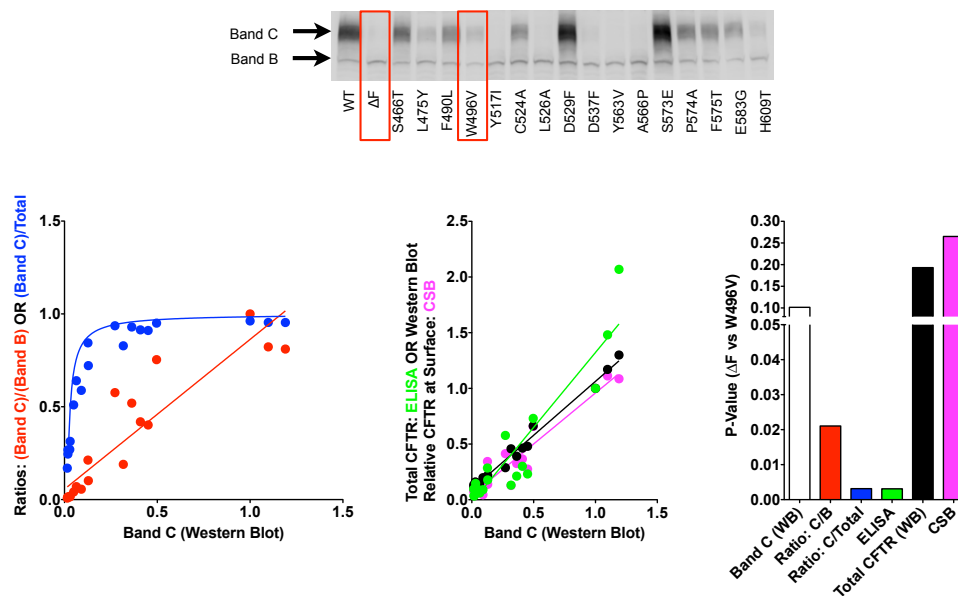


Figure S5. Comparison of Various Methods for Quantification of Maturation of CFTR. (A) Representative western blot (mAb 596) of WT, $\Delta F508$, and sixteen 508-coupled positions as described in Figure 2C. Band C and Band B from three independent experiments were quantified by densitometry and plotted using common methods for comparisons of mature CFTR. (B) Plot of normalized ratios Band C/Band B red filled circles and linear fit, and of Band C/Total (Band B + Band C) blue filled circles and fit. (C) Total CFTR as measured by ELISA linearly correlates with relative quantity of Band C, as do total CFTR as measured by densitometry and mature CFTR protein as measured by cell surface biotinylation. (D) Statistical parameters for the five. W496V CFTR has the lowest quantity of Band C, and is significantly different from $\Delta F508$ CFTR, p -value < 0.05 , for three of the five methods; Band C/Band B, Band C/Total, and ELISA.

Table S1. Crystallographic and Refinement Data for the Murine DF508 Structure.

Parameter	Value
Space Group	P4 ₂ ,2
Unit cell dimensions (Å)	170.5
a	
b	170.5
c	109.4
a, b, g (°)	90, 90, 90
Resolution (Å)	44.9-2.25 (2.28-2.25)*
Completeness (%)	100 (100)
Multiplicity	11.2 (11.3)
Unique reflections	76,676 (2,535)
$R_{\text{merge}}^{\dagger}$	0.074 (0.858)
I/s_1	34.4 (2.7)
Wilson B (Å ²)	45.7
Refinement	
Resolution (Å)	49.8-2.25
No. non-solvent atoms	8,505
No. solvent atoms	291
Cutoff F_o/s_{F_o}	0
Avg. B-factors	
non-solvent (Å ²)	52.8

solvent (Å ²)	45.3
R-values	0.181
<i>R_{work}</i>	
<i>R_{free}</i>	0.227
Ramachandran statistics[§]	0.0
outliers (%)	
most favored region (%)	96.9
r.m.s. deviations	0.007
Bonds (Å)	
Angles (°)	1.1

*Values in parentheses are for the highest resolution shell.

[†] $R_{sym} = \frac{\sum_h \sum_i |I_{h,i} - \langle I_h \rangle|}{\sum_h \sum_i I_{h,i}}$ where the outer sum (h) is over the unique reflections and the inner sum (i) is over the set of independent observations of each unique reflection.

[§]From MolProbity (Davis et al., 2007).

Table S2. Impact of Suppressor Mutations on Δ F508 NBD1 Folding, Maturation.

		Relative Yield NBD1 (β -gal.) (n)	Relative Yield CFTR (ELISA) (n)	Relative Conductance (10 μ M Forskolin + 100 μ IBMX) (n=3)	Relative Conductance (10 μ M Forskolin + 100 μ M IBMX + 20 μ M Inh-172) (n=3)	Current Density (pA/pF) (10 μ M Forskolin + 100 μ IBMX) (n)	Current Density (pA/pF) (10 μ M Forskolin + 100 μ M IBMX + 10 μ M Inh-172) (n)
WT	WT	1.00 \pm .03 (18)	1.00 \pm .03 (6)	1.00 \pm 0.05	0.18 \pm 0.13	82 \pm 2 (5)	1.1 \pm 0.1 (5)
	Δ F508	0.43 \pm 0.03 (18)	0.11 \pm .01 (6)	0.17 \pm 0.03	0.22 \pm 0.03	1.7 \pm 0.1 (5)	0.4 \pm 0.2 (4)
	R1070W	N/A	0.22 \pm .02 (3)	0.47 \pm 0.03	0.21 \pm 0.10		
Δ F508	I539T	0.79 \pm .03 (9)	0.14 \pm 0.01 (3)	0.21 \pm 0.08	0.29 \pm 0.10	0.38 \pm 0.03 (6)	0.23 \pm 0.05 (6)
	G550E	0.78 \pm .03 (9)	0.17 \pm 0.02 (3)				
	R553M	0.59 \pm .06 (9)	0.11 \pm 0.01 (3)				
	R555K	1.03 \pm .06 (9)	0.18 \pm 0.01 (3)	0.25 \pm 0.05	0.22 \pm 0.03	18 \pm 6 (6)	0.46 \pm 0.05 (6)
	G550E- R553M- R555K (3M)	0.67 \pm .0 (9)	0.16 \pm 0.01 (3)				
	R1070W	N/A	0.17 \pm 0.03 (3)	0.48 \pm 0.07	0.21 \pm 0.10	27 \pm 9 (5)	1.1 \pm 0.2 (5)
Δ F508- R1070W	I539T	N/A	0.76 \pm 0.03 (6)	1.71 \pm 0.23	0.35 \pm 0.10	88 \pm 8 (6)	1.2 \pm 0.1 (6)
	G550E	N/A	0.35 \pm 0.03 (6)				
	R553M	N/A	0.20 \pm 0.02 (6)				
	R555K	N/A	0.62 \pm 0.04 (6)	1.90 \pm 0.42	0.31 \pm 0.06	76 \pm 5 (6)	0.8 \pm 0.2 (6)
	G550E- R553M- R555K (3M)	N/A	0.84 \pm 0.06 (6)				

Bibliography

- Accurso, F.J., Rowe, S.M., Clancy, J.P., Boyle, M.P., Dunitz, J.M., Durie, P.R., Sagel, S.D., Hornick, D.B., Konstan, M.W., Donaldson, S.H., *et al.* (2010a). Effect of VX-770 in persons with cystic fibrosis and the G551D-CFTR mutation. *N Engl J Med* 363, 1991-2003.
- Accurso, F.J., Rowe, S.M., Clancy, J.P., Boyle, M.P., Dunitz, J.M., Durie, P.R., Sagel, S.D., Hornick, D.B., Konstan, M.W., Donaldson, S.H., *et al.* (2010b). Effect of VX-770 in persons with cystic fibrosis and the G551D-CFTR mutation. *The New England journal of medicine* 363, 1991-2003.
- Adams, P.D., Afonine, P.V., Bunkóczi, G., Chen, V.B., Davis, I.W., Echols, N., Headd, J.J., Hung, W., Kapral, G.J., Grosse-Kunstleve, R.W., *et al.* (2010). PHENIX: a comprehensive Python-based system for macromolecular structure determination. *Acta Crystallographica D* 66, 213-221.
- Aller, S.G., Yu, J., Ward, A., Weng, Y., Chittaboina, S., Zhuo, R., Harrell, P.M., Trinh, Y.T., Zhang, Q., Urbatsch, I.L., *et al.* (2009). Structure of P-glycoprotein reveals a molecular basis for poly-specific drug binding. *Science* 323, 1718-1722.
- Altschul, S.F., Madden, T.L., Schaffer, A.A., Zhang, J., Zhang, Z., Miller, W., and Lipman, D.J. (1997). Gapped BLAST and PSI-BLAST: a new generation of protein database search programs. *Nucleic acids research* 25, 3389-3402.
- Araujo, F.G., Novaes, F.C., Santos, N.P., Martins, V.C., Souza, S.M., Santos, S.E., and Ribeiro-dos-Santos, A.K. (2005). Prevalence of deltaF508, G551D, G542X, and R553X mutations among cystic fibrosis patients in the North of Brazil. *Braz J Med Biol Res* 38, 11-15.
- Atwell, S., Brouillette, C.G., Conners, K., Emtage, S., Gheyi, T., Guggino, W.B., Hendle, J., Hunt, J.F., Lewis, H.A., Lu, F., *et al.* Structures of a minimal human CFTR first nucleotide-binding domain as a monomer, head-to-tail homodimer, and pathogenic mutant. *Protein Eng Des Sel*.
- Atwell, S., Brouillette, C.G., Conners, K., Emtage, S., Gheyi, T., Guggino, W.B., Hendle, J., Hunt, J.F., Lewis, H.A., Lu, F., *et al.* (2010). Structures of a minimal human CFTR first nucleotide-binding domain as a monomer, head-to-tail homodimer, and pathogenic mutant. *Protein Eng Des Sel* 23, 375-384.
- Awayn, N.H., Rosenberg, M.F., Kamis, A.B., Aleksandrov, L.A., Riordan, J.R., and Ford, R.C. (2005). Crystallographic and single-particle analyses of native- and nucleotide-bound forms of the cystic fibrosis transmembrane conductance regulator (CFTR) protein. *Biochemical Society transactions* 33, 996-999.
- Baker, J.M., Hudson, R.P., Kanelis, V., Choy, W.Y., Thibodeau, P.H., Thomas, P.J., and Forman-Kay, J.D. (2007). CFTR regulatory

- region interacts with NBD1 predominantly via multiple transient helices. *Nat Struct Mol Biol* *14*, 738-745.
- Berger, A.L., Ikuma, M., and Welsh, M.J. (2005). Normal gating of CFTR requires ATP binding to both nucleotide-binding domains and hydrolysis at the second nucleotide-binding domain. *Proc Natl Acad Sci U S A* *102*, 455-460.
- Biemans-Oldehinkel, E., Doeven, M.K., and Poolman, B. (2006). ABC transporter architecture and regulatory roles of accessory domains. *FEBS Lett* *580*, 1023-1035.
- Bompadre, S.G., Li, M., and Hwang, T.C. (2008). Mechanism of G551D-CFTR (cystic fibrosis transmembrane conductance regulator) potentiation by a high affinity ATP analog. *J Biol Chem* *283*, 5364-5369.
- Bompadre, S.G., Sohma, Y., Li, M., and Hwang, T.C. (2007). G551D and G1349D, two CF-associated mutations in the signature sequences of CFTR, exhibit distinct gating defects. *J Gen Physiol* *129*, 285-298.
- Briggs, D., Stephens, C., Vaughan, R., Welsh, K., and Black, C. (1993). A molecular and serologic analysis of the major histocompatibility complex and complement component C4 in systemic sclerosis. *Arthritis Rheum* *36*, 943-954.
- Brown, C.R., Hong-Brown, L.Q., Biwersi, J., Verkman, A.S., and Welch, W.J. (1996). Chemical chaperones correct the mutant phenotype of the delta F508 cystic fibrosis transmembrane conductance regulator protein. *Cell stress & chaperones* *1*, 117-125.
- Bulteau-Pignoux, L., Derand, R., Metaye, T., Joffre, M., and Becq, F. (2002). Genistein modifies the activation kinetics and magnitude of phosphorylated wild-type and G551D-CFTR chloride currents. *J Membr Biol* *188*, 175-182.
- Cai, Z., Taddei, A., and Sheppard, D.N. (2006). Differential sensitivity of the cystic fibrosis (CF)-associated mutants G551D and G1349D to potentiators of the cystic fibrosis transmembrane conductance regulator (CFTR) Cl⁻ channel. *J Biol Chem* *281*, 1970-1977.
- Cashman, S.M., Patino, A., Martinez, A., Garcia-Delgado, M., Miedzybrodzka, Z., Schwarz, M., Shrimpton, A., Ferec, C., Raguene, O., Macek, M., Jr., *et al.* (1995). Identical intragenic microsatellite haplotype found in cystic fibrosis chromosomes bearing mutation G551D in Irish, English, Scottish, Breton and Czech patients. *Hum Hered* *45*, 6-12.
- Chan, T.C., Chang, C.J., Koonchanok, N.M., and Geahlen, R.L. (1993). Selective inhibition of the growth of ras-transformed human bronchial epithelial cells by emodin, a protein-tyrosine kinase inhibitor. *Biochem Biophys Res Commun* *193*, 1152-1158.

- Chang, G., and Roth, C.B. (2001). Structure of MsbA from *E. coli*: a homolog of the multidrug resistance ATP binding cassette (ABC) transporters. *Science* 293, 1793-1800.
- Chang, G., Roth, C.B., Reyes, C.L., Pornillos, O., Chen, Y.J., and Chen, A.P. (2006). Retraction. *Science* 314, 1875.
- Chang, J.D., Xu, Y., Raychowdhury, M.K., and Ware, J.A. (1993a). Molecular cloning and expression of a cDNA encoding a novel isoenzyme of protein kinase C (nPKC). A new member of the nPKC family expressed in skeletal muscle, megakaryoblastic cells, and platelets. *J Biol Chem* 268, 14208-14214.
- Chang, X.B., Tabcharani, J.A., Hou, Y.X., Jensen, T.J., Kartner, N., Alon, N., Hanrahan, J.W., and Riordan, J.R. (1993b). Protein kinase A (PKA) still activates CFTR chloride channel after mutagenesis of all 10 PKA consensus phosphorylation sites. *J Biol Chem* 268, 11304-11311.
- Chang, Z.L., and Beezhold, D.H. (1993). Protein kinase C activation in human monocytes: regulation of PKC isoforms. *Immunology* 80, 360-366.
- Cheng, S.H., Gregory, R.J., Marshall, J., Paul, S., Souza, D.W., White, G.A., O'Riordan, C.R., and Smith, A.E. (1990). Defective intracellular transport and processing of CFTR is the molecular basis of most cystic fibrosis. *Cell* 63, 827-834.
- Choi, J.Y., Joo, N.S., Krouse, M.E., Wu, J.V., Robbins, R.C., Ianowski, J.P., Hanrahan, J.W., and Wine, J.J. (2007). Synergistic airway gland mucus secretion in response to vasoactive intestinal peptide and carbachol is lost in cystic fibrosis. *J Clin Invest* 117, 3118-3127.
- Clamp, M., Cuff, J., Searle, S.M., and Barton, G.J. (2004). The Jalview Java alignment editor. *Bioinformatics* 20, 426-427.
- Comer, D.M., Ennis, M., McDowell, C., Beattie, D., Rendall, J., Hall, V., and Elborn, J.S. (2009). Clinical phenotype of cystic fibrosis patients with the G551D mutation. *Qjm* 102, 793-798.
- Cotten, J.F., Ostedgaard, L.S., Carson, M.R., and Welsh, M.J. (1996). Effect of cystic fibrosis-associated mutations in the fourth intracellular loop of cystic fibrosis transmembrane conductance regulator. *J Biol Chem* 271, 21279-21284.
- Cui, L., Aleksandrov, L., Chang, X.B., Hou, Y.X., He, L., Hegedus, T., Gentzsch, M., Aleksandrov, A., Balch, W.E., and Riordan, J.R. (2007). Domain interdependence in the biosynthetic assembly of CFTR. *J Mol Biol* 365, 981-994.
- Cutting, G.R. (1993). Spectrum of mutations in cystic fibrosis. *J Bioenerg Biomembr* 25, 7-10.
- Dabovic, B.B., Radojkovic, D., Minic, P., Savic, J., and Savic, A. (1992). Frequency of the delta F508 deletion and G551D, R553X and G542X mutations in Yugoslav CF patients. *Hum Genet* 88, 699-700.

- Dannhoffer, L., Billet, A., Jollivet, M., Melin-Heschel, P., Faveau, C., and Becq, F. (2011). Stimulation of Wild-Type, F508del- and G551D-CFTR Chloride Channels by Non-Toxic Modified pyrrolo[2,3-b]pyrazine Derivatives. *Front Pharmacol* 2, 48.
- Dassa, E., and Hofnung, M. (1985). [Homologies between integral proteins of the inner membrane of binding protein transport systems in enterobacteria]. *Annales de l'Institut Pasteur* 136A, 281-288.
- Davies, M.V., Chang, H.W., Jacobs, B.L., and Kaufman, R.J. (1993). The E3L and K3L vaccinia virus gene products stimulate translation through inhibition of the double-stranded RNA-dependent protein kinase by different mechanisms. *J Virol* 67, 1688-1692.
- Davis, I.W., Leaver-Fay, A., Chen, V.B., Block, J.N., Kapral, G.J., Wang, X., Murray, L.W., Arendall, W.B., Snoeyink, J., Richardson, J.S., *et al.* (2007). MolProbity: all-atom contacts and structure validation for proteins and nucleic acids. *Nucleic Acids Research* 35, W375-W383.
- Dawson, R.J., Hollenstein, K., and Locher, K.P. (2007). Uptake or extrusion: crystal structures of full ABC transporters suggest a common mechanism. *Molecular microbiology* 65, 250-257.
- Dawson, R.J., and Locher, K.P. (2006). Structure of a bacterial multidrug ABC transporter. *Nature* 443, 180-185.
- Dawson, R.J., and Locher, K.P. (2007). Structure of the multidrug ABC transporter Sav1866 from *Staphylococcus aureus* in complex with AMP-PNP. *FEBS Lett* 581, 935-938.
- Dean, M., and Allikmets, R. (1995). Evolution of ATP-binding cassette transporter genes. *Curr Opin Genet Dev* 5, 779-785.
- Dean, M., and Annilo, T. (2005). Evolution of the ATP-binding cassette (ABC) transporter superfamily in vertebrates. *Annu Rev Genomics Hum Genet* 6, 123-142.
- DeCarvalho, A.C., Gansheroff, L.J., and Teem, J.L. (2002). Mutations in the nucleotide binding domain 1 signature motif region rescue processing and functional defects of cystic fibrosis transmembrane conductance regulator delta f508. *J Biol Chem* 277, 35896-35905.
- Dekker, J.P., Fodor, A., Aldrich, R.W., and Yellen, G. (2004). A perturbation-based method for calculating explicit likelihood of evolutionary co-variance in multiple sequence alignments. *Bioinformatics* 20, 1565-1572.
- Delaney, S.J., Alton, E.W., Smith, S.N., Lunn, D.P., Farley, R., Lovelock, P.K., Thomson, S.A., Hume, D.A., Lamb, D., Porteous, D.J., *et al.* (1996). Cystic fibrosis mice carrying the missense mutation G551D replicate human genotype-phenotype correlations. *Embo J* 15, 955-963.

- Denning, G.M., Anderson, M.P., Amara, J.F., Marshall, J., Smith, A.E., and Welsh, M.J. (1992). Processing of mutant cystic fibrosis transmembrane conductance regulator is temperature-sensitive. *Nature* **358**, 761-764.
- Derand, R., Bulteau-Pignoux, L., and Becq, F. (2002). The cystic fibrosis mutation G551D alters the non-Michaelis-Menten behavior of the cystic fibrosis transmembrane conductance regulator (CFTR) channel and abolishes the inhibitory Genistein binding site. *J Biol Chem* **277**, 35999-36004.
- Derand, R., Bulteau-Pignoux, L., and Becq, F. (2003). Comparative pharmacology of the activity of wild-type and G551D mutated CFTR chloride channel: effect of the benzimidazolone derivative NS004. *J Membr Biol* **194**, 109-117.
- Derand, R., Bulteau-Pignoux, L., Mettey, Y., Zegarra-Moran, O., Howell, L.D., Randak, C., Galiotta, L.J., Cohn, J.A., Norez, C., Romio, L., *et al.* (2001). Activation of G551D CFTR channel with MPB-91: regulation by ATPase activity and phosphorylation. *American journal of physiology Cell physiology* **281**, C1657-1666.
- Devor, D.C., Bridges, R.J., and Pilewski, J.M. (2000). Pharmacological modulation of ion transport across wild-type and DeltaF508 CFTR-expressing human bronchial epithelia. *American journal of physiology* **279**, C461-479.
- Doige, C.A., and Ames, G.F. (1993). ATP-dependent transport systems in bacteria and humans: relevance to cystic fibrosis and multidrug resistance. *Annual review of microbiology* **47**, 291-319.
- Dork, T., Wulbrand, U., Richter, T., Neumann, T., Wolfes, H., Wulf, B., Maass, G., and Tummeler, B. (1991). Cystic fibrosis with three mutations in the cystic fibrosis transmembrane conductance regulator gene. *Hum Genet* **87**, 441-446.
- Du, K., Sharma, M., and Lukacs, G.L. (2005). The DeltaF508 cystic fibrosis mutation impairs domain-domain interactions and arrests post-translational folding of CFTR. *Nat Struct Mol Biol* **12**, 17-25.
- Duthie, A., Doherty, D.G., Williams, C., Scott-Jupp, R., Warner, J.O., Tanner, M.S., Williamson, R., and Mowat, A.P. (1992). Genotype analysis for delta F508, G551D and R553X mutations in children and young adults with cystic fibrosis with and without chronic liver disease. *Hepatology* **15**, 660-664.
- Emsley, P., and Cowtan, K. (2004). Coot: Model-building tools for molecular graphics. *Acta Crystallographica Section D: Biological Crystallography* **60**, 2126-2132.
- Fang, F.C., McClelland, M., Guiney, D.G., Jackson, M.M., Hartstein, A.I., Morthland, V.H., Davis, C.E., McPherson, D.C., and Welsh, J. (1993). Value of molecular epidemiologic analysis in a nosocomial methicillin-resistant *Staphylococcus aureus* outbreak. *Jama* **270**, 1323-1328.

- Fetsch, E.E., and Davidson, A.L. (2002). Vanadate-catalyzed photocleavage of the signature motif of an ATP-binding cassette (ABC) transporter. *Proc Natl Acad Sci U S A* 99, 9685-9690.
- Fodor, A.A., and Aldrich, R.W. (2004). Influence of conservation on calculations of amino acid covariance in multiple sequence alignments. *Proteins* 56, 211-221.
- French, S., and Wilson, K. (1978). On the treatment of negative intensity observations. *Acta Crystallographica Section A, Crystal Physics, Diffraction, Theoretical and General Crystallography* 34, 517-525.
- Fulmer, S.B., Schwiebert, E.M., Morales, M.M., Guggino, W.B., and Cutting, G.R. (1995). Two cystic fibrosis transmembrane conductance regulator mutations have different effects on both pulmonary phenotype and regulation of outwardly rectified chloride currents. *Proc Natl Acad Sci U S A* 92, 6832-6836.
- Goh, C.S., Bogan, A.A., Joachimiak, M., Walther, D., and Cohen, F.E. (2000). Co-evolution of proteins with their interaction partners. *J Mol Biol* 299, 283-293.
- Gregory, R.J., Rich, D.P., Cheng, S.H., Souza, D.W., Paul, S., Manavalan, P., Anderson, M.P., Welsh, M.J., and Smith, A.E. (1991). Maturation and function of cystic fibrosis transmembrane conductance regulator variants bearing mutations in putative nucleotide-binding domains 1 and 2. *Molecular and cellular biology* 11, 3886-3893.
- Higgins, C.F. (1992). ABC transporters: from microorganisms to man. *Annual review of cell biology* 8, 67-113.
- Hoelen, H., Kleizen, B., Schmidt, A., Richardson, J., Charitou, P., Thomas, P.J., and Braakman, I. (2010). The primary folding defect and rescue of DeltaF508 CFTR emerge during translation of the mutant domain. *PLoS One* 5, e15458.
- Hollenstein, K., Frei, D.C., and Locher, K.P. (2007). Structure of an ABC transporter in complex with its binding protein. *Nature* 446, 213-216.
- Hopfner, K.P., Karcher, A., Shin, D.S., Craig, L., Arthur, L.M., Carney, J.P., and Tainer, J.A. (2000). Structural biology of Rad50 ATPase: ATP-driven conformational control in DNA double-strand break repair and the ABC-ATPase superfamily. *Cell* 101, 789-800.
- Howell, L.D., Borchardt, R., and Cohn, J.A. (2000). ATP hydrolysis by a CFTR domain: pharmacology and effects of G551D mutation. *Biochem Biophys Res Commun* 271, 518-525.
- Huang, S.Y., Bolser, D., Liu, H.Y., Hwang, T.C., and Zou, X. (2009). Molecular modeling of the heterodimer of human CFTR's nucleotide-binding domains using a protein-protein docking approach. *Journal of molecular graphics & modelling* 27, 822-828.

- Hung, L.W., Wang, I.X., Nikaido, K., Liu, P.Q., Ames, G.F., and Kim, S.H. (1998). Crystal structure of the ATP-binding subunit of an ABC transporter. *Nature* 396, 703-707.
- Hutt, D.M., Herman, D., Rodrigues, A.P., Noel, S., Pilewski, J.M., Matteson, J., Hoch, B., Kellner, W., Kelly, J.W., Schmidt, A., *et al.* Reduced histone deacetylase 7 activity restores function to misfolded CFTR in cystic fibrosis. *Nature chemical biology* 6, 25-33.
- Illek, B., Zhang, L., Lewis, N.C., Moss, R.B., Dong, J.Y., and Fischer, H. (1999). Defective function of the cystic fibrosis-causing missense mutation G551D is recovered by genistein. *The American journal of physiology* 277, C833-839.
- Jobin, R.M., Ginsberg, J., Matowe, W.C., and Chang, J.P. (1993). Downregulation of protein kinase C levels leads to inhibition of GnRH-stimulated gonadotropin secretion from dispersed pituitary cells of goldfish. *Neuroendocrinology* 58, 2-10.
- Jones, P.M., and George, A.M. (1999). Subunit interactions in ABC transporters: towards a functional architecture. *FEMS microbiology letters* 179, 187-202.
- Jones, P.M., and George, A.M. (2004). The ABC transporter structure and mechanism: perspectives on recent research. *Cell Mol Life Sci* 61, 682-699.
- Kanelis, V., Hudson, R.P., Thibodeau, P.H., Thomas, P.J., and Forman-Kay, J.D. NMR evidence for differential phosphorylation-dependent interactions in WT and DeltaF508 CFTR. *Embo J* 29, 263-277.
- Kass, I., and Horovitz, A. (2002). Mapping pathways of allosteric communication in GroEL by analysis of correlated mutations. *Proteins* 48, 611-617.
- Kleizen, B., van Vlijmen, T., de Jonge, H.R., and Braakman, I. (2005). Folding of CFTR is predominantly cotranslational. *Molecular cell* 20, 277-287.
- Ko, F.N., Chang, Y.L., Kuo, Y.H., Lin, Y.L., and Teng, C.M. (1993). Daphnoretin, a new protein kinase C activator isolated from *Wikstroemia indica* C.A. Mey. *Biochem J* 295 (Pt 1), 321-327.
- Ko, S.B., Zeng, W., Dorwart, M.R., Luo, X., Kim, K.H., Millen, L., Goto, H., Naruse, S., Soyombo, A., Thomas, P.J., *et al.* (2004). Gating of CFTR by the STAS domain of SLC26 transporters. *Nature cell biology* 6, 343-350.
- Krasnov, K.V., Tzetis, M., Cheng, J., Guggino, W.B., and Cutting, G.R. (2008). Localization studies of rare missense mutations in cystic fibrosis transmembrane conductance regulator (CFTR) facilitate interpretation of genotype-phenotype relationships. *Hum Mutat* 29, 1364-1372.
- Kuchynkova, Z., Macek, M., Jr., Holcat, M., and Macek, M. (1995). [Detection of the G551D mutation in a patient with nasal polyps]. *Cas Lek Cesk* 134, 212-213.

- Kunichika, K., Hashimoto, Y., and Imoto, T. (2002). Robustness of hen lysozyme monitored by random mutations. *Protein Eng* 15, 805-809.
- Kunzelmann, K., Kiser, G.L., Schreiber, R., and Riordan, J.R. (1997). Inhibition of epithelial Na⁺ currents by intracellular domains of the cystic fibrosis transmembrane conductance regulator. *FEBS Lett* 400, 341-344.
- Larkin, M.A., Blackshields, G., Brown, N.P., Chenna, R., McGettigan, P.A., McWilliam, H., Valentin, F., Wallace, I.M., Wilm, A., Lopez, R., *et al.* (2007). Clustal W and Clustal X version 2.0. *Bioinformatics* 23, 2947-2948.
- Leslie, E.M., Deeley, R.G., and Cole, S.P. (2001). Toxicological relevance of the multidrug resistance protein 1, MRP1 (ABCC1) and related transporters. *Toxicology* 167, 3-23.
- Lewis, H.A., Buchanan, S.G., Burley, S.K., Conners, K., Dickey, M., Dorwart, M., Fowler, R., Gao, X., Guggino, W.B., Hendrickson, W.A., *et al.* (2004a). Structure of nucleotide-binding domain 1 of the cystic fibrosis transmembrane conductance regulator. *EMBO Journal* 23, 282-293.
- Lewis, H.A., Buchanan, S.G., Burley, S.K., Conners, K., Dickey, M., Dorwart, M., Fowler, R., Gao, X., Guggino, W.B., Hendrickson, W.A., *et al.* (2004b). Structure of nucleotide-binding domain 1 of the cystic fibrosis transmembrane conductance regulator. *Embo J* 23, 282-293.
- Lewis, H.A., Wang, C., Zhao, X., Hamuro, Y., Conners, K., Kearins, M.C., Lu, F., Sauder, J.M., Molnar, K.S., Coales, S.J., *et al.* Structure and dynamics of NBD1 from CFTR characterized using crystallography and hydrogen/deuterium exchange mass spectrometry. *J Mol Biol* 396, 406-430.
- Lewis, H.A., Wang, C., Zhao, X., Hamuro, Y., Conners, K., Kearins, M.C., Lu, F., Sauder, J.M., Molnar, K.S., Coales, S.J., *et al.* (2010). Structure and dynamics of NBD1 from CFTR characterized using crystallography and hydrogen/deuterium exchange mass spectrometry. *J Mol Biol* 396, 406-430.
- Lewis, H.A., Zhao, X., Wang, C., Sauder, J.M., Rooney, I., Noland, B.W., Lorimer, D., Kearins, M.C., Conners, K., Condon, B., *et al.* (2005). Impact of the deltaF508 mutation in first nucleotide-binding domain of human cystic fibrosis transmembrane conductance regulator on domain folding and structure. *J Biol Chem* 280, 1346-1353.
- Linsdell, P., Zheng, S.X., and Hanrahan, J.W. (1998). Non-pore lining amino acid side chains influence anion selectivity of the human CFTR Cl⁻ channel expressed in mammalian cell lines. *The Journal of physiology* 512 (Pt 1), 1-16.

- Locher, K.P., Lee, A.T., and Rees, D.C. (2002). The E. coli BtuCD structure: a framework for ABC transporter architecture and mechanism. *Science* 296, 1091-1098.
- Lockless, S.W., and Ranganathan, R. (1999). Evolutionarily conserved pathways of energetic connectivity in protein families. *Science* 286, 295-299.
- Loo, T.W., Bartlett, M.C., and Clarke, D.M. (2002). The "LSGGQ" motif in each nucleotide-binding domain of human P-glycoprotein is adjacent to the opposing walker A sequence. *J Biol Chem* 277, 41303-41306.
- Lu, L., Wang, L.S., Cooper, R.J., Liu, H.J., Turner, K., Weich, N., and Broxmeyer, H.E. (2000). Suppressive effects of TNF-alpha, TGF-beta1, and chemokines on megakaryocytic colony formation in CD34+ cells derived from umbilical cord blood compared with mobilized peripheral blood and bone marrow. *J Hematother Stem Cell Res* 9, 195-204.
- Lukacs, G.L., Mohamed, A., Kartner, N., Chang, X.B., Riordan, J.R., and Grinstein, S. (1994). Conformational maturation of CFTR but not its mutant counterpart (delta F508) occurs in the endoplasmic reticulum and requires ATP. *Embo J* 13, 6076-6086.
- Madaoui, H., and Guerois, R. (2008). Coevolution at protein complex interfaces can be detected by the complementarity trace with important impact for predictive docking. *Proc Natl Acad Sci U S A* 105, 7708-7713.
- Mall, M., Bleich, M., Kuehr, J., Brandis, M., Greger, R., and Kunzelmann, K. (1999). CFTR-mediated inhibition of epithelial Na+ conductance in human colon is defective in cystic fibrosis. *The American journal of physiology* 277, G709-716.
- Matthews, B.W. (2007). Five retracted structure reports: inverted or incorrect? *Protein Sci* 16, 1013-1016.
- McCarty, N.A. (2000). Permeation through the CFTR chloride channel. *J Exp Biol* 203, 1947-1962.
- McLachlan, A.D. (1971). Tests for comparing related amino-acid sequences. Cytochrome c and cytochrome c 551. *J Mol Biol* 61, 409-424.
- McMorrán, B.J., Palmer, J.S., Lunn, D.P., Oceandy, D., Costelloe, E.O., Thomas, G.R., Hume, D.A., and Wainwright, B.J. (2001). G551D CF mice display an abnormal host response and have impaired clearance of Pseudomonas lung disease. *Am J Physiol Lung Cell Mol Physiol* 281, L740-747.
- Mendoza, J.L., and Thomas, P.J. (2007). Building an understanding of cystic fibrosis on the foundation of ABC transporter structures. *J Bioenerg Biomembr* 39, 499-505.
- Moody, J.E., Millen, L., Binns, D., Hunt, J.F., and Thomas, P.J. (2002). Cooperative, ATP-dependent association of the nucleotide

- binding cassettes during the catalytic cycle of ATP-binding cassette transporters. *J Biol Chem* 277, 21111-21114.
- Moran, O. Model of the cAMP activation of chloride transport by CFTR channel and the mechanism of potentiators. *Journal of theoretical biology* 262, 73-79.
- Mornon, J.P., Lehn, P., and Callebaut, I. (2009). Molecular models of the open and closed states of the whole human CFTR protein. *Cell Mol Life Sci* 66, 3469-3486.
- Murzin, A.G., Brenner, S.E., Hubbard, T., and Chothia, C. (1995). SCOP: a structural classification of proteins database for the investigation of sequences and structures. *J Mol Biol* 247, 536-540.
- Nikaido, K., Liu, P.Q., and Ames, G.F. (1997). Purification and characterization of HisP, the ATP-binding subunit of a traffic ATPase (ABC transporter), the histidine permease of *Salmonella typhimurium*. Solubility, dimerization, and ATPase activity. *J Biol Chem* 272, 27745-27752.
- Noel, S., Faveau, C., Norez, C., Rogier, C., Mettey, Y., and Becq, F. (2006). Discovery of pyrrolo[2,3-b]pyrazines derivatives as submicromolar affinity activators of wild type, G551D, and F508del cystic fibrosis transmembrane conductance regulator chloride channels. *J Pharmacol Exp Ther* 319, 349-359.
- Oceandy, D., McMorran, B., Schreiber, R., Wainwright, B.J., and Kunzelmann, K. (2003). GFP-tagged CFTR transgene is functional in the G551D cystic fibrosis mouse colon. *J Membr Biol* 192, 159-167.
- Olmea, O., and Valencia, A. (1997). Improving contact predictions by the combination of correlated mutations and other sources of sequence information. *Fold Des* 2, S25-32.
- Orengo, C.A., Michie, A.D., Jones, S., Jones, D.T., Swindells, M.B., and Thornton, J.M. (1997). CATH--a hierarchic classification of protein domain structures. *Structure* 5, 1093-1108.
- Otwinowski, Z., and Minor, W. (1997). Processing of X-ray diffraction data collected in oscillation mode. *Methods in Enzymology* 276, 307-326.
- Parad, R.B. (1996). Heterogeneity of phenotype in two cystic fibrosis patients homozygous for the CFTR exon 11 mutation G551D. *J Med Genet* 33, 711-713.
- Pasyk, S., Li, C., Ramjeesingh, M., and Bear, C.E. (2009). Direct interaction of a small-molecule modulator with G551D-CFTR, a cystic fibrosis-causing mutation associated with severe disease. *Biochem J* 418, 185-190.
- Pazos, F., and Valencia, A. (2008). Protein co-evolution, co-adaptation and interactions. *Embo J* 27, 2648-2655.
- Pedemonte, N., Lukacs, G.L., Du, K., Caci, E., Zegarra-Moran, O., Galletta, L.J., and Verkman, A.S. (2005a). Small-molecule correctors of defective DeltaF508-CFTR cellular processing

- identified by high-throughput screening. *J Clin Invest* 115, 2564-2571.
- Pedemonte, N., Sonawane, N.D., Taddei, A., Hu, J., Zegarra-Moran, O., Suen, Y.F., Robins, L.I., Dicus, C.W., Willenbring, D., Nantz, M.H., *et al.* (2005b). Phenylglycine and sulfonamide correctors of defective delta F508 and G551D cystic fibrosis transmembrane conductance regulator chloride-channel gating. *Molecular pharmacology* 67, 1797-1807.
- Pei, J., and Grishin, N.V. (2001). AL2CO: calculation of positional conservation in a protein sequence alignment. *Bioinformatics* 17, 700-712.
- Pei, J., Kim, B.H., and Grishin, N.V. (2008a). PROMALS3D: a tool for multiple protein sequence and structure alignments. *Nucleic acids research* 36, 2295-2300.
- Pei, J., Tang, M., and Grishin, N.V. (2008b). PROMALS3D web server for accurate multiple protein sequence and structure alignments. *Nucleic acids research* 36, W30-34.
- Pissarra, L.S., Farinha, C.M., Xu, Z., Schmidt, A., Thibodeau, P.H., Cai, Z., Thomas, P.J., Sheppard, D.N., and Amaral, M.D. (2008). Solubilizing mutations used to crystallize one CFTR domain attenuate the trafficking and channel defects caused by the major cystic fibrosis mutation. *Chem Biol* 15, 62-69.
- Pjura, P., Matsumura, M., Baase, W.A., and Matthews, B.W. (1993). Development of an in vivo method to identify mutants of phage T4 lysozyme of enhanced thermostability. *Protein Sci* 2, 2217-2225.
- Protasevich, I., Yang, Z., Wang, C., Atwell, S., Zhao, X., Emtage, S., Wetmore, D., Hunt, J.F., and Brouillette, C.G. (2010). Thermal unfolding studies show the disease causing F508del mutation in CFTR thermodynamically destabilizes nucleotide-binding domain 1. *Protein Sci* 19, 1917-1931.
- Qu, B.H., Strickland, E., and Thomas, P.J. (1997a). Cystic fibrosis: a disease of altered protein folding. *J Bioenerg Biomembr* 29, 483-490.
- Qu, B.H., Strickland, E.H., and Thomas, P.J. (1997b). Localization and suppression of a kinetic defect in cystic fibrosis transmembrane conductance regulator folding. *J Biol Chem* 272, 15739-15744.
- Qu, B.H., and Thomas, P.J. (1996). Alteration of the cystic fibrosis transmembrane conductance regulator folding pathway. *J Biol Chem* 271, 7261-7264.
- Quinton, P.M., and Reddy, M.M. (1992). Control of CFTR chloride conductance by ATP levels through non-hydrolytic binding. *Nature* 360, 79-81.
- Reiss, J., Ellermeyer, U., Schloesser, M., Fuhrmann, W., Drews, D., and Posselt, H.G. (1993). Two cystic fibrosis patients with the genotype G542X/G551D. *Hum Genet* 91, 78-79.

- Reyes, C.L., and Chang, G. (2005). Structure of the ABC transporter MsbA in complex with ADP.vanadate and lipopolysaccharide. *Science* 308, 1028-1031.
- Rich, D.P., Anderson, M.P., Gregory, R.J., Cheng, S.H., Paul, S., Jefferson, D.M., McCann, J.D., Klinger, K.W., Smith, A.E., and Welsh, M.J. (1990). Expression of cystic fibrosis transmembrane conductance regulator corrects defective chloride channel regulation in cystic fibrosis airway epithelial cells. *Nature* 347, 358-363.
- Riordan, J.R. (2008). CFTR function and prospects for therapy. *Annual review of biochemistry* 77, 701-726.
- Riordan, J.R., Rommens, J.M., Kerem, B., Alon, N., Rozmahel, R., Grzelczak, Z., Zielenski, J., Lok, S., Plavsic, N., Chou, J.L., *et al.* (1989). Identification of the cystic fibrosis gene: cloning and characterization of complementary DNA. *Science* 245, 1066-1073.
- Robert, R., Carlile, G.W., Liao, J., Balghi, H., Lesimple, P., Liu, N., Kus, B., Rotin, D., Wilke, M., de Jonge, H.R., *et al.* (2010). Correction of the Delta phe508 cystic fibrosis transmembrane conductance regulator trafficking defect by the bioavailable compound glafenine. *Mol Pharmacol* 77, 922-930.
- Robert, R., Carlile, G.W., Pavel, C., Liu, N., Anjos, S.M., Liao, J., Luo, Y., Zhang, D., Thomas, D.Y., and Hanrahan, J.W. (2008). Structural analog of sildenafil identified as a novel corrector of the F508del-CFTR trafficking defect. *Mol Pharmacol* 73, 478-489.
- Rosenberg, M.F., Kamis, A.B., Aleksandrov, L.A., Ford, R.C., and Riordan, J.R. (2004). Purification and crystallization of the cystic fibrosis transmembrane conductance regulator (CFTR). *J Biol Chem* 279, 39051-39057.
- Roxo-Rosa, M., Xu, Z., Schmidt, A., Neto, M., Cai, Z., Soares, C.M., Sheppard, D.N., and Amaral, M.D. (2006). Revertant mutants G550E and 4RK rescue cystic fibrosis mutants in the first nucleotide-binding domain of CFTR by different mechanisms. *Proc Natl Acad Sci U S A* 103, 17891-17896.
- Sampson, H.M., Robert, R., Liao, J., Matthes, E., Carlile, G.W., Hanrahan, J.W., and Thomas, D.Y. (2011). Identification of a NBD1-binding pharmacological chaperone that corrects the trafficking defect of F508del-CFTR. *Chem Biol* 18, 231-242.
- Sanguolo, F., Maceratesi, P., Mesoraca, A., Botta, A., Cavicchini, A., Novelli, G., and Dallapiccola, B. (1995). Simultaneous detection of delta F508, G542X, N1303K, G551D, and 1717-1G-->A cystic fibrosis alleles by a multiplex DNA enzyme immunoassay. *Int J Clin Lab Res* 25, 142-145.
- Saraste, M., Sibbald, P.R., and Wittinghofer, A. (1990). The P-loop--a common motif in ATP- and GTP-binding proteins. *Trends in biochemical sciences* 15, 430-434.

- Saurin, W., and Dassa, E. (1994). Sequence relationships between integral inner membrane proteins of binding protein-dependent transport systems: evolution by recurrent gene duplications. *Protein Sci* 3, 325-344.
- Schmitt, L., and Tampe, R. (2002). Structure and mechanism of ABC transporters. *Current opinion in structural biology* 12, 754-760.
- Schreiber, R., Hopf, A., Mall, M., Greger, R., and Kunzelmann, K. (1999). The first-nucleotide binding domain of the cystic-fibrosis transmembrane conductance regulator is important for inhibition of the epithelial Na⁺ channel. *Proc Natl Acad Sci U S A* 96, 5310-5315.
- Schrodinger, LLC (2010). The PyMOL Molecular Graphics System, Version 1.3r1.
- Seibert, F.S., Linsdell, P., Loo, T.W., Hanrahan, J.W., Riordan, J.R., and Clarke, D.M. (1996). Cytoplasmic loop three of cystic fibrosis transmembrane conductance regulator contributes to regulation of chloride channel activity. *J Biol Chem* 271, 27493-27499.
- Serohijos, A.W., Hegedus, T., Aleksandrov, A.A., He, L., Cui, L., Dokholyan, N.V., and Riordan, J.R. (2008). Phenylalanine-508 mediates a cytoplasmic-membrane domain contact in the CFTR 3D structure crucial to assembly and channel function. *Proc Natl Acad Sci U S A* 105, 3256-3261.
- Sheppard, D.N., Rich, D.P., Ostedgaard, L.S., Gregory, R.J., Smith, A.E., and Welsh, M.J. (1993). Mutations in CFTR associated with mild-disease-form Cl⁻ channels with altered pore properties. *Nature* 362, 160-164.
- Smith, P.C., Karpowich, N., Millen, L., Moody, J.E., Rosen, J., Thomas, P.J., and Hunt, J.F. (2002). ATP binding to the motor domain from an ABC transporter drives formation of a nucleotide sandwich dimer. *Molecular cell* 10, 139-149.
- Smith, S.N., Delaney, S.J., Dorin, J.R., Farley, R., Geddes, D.M., Porteous, D.J., Wainwright, B.J., and Alton, E.W. (1998). Effect of IBMX and alkaline phosphatase inhibitors on Cl⁻ secretion in G551D cystic fibrosis mutant mice. *The American journal of physiology* 274, C492-499.
- Socolich, M., Lockless, S.W., Russ, W.P., Lee, H., Gardner, K.H., and Ranganathan, R. (2005). Evolutionary information for specifying a protein fold. *Nature* 437, 512-518.
- Sonnhammer, E.L., Eddy, S.R., and Durbin, R. (1997). Pfam: a comprehensive database of protein domain families based on seed alignments. *Proteins* 28, 405-420.
- Stagg, S.M., LaPointe, P., Razvi, A., Gurkan, C., Potter, C.S., Carragher, B., and Balch, W.E. (2008). Structural basis for cargo regulation of COPII coat assembly. *Cell* 134, 474-484.
- Story, R.M., Weber, I.T., and Steitz, T.A. (1992). The structure of the E. coli recA protein monomer and polymer. *Nature* 355, 318-325.

- Stratford, F.L., Ramjeesingh, M., Cheung, J.C., Huan, L.J., and Bear, C.E. (2007). The Walker B motif of the second nucleotide-binding domain (NBD2) of CFTR plays a key role in ATPase activity by the NBD1-NBD2 heterodimer. *Biochem J* 401, 581-586.
- Suaud, L., Carattino, M., Kleyman, T.R., and Rubenstein, R.C. (2002). Genistein improves regulatory interactions between G551D-cystic fibrosis transmembrane conductance regulator and the epithelial sodium channel in *Xenopus* oocytes. *J Biol Chem* 277, 50341-50347.
- Teem, J.L., Berger, H.A., Ostedgaard, L.S., Rich, D.P., Tsui, L.C., and Welsh, M.J. (1993). Identification of revertants for the cystic fibrosis delta F508 mutation using STE6-CFTR chimeras in yeast. *Cell* 73, 335-346.
- Teem, J.L., Carson, M.R., and Welsh, M.J. (1996). Mutation of R555 in CFTR-delta F508 enhances function and partially corrects defective processing. *Receptors Channels* 4, 63-72.
- Thibodeau, P.H., Brautigam, C.A., Machius, M., and Thomas, P.J. (2005). Side chain and backbone contributions of Phe508 to CFTR folding. *Nat Struct Mol Biol* 12, 10-16.
- Thibodeau, P.H., Richardson, J.M., 3rd, Wang, W., Millen, L., Watson, J., Mendoza, J.L., Du, K., Fischman, S., Senderowitz, H., Lukacs, G.L., *et al.* (2010). The cystic fibrosis-causing mutation deltaF508 affects multiple steps in cystic fibrosis transmembrane conductance regulator biogenesis. *J Biol Chem* 285, 35825-35835.
- Thomas, G.R., Costelloe, E.A., Lunn, D.P., Stacey, K.J., Delaney, S.J., Passey, R., McGlenn, E.C., McMorran, B.J., Ahadizadeh, A., Geczy, C.L., *et al.* (2000). G551D cystic fibrosis mice exhibit abnormal regulation of inflammation in lungs and macrophages. *J Immunol* 164, 3870-3877.
- Thomas, P.J., Ko, Y.H., and Pedersen, P.L. (1992a). Altered protein folding may be the molecular basis of most cases of cystic fibrosis. *FEBS Lett* 312, 7-9.
- Thomas, P.J., Shenbagamurthi, P., Sondek, J., Hulihan, J.M., and Pedersen, P.L. (1992b). The cystic fibrosis transmembrane conductance regulator. Effects of the most common cystic fibrosis-causing mutation on the secondary structure and stability of a synthetic peptide. *J Biol Chem* 267, 5727-5730.
- Van Goor, F., Hadida, S., Grootenhuys, P.D., Burton, B., Cao, D., Neuberger, T., Turnbull, A., Singh, A., Joubran, J., Hazlewood, A., *et al.* (2009). Rescue of CF airway epithelial cell function in vitro by a CFTR potentiator, VX-770. *Proc Natl Acad Sci U S A* 106, 18825-18830.
- Van Goor, F., Straley, K.S., Cao, D., Gonzalez, J., Hadida, S., Hazlewood, A., Joubran, J., Knapp, T., Makings, L.R., Miller, M., *et al.* (2006). Rescue of DeltaF508-CFTR trafficking and gating in

- human cystic fibrosis airway primary cultures by small molecules. *Am J Physiol Lung Cell Mol Physiol* 290, L1117-1130.
- Vergani, P., Lockless, S.W., Nairn, A.C., and Gadsby, D.C. (2005). CFTR channel opening by ATP-driven tight dimerization of its nucleotide-binding domains. *Nature* 433, 876-880.
- Vergani, P., Nairn, A.C., and Gadsby, D.C. (2003). On the mechanism of MgATP-dependent gating of CFTR Cl⁻ channels. *J Gen Physiol* 121, 17-36.
- Walker, J.E., Saraste, M., Runswick, M.J., and Gay, N.J. (1982). Distantly related sequences in the alpha- and beta-subunits of ATP synthase, myosin, kinases and other ATP-requiring enzymes and a common nucleotide binding fold. *Embo J* 1, 945-951.
- Wang, C., Protasevich, I., Yang, Z., Seehausen, D., Skalak, T., Zhao, X., Atwell, S., Spencer Emtage, J., Wetmore, D.R., Brouillette, C.G., *et al.* (2010). Integrated biophysical studies implicate partial unfolding of NBD1 of CFTR in the molecular pathogenesis of F508del cystic fibrosis. *Protein Sci* 19, 1932-1947.
- Wang, X., Venable, J., LaPointe, P., Hutt, D.M., Koulov, A.V., Coppinger, J., Gurkan, C., Kellner, W., Matteson, J., Plutner, H., *et al.* (2006a). Hsp90 cochaperone Aha1 downregulation rescues misfolding of CFTR in cystic fibrosis. *Cell* 127, 803-815.
- Wang, Y., Soyombo, A.A., Shcheynikov, N., Zeng, W., Dorwart, M., Marino, C.R., Thomas, P.J., and Muallem, S. (2006b). Slc26a6 regulates CFTR activity in vivo to determine pancreatic duct HCO₃⁻ secretion: relevance to cystic fibrosis. *Embo J* 25, 5049-5057.
- Waterhouse, A.M., Procter, J.B., Martin, D.M., Clamp, M., and Barton, G.J. (2009). Jalview Version 2--a multiple sequence alignment editor and analysis workbench. *Bioinformatics* 25, 1189-1191.
- Wei, L., Vankeerberghen, A., Jaspers, M., Cassiman, J., Nilius, B., and Cuppens, H. (2000). Suppressive interactions between mutations located in the two nucleotide binding domains of CFTR. *FEBS Lett* 473, 149-153.
- Welsh, M.J., and Smith, A.E. (1993). Molecular mechanisms of CFTR chloride channel dysfunction in cystic fibrosis. *Cell* 73, 1251-1254.
- Wigley, W.C., Stidham, R.D., Smith, N.M., Hunt, J.F., and Thomas, P.J. (2001). Protein solubility and folding monitored in vivo by structural complementation of a genetic marker protein. *Nat Biotechnol* 19, 131-136.
- Wigley, W.C., Vijayakumar, S., Jones, J.D., Slaughter, C., and Thomas, P.J. (1998). Transmembrane domain of cystic fibrosis transmembrane conductance regulator: design, characterization, and secondary structure of synthetic peptides m1-m6. *Biochemistry* 37, 844-853.

- Younger, J.M., Fan, C.Y., Chen, L., Rosser, M.F., Patterson, C., and Cyr, D.M. (2005). Cystic fibrosis transmembrane conductance regulator as a model substrate to study endoplasmic reticulum protein quality control in mammalian cells. *Methods in molecular biology* (Clifton, NJ) *301*, 293-303.
- Yu, Y.C., Miki, H., Nakamura, Y., Hanyuda, A., Matsuzaki, Y., Abe, Y., Yasui, M., Tanaka, K., Hwang, T.C., Bompadre, S.G., *et al.* (2011). Curcumin and genistein additively potentiate G551D-CFTR. *J Cyst Fibros* *10*, 243-252.
- Zegarra-Moran, O., Romio, L., Folli, C., Caci, E., Becq, F., Vierfond, J.M., Mettey, Y., Cabrini, G., Fanen, P., and Galiotta, L.J. (2002). Correction of G551D-CFTR transport defect in epithelial monolayers by genistein but not by CPX or MPB-07. *Br J Pharmacol* *137*, 504-512.
- Zhang, L., Aleksandrov, L.A., Zhao, Z., Birtley, J.R., Riordan, J.R., and Ford, R.C. (2009). Architecture of the cystic fibrosis transmembrane conductance regulator protein and structural changes associated with phosphorylation and nucleotide binding. *Journal of structural biology* *167*, 242-251.
- Zolnerciks, J.K., Wooding, C., and Linton, K.J. (2007). Evidence for a Sav1866-like architecture for the human multidrug transporter P-glycoprotein. *Faseb J*.